2023

# Quantification and identification of neuro-electrophysiological markers and brain network for biomedical applications

Shu Kang

# Quantification and identification of neuro-electrophysiological markers and brain network for biomedical applications

by

Shu Kang

Presented to the Faculty of the Graduate School of
The University of Texas at Arlington in Partial Fulfillment
of the Requirements for the Degree of

DOCTOR OF PHILOSOPHY

THE UNIVERSITY OF TEXAS AT ARLINGTON

August 2023

## Acknowledgements

I write to convey my heartfelt gratitude and sincere appreciation as I approach the Mont Blanc of my doctoral journey. As I reflect on this odyssey, I am humbled and deeply thankful for the invaluable support and guidance I have received.

Foremost, I extend my utmost gratitude to my esteemed supervisor Prof. Hanli Liu for her unwavering support and guidance in shaping my academic growth. She encouraged me to transcend limitations and pursue innovation. Her discerning perspectives have challenged and inspired me to reach new heights in my academic pursuits.

Furthermore, I want to express my sincere appreciation to Dr. Lina Chalak for leading me into the research of neonatal brain injury. Her profound passion for cutting-edge research and a dedication to excellence deeply influences me. I feel incredibly fortunate to work with her and her exceptional research team members Drs. Rong Zhang, Srinivas Kota, and Yulun Liu.

To all my esteemed committee members Drs. Hanli Liu, Lina Chalak, Srinivas Kota, and George Alexandrakis, I am profoundly grateful for their invaluable support and comments throughout my Ph.D. journey. Their rigorous assessment and insightful feedback have been pivotal in enhancing the quality and rigor of my research.

Also, I wish to extend my heartfelt gratitude to my colleagues Drs. Srinivas Kota, Xinlong Wang, Sadra Shahdadian, and Yunlun Liu for their inspiration, suggestions, and support. Drs. Srinivas Kota, Xinlong Wang, and Sadra Shahdadian always wholeheartedly sharing their research experience with me. They introduced me to new approaches and provided invaluable suggestions in signal processing, data analysis, and manuscript writing. And Dr. Yulun Liu helped me with rigorous statistical analysis.

In addition to the individuals mentioned earlier, I am thankful to my former and current lab colleagues, Drs. Anqi Wu, Yudhajit Das, Nghi Truong, Akhil Chaudhari, Tyrell Pruitt, and Hashini Wanniarachchi. I am deeply aware of the collective effort and collaboration that have brought me to this juncture.

To my beloved family and loved ones, I‘m deeply grateful for their unconditional support. Their belief in my abilities and resilience has been my constant source of strength.

With warmest regards,
Shu

July 31, 2023

# Abstract

Quantification and identification of neuro-electrophysiological markers and brain network for biomedical applications

Shu Kang, Ph.D.

The University of Texas at Arlington, 2023

*Supervising Professor: Dr. Hanli Liu*

Electroencephalogram (EEG) can detect and monitor neuro-electrophysiological signals in the human brain, including assessing brain function in newborns at risk of neurological injury and healthy adults undergoing intervention with prefrontal transcranial photobiomodulation (tPBM). Moreover, EEG-based brain functional connectivity can be assessed in either resting-state or task-based measurements using graph-theoretical network modeling. However, the management of newborns with mild hypoxic ischemic encephalopathy (HIE) is controversial, and no study has investigated the EEG-based brain network and information flow resulting from HIE. Also, the underlying electrophysiological mechanism of tPBM is still unclear, and further research is needed to determine optimal parameters for tPBM applications. My dissertation targets these gaps to (1) evaluate the potential of predicting neurodevelopmental outcomes of newborns with HIE using the brain state of newborn (BSN) measured within the first day of life; (2) investigate the brain network in newborns with HIE; and (3) compare electrophysiological modulations of the human brain in response to left and right prefrontal tPBM using 800-nm laser.

In Chapter 2, I aimed to predict neurodevelopmental outcomes at two years of age using BSN that was derived from EEG data collected on the first day of life. The results showed that BSN can distinguish normal and HIE cases and has strong correlation with a clinical assessment score (i.e., the concomitant Total Sanart Score). BSN were also differentiated between neonates with normal and abnormal neurodevelopmental outcomes at the age of two years. Additionally,

higher BSN values indicate a reduction in the odds of HIE occurrence and of abnormal neurodevelopmental outcomes in global, cognitive, language, and motor skills. The findings confirm that BSN is a sensitive real-time biomarker for monitoring the dynamic progression of neonatal encephalopathy.

In Chapter 3, I targeted the assessment of brain network in newborns with HIE. Based on the first 30 minutes of available clean eight-channel EEG data, I quantified the global brain connectivity parameters in newborns with HIE, followed by comparisons with those from healthy newborns and adults. Furthermore, nodal graphical brain connectivity and region-wise networks were also investigated. The major findings indicate that the neural networks of neonates affected by HIE exhibited a notable reduction of overall efficiency compared to both healthy neonates and adults. However, significant distinctions in these fundamental metrics were not observed between the mild and moderate HIE cohorts, implying the necessity for prompt and efficacious medical intervention even for newborns with mild HIE to mitigate potential adverse outcomes.

In Chapter 4, I explored electrophysiological modulations of the brain in response to left/right prefrontal 800-nm tPBM. Recent literature supports tPBM's capacity to enhance cerebral blood flow and oxygenation and thus to improve cognitive performance. A total of 26 subjects underwent 7-min resting-state 19-channel EEG recordings before and after tPBM/sham stimulation on the left/right forehead, in a single-blind crossover design with randomized sham and tPBM sequences. Global and regional GTA-derived brain networks were assessed and compared between the tPBM and sham conditions. My results indicated site-specific effects of tPBM, with distinct EEG network changes induced by left and right prefrontal tPBM.

# Table of Contents

# List of Illustrations

# Chapter 1

# Introduction

## 1.1. Background of Hypoxic-Ischemic Encephalopathy (HIE)

Clinically presenting as neonatal encephalopathy (NE), HIE is a leading cause of long-term disability and death in newborns. As a dynamic condition that evolves over time, HIE can cause the extent of brain injury to worsen rapidly if untreated. In clinical practice, neonatal HIE severity is classified as mild, moderate, or severe. The assessment of HIE severity and prognosis is crucial for guiding appropriate clinical interventions and predicting neurodevelopmental outcomes.

## 1.2. Treatment and challenges of HIE

Targeting moderate to severe HIE, the current standard treatment whole-body therapeutic hypothermia (TH) is suggested to be initiated for moderate and severe encephalopathy within six hours of birth to be effective. TH involves cooling the body temperature of the newborn with HIE to 33.5°C for 72 hours to reduce the metabolic rate and decrease inflammation in the brain, followed by a gradual rewarming process at a rate of 0.5°C per one to two hours for the subsequent six hours. Newborns with mild encephalopathy will undergo late hypothermia if they progress to more severe encephalopathy or experience seizures within the first day of life. However, management of mild HIE is controversial. Accurately identifying mild HIE immediately after birth is challenging, and there is strong biological plausibility and preclinical evidence supporting that the newborns with mild encephalopathy are at a significant risk of adverse outcomes.

## 1.3. Conventional monitoring tools

Accurate and continuous measures of brain health are essential for prompt treatment decisions on infants with HIE, including newborns with mild NE. As a non-invasive neuroimaging tool, continuous scalp multichannel electroencephalography (EEG) is recommended for detecting and

monitoring neuro-electrophysiological signals in the brain of newborns at risk of neurological injury. This includes assessing brain function in newborns with seizures and HIE.

On the other hand, we can quantify the modulation effects caused by tPBM on brain functional connectivity based on EEG recording. Specifically, employing graph theory metrics, we can evaluate the alterations in brain network and information flow induced by tPBM. Representing the brain as a network of interconnected nodes which refer to brain regions) and edges which indicate the connections between regions, graph theory-based brain network analysis (GTA-based) enables the intricacies of connections and communication patterns within the brain.

### 1.4. Background of Prefrontal transcranial photobiomodulation (tPBM)

tPBM has emerged as a promising non-invasive intervention with the potential to enhance cognitive function, particularly in the domains of attention, memory, and executive function. Recent research has demonstrated its memory-enhancing effects in both healthy individuals and patients with specific neurological conditions. By targeting specific brain regions, tPBM has been shown to increase cerebral blood flow and oxygenation by working on cytochrome c oxidase, leading to enhanced neuronal activity and improved cognitive performance. Additionally, some studies suggest that tPBM may influence the levels of neurotransmitters like dopamine and serotonin, which play crucial roles in cognitive processes such as attention and memory.

### 1.5.Challenges of tPBM

The electrophysiological mechanism of tPBM remains unclear, necessitating further research to identify optimal parameters for tPBM applications, including wavelength and treatment location. Previous studies have primarily examined tPBM's effects on brain activity from hemodynamic, metabolic, or electrophysiological perspectives. However, to date, no research has explored the systemic modulation of the brain in response to left and right prefrontal tPBM using 800-nm laser.

### 1.6. Rationale of this thesis

HIE evolves over time and the extent of brain injury can worsen rapidly if left untreated, leading to death or long-term disabilities such as cerebral palsy, seizures, and developmental delay. Current treatment for HIE includes TH, by cooling the body temperature of the newborn to reduce metabolic rate and decrease inflammation in the brain. This treatment must be initiated within six hours of birth to be effective. However, grading of severity of encephalopathy using neurological exams such as modified sarnat score may not be accurate due to the potential progression of encephalopathy severity. Recent reports have shown that newborns with mild encephalopathy experience poor neurodevelopmental outcomes. Therefore, prompt intervention within the first 6 hours of life is critical and crucial in reducing the risk of long-term neurological deficits and improving survival chances, which requires accurate and continuous quantitative biomarkers.

In neonates with HIE, acute kidney injury (AKI) is prevalent in approximately 40% of cases and serves as a separate risk determinant, leading to compromised neurodevelopmental progress and heightened mortality rates. According to the latest research Effects of photobiomodulation and caffeine treatment on acute kidney injury in a hypoxic ischemic neonatal rat model (Groves et al., 2023), tPBM using 670-nm red light has been found can reduce AKI caused by HIE in the modified Rice-Vannucci model. Therefore, if further research can substantiate that AKI can also be ameliorated by tPBM in neonates with HIE, this could offer a potential pathway for advancing therapeutic treatments for neonatal HIE.

Previous studies investigating the effects of tPBM on brain activity have predominantly focused on hemodynamic and metabolic, or electrophysiological viewpoints. To date, no research has assessed the systemic modulation of the brain in response to left and right prefrontal tPBM using 800-nm laser. Hence, a more comprehensive understanding of the mechanisms underlying

tPBM can be achieved by examining the topological networks and their modulation in response to tPBM using a different wavelength. On the other hand, exploring the modulation effects of tPBM in healthy adults may serve as a critical reference for the subsequent stages of research focused on applying tPBM therapy and selecting parameters in newborns with HIE.

Therefore, I focused on quantifying and identifying EEG-derived electrophysiological markers and brain networks for two clinical and biomedical applications in my dissertation. The clinical application targeting neonatal HIE encompassed two aims: Aim 1 aimed to monitor evolving encephalopathy using the Brain State of Newborn (BSN) which quantifies EEG background activity. The purpose was to accurately and timely differentiate cases who may benefit from neuroprotective therapies, on the first day of life. Aim 2 involved investigating brain connectivity in newborns with mild and moderate HIE. This may provide insight into the underlying neural mechanisms of HIE and help to identify potential patterns for early diagnosis and intervention that can reduce the risk of long-term neurological impairments. In the second biomedical application, my objective was to explore the modulation effects of 800-nm left/right prefrontal tPBM in healthy young adults. Aim 3 serves as an investigation of optimal parameters for tPBM therapy.

Specific aims under three aims are listed below:

Aim 1(a): to determine if the Brain State Network (BSN) could provide real-time, automated monitoring and interpretation of encephalopathy grade in HIE cases, which might necessitate intervention within 6 hours.

Aim 1(b): to examine the relationship between BSN measurements taken on the first day of life and the severity of neurodevelopmental impairment outcomes in infants affected by HIE at two years of age.

Aim 2(a): to study the brain power spectral density (PSD) of neonatal HIE.

Aim 2(b): to explore the global topographical connectivity in neonatal HIE and healthy newborns.

Aim 2(c): to compare the nodal topographical connectivity in infants with mild and moderate HIE.

Aim 3(a): to investigate the global and nodal brain connectivity modulated by 800-nm left prefrontal tPBM.

Aim 3(b): to study the modulation effects of 800-nm right prefrontal tPBM on neurophysiological networks.

### 1.7.Organization of this thesis

This dissertation has 6 chapters, which consist of one manuscript ready for submission (Chapter 2), and two manuscripts that are in preparation for submission to scientific journal (Chapter 3 and 4). Chapter 1 is a brief introduction of the HIE and tPBM, current treatment for HIE, challenges of HIE management and tPBM, conventional monitoring tools and need for biomarkers to guide therapeutic decision-making and early prediction of neurodevelopmental impairment in newborns with HIE. Chapter 2 investigates if EEG-derived automated bedside brain state trend correlates with encephalopathy grade and neurodevelopmental outcome in newborns with HIE. Chapter 3 aims to study the neurophysiological networks for newborns with Mild and Moderate HIE. In Chapter 4, the effects of both left and right prefrontal 800-nm tPBM on neurophysiological networks were determined, and distinct site-specific effects were observed. Furthermore, Chapter 5 discussed serval directions of future studies, focusing on the prediction of long-term severities of newborns with HIE and advanced management in their first 72 hours of life. Finally, Chapter 6 summarizes the conclusions of all three aims in this dissertation.

# Chapter 2

# Brain State of Newborn (BSN) Predicts Encephalopathy Severity and Neurodevelopmental Outcome in Newborns with Hypoxic-Ischemic Encephalopathy

## 2.1 Introduction

Hypoxic ischemic encephalopathy (HIE) is one of the leading causes of mortality and morbidity in newborns worldwide [1]. HIE occurs when the fetal brain is deprived of oxygen and blood supply [2] and the encephalopathy severity is classified as mild, moderate, or severe grades within six hours after birth [3-5]. While therapeutic hypothermia (TH) [6] is standard clinical care for moderate and severe grades in developed countries, the management of mild HIE is controversial [7] due to difficult clinical classification and progression of encephalopathy grade. Mild HIE accounts for 50% of total HIE [8]. Newborns with mild HIE and worsening symptoms in the first day of life are often treated with TH using a late hypothermia protocol, but its effectiveness may be limited if it is initiated after six hours of life [9].

Electroencephalogram (EEG) monitoring is routinely used to detect seizures and predict outcomes in HIE [10]. We and others have studied Qualitative and quantitative metrics, such as background EEG activity, amplitude-integrated EEG (aEEG), spectral power, and connectivity, for prognosis [11-14]. However, due to the lack of continuous interpretation, these biomarkers have not been available to be used for timely interventions.

Moghadam et al. proposed a novel biomarker called the brain state of newborn (BSN), which uses deep learning and expert-scored EEG background activity [15]. This method achieved 92% accuracy and was validated with EEG datasets from other sources. This cloud-based tool provides BSN values range from 0 to 100 which are based on EEG background activity and sleep

state trend, where 0 represents inactive EEG background activity and 100 indicates gradual improvement.

The aim of this study is to evaluate BSN measured within the first day of life in newborns with different grades of encephalopathy and correlate it with the Total Sarnat Score (TSS) from modified Sarnat exam and predict neurodevelopmental outcomes at two years of age. Our hypothesis is that BSN has the potential to accurately and timely differentiate in the first day of life cases who may benefit from neuroprotective therapies.

## 2.2 Method

### 2.2.1 Study participants

#### 2.2.1.1 HIE cohort

Term newborns (≥36 weeks' gestation) at Parkland Hospital (Dallas, TX) who met the following criteria were recruited for this prospective study between 2017 and 2019: 1) a history of an acute perinatal event (e.g., placental abruption, cord prolapse, decreased fetal heart rate), 2) umbilical cord arterial pH or arterial blood gas pH of ≤ 7.0 or base deficit ≥ 15 mmol/L at < 1 hour postnatal age, and 3) signs of encephalopathy. Newborns were excluded from the study if they had any genetic or congenital condition, birthweight < 1800 g, and/or head circumference < 30 cm, as these factors can interfere with the primary outcome. The study was approved by the Institutional Review Board at University of Texas Southwestern Medical Center, and written informed consent was obtained from a parent of each newborn prior to enrollment.

The newborns were evaluated within 6 h after birth using a modified Sarnat exam to determine the severity of encephalopathy that included 1) level of consciousness, 2) spontaneous activity, 3) posture, 4) tone, 5) primitive reflexes (suck, moro), and 6) autonomic system (pupils, heart rate, respirations), with scores of normal (0), mild (1), moderate (2), or severe (3). The TSS

was determined by adding the scores for each of the six categories, which ranges from 0 to 18 [5], where 0 represents normal in all six categories, and 18 represents severe encephalopathy in all six categories. The clinical grade of encephalopathy was determined by the number of Sarnat abnormalities, with classifications ranging from mild to moderate or severe. In cases where equal numbers of abnormalities were observed, the grade was determined by the degree of reduced level of consciousness.

Whole-body therapeutic hypothermia (TH) was initiated within 6 h after birth for newborns with moderate and severe encephalopathy, following the National Institute of Child Health and Human Development (NICHD) protocol [6]. A servo-controlled blanket (Blanketrol II, Cincinnati Sub-Zero Products LLC, OH, USA) was used to maintain a core body temperature of 33.5 °C for 72 hours, followed by rewarming at a rate of 0.5°C per one to two hours for the next six hours. Newborns with mild encephalopathy received normothermia as per the standard of care. TH was initiated in accordance with the NICHD late hypothermia protocol if they progressed to more severe encephalopathy or experienced seizures within the first day of life [9].

Neurodevelopmental impairment at age of two years was death or disability defined by a cognition, language, or motor score < 85 on the Bayley Scales of Infant Toddler Development, third edition (BSID-III) [5, 16, 17], which was performed by certified professionals in the follow up clinic at 18-24 months of age.

Continuous EEG acquisition was initiated at a sampling rate of 256 Hz as soon as newborns were admitted. EEG (Nihon Kohden America Inc., Irvine, CA) data were acquired from eight scalp electrodes (Fz, C3, Cz, C4, P3, P4, O1, O2) that are referenced to the midpareital electrode (Pz), placed according to the modified 10-20 montage for newborns [18]. The Component Neuromonitoring System (CNS Monitor) (Moberg Research, Inc., Ambler, PA,

USA) was used to interface EEG and other physiological signals at the bedside. The EEG data were obtained from CNS monitor and processed offline using MATLAB (MathWorks Inc., Natick, MA, USA).

Central and parietal electrodes were chosen for analysis because they reflect watershed injury patterns on MRI that are commonly observed in cases of HIE [19-21]. Inter-hemispheric (C3-C4, P3-P4) and intra-hemispheric (C3-P3, C4-P4) bipolar EEG data were obtained by taking a difference between pair of electrodes. The bipolar EEG data were high pass filtered at 0.3 Hz using a Butterworth filter of order 4.

#### 2.2.1.2 Control Cohort

EEG data were collected using a NicoletOne system (Cardinal Healthcare/Natus, USA) at sampling rate of 256 Hz from four need electrodes (F3, F4, P3, and P4). All the bipolar signals (F3-P3, F4-P4, F3-F4, and P3-P4) were obtained for further analysis. EEG review was normal, and no neurological abnormalities were identified in this cohort.

### 2.2.2 Brain State of Newborn (BSN)

An automated cloud service tool (**https://babacloud.fi/**) was employed to calculate BSN and identify seizures and artifacts for every two seconds segments of data**[15]**. BSN was derived from EEG background activity and sleep state trend. The BSN values ranged from 0 to 100, with indicating inactive cerebral activity and a gradual improvement in cerebral recovery represented by an increase to 100. The mean BSN value was calculated for the first hour of artifact-free segments from four bipolar electrode pairs for statistical analysis.

### 2.2.3 Statistical analysis

Demographic and clinical characteristics of newborns, stratified by non-mild HIE (including mild-moderate, moderate, and severe) and mild HIE, were summarized with descriptive

statistics, where continuous variables were presented as means with standard deviations or medians with interquartile ranges (IQRs), and categorical variables were presented with counts with percentages. The non-mild and mild HIE groups were compared using Student's t-test or Wilcoxon rank-sum test for continuous variables, while $\chi^2$ test or Fisher's exact test for comparisons among categorical variables. Univariate linear regression analysis was performed to determine the association between BSN and TSS. The assumptions for linear regression model, including normality of residuals and homoscedasticity, were evaluated using Shapiro-Wilk test and Breusch-Pagan test. Univariate logistic regression models were used to assess the relationships of BSN on Bayley-III neurodevelopmental outcomes, including global, cognitive, language, and motor outcomes. To evaluate the prediction ability of BSN on Bayley-III neurodevelopmental outcomes, we conducted the receiver operating characteristic (ROC) curve, with the area under the ROC curve (AUC). The optimal cut-off values of BSN were obtained with the Youden method to distinguish between normal and abnormal neurodevelopmental outcomes in infants. Results were reported as odds ratios with 95% confidence intervals in logistic regression models, and regression coefficients with 95% confidence intervals in linear regression models. A 2-tailed *p* value less than 0.05 was considered the threshold for statistical significance. All statistical analyses were performed using R version 4.2.2.

## 2.3 Results

A total of 45 newborns with symptoms ranging from mild to severe encephalopathy, as determined by the modified Sarnat exam within the first six hours after birth, were recruited for this study. Among them, 26 newborns were initially classified as mild in the first six hours of life. However, seven of those infants later developed seizures or displayed worsening symptoms

of encephalopathy, leading to their reclassification as mild-moderate. Maternal and neonatal characteristics of the cohort are provided in Table 2-1. The non-mild group consisted of mild-moderate, moderate, and severe grades, while the mild group consisted of 19 newborns. Two newborns with severe grade died in the first week of life following redirection of care.

The severity of encephalopathy was associated with lower Apgar scores, the presence of meconium, and longer hospital stays (Table 2-1). Out of 45 infants eight were lost two-years follow up (6 mild, 2 moderate). There was no statistically significant difference in BSID-III scores between the mild and non-mild groups. An abnormal score in cognition, language, or motor skills was defined as a BSID-III score < 85. For global outcome, any of the three scores < 85 was considered abnormal. Normal newborns (GA 40 [39 42]) with no neurological abnormalities were included benchmark the study cohort (GA 39 [38 40]) and their neurodevelopmental outcome was recorded normal.

Figure 2-1 illustrates the BSN values for both normal newborns and newborns with HIE. It is evident that normal newborns have higher BSN values compared to the study cohort. Figure 2-2 (a) to (d) provides examples of BSN trends with the classifier's confidence on given BSN values for one of the newborns in each encephalopathy grade (normal, mild, moderate, and severe), along with the distribution of average BSN values for all newborns in each group (Figure 2-2 e).

**Table 2-1.** Maternal and neonatal characteristics of the HIE cohort

| Characteristics | Overall | Encephalopathy Grade | |
|---|---|---|---|
| | | Mild | Non-Mild |
| Total N | 45 | 19 | 26 |
| Male: N (%) | 29 (64) | 14 (74) | 15 (58) |
| Gestational Age (weeks), median [IQR] | 39 [38 40] | 39 [38 40] | 39 [38 40] |
| Birth Weight (kg) | 3.3 (0.7) | 3.4 (0.6) | 3.3 (0.8) |
| Apgar 1 minute, median [IQR]* | 2 [1 4] | 3 [2 5] | 1 [1 2] |
| Apgar 5 minute, median [IQR]* | 6 [4 7] | 7 [6 8] | 5 [2 6] |
| Umbilical Cord Gas pH | 7 (0.1) | 7(0.1) | 7(0.2) |
| Base Deficit | 17.1 (6.1) | 17.4 (3.6) | 17 (7.5) |
| Abnormal MRI (Global): N (%) | 12 (27) | 4 (21) | 8 (31) |
| Maternal Race/Ethnicity: N (%) | | | |
| *Caucasian non-Hispanic* | 2 (4) | 1 (5) | 1 (4) |
| *Black non-Hispanic* | 10 (22) | 4 (21) | 6 (23) |
| *Hispanic* | 31 (69) | 13 (68) | 18 (69) |
| *Other non-Hispanic* | 2 (4) | 1 (5) | 1 (4) |
| Delivery Mode: N (%) | | | |
| *C/S* | 29 (64) | 12 (63) | 17 (65) |
| *Vaginal* | 16 (36) | 7 (37) | 9 (35) |
| Maternal Risk Factors: N (%) | | | |
| *Hypertension* | 10 (22) | 4 (21) | 6 (23) |
| *Diabetes* | 5 (11) | 4 (21) | 1 (4) |
| *Pre-eclampsia* | 12 (27) | 4 (21) | 8 (31) |
| Labor Complications: N (%) | | | |
| *Meconium** | 12 (27) | 2 (11) | 10 (38) |
| *Umbilical Cord Prolapse* | 1 (2) | 0 | 1 (4) |
| *Placental Abruption* | 4 (9) | 1 (5) | 3 (12) |
| *Uterine Rupture* | 4 (9) | 2 (11) | 2 (8) |
| *Maternal Chorioamnionitis* | 13 (29) | 6 (32) | 7 (27) |
| *Placental Chorioamnionitis* | 23 (51) | 10 (53) | 13 (50) |
| Disposition: | | | |
| DOL at discharge, median [IQR]* | 9 [6 17] | 6 [5 7] | 14 [9 20] |
| Death prior to discharge, N (%) | 2 (4) | 0 | 2 (8) |
| Neurodevelopmental Outcome: | | | |
| Total N | 37 | 13 | 24 |
| Composite, death or disability N (%) | 32 (86) | 11 (85) | 21 (88) |
| BSID Score: median [IQR] | | | |
| Cognition | 85 [75 90] | 83 [75 95] | 85 [80 90] |
| Language | 73 [60 79] | 73 [59 80] | 71 [62 79] |
| Motor | 94 [88 100] | 94 [78 100] | 94 [92 102] |

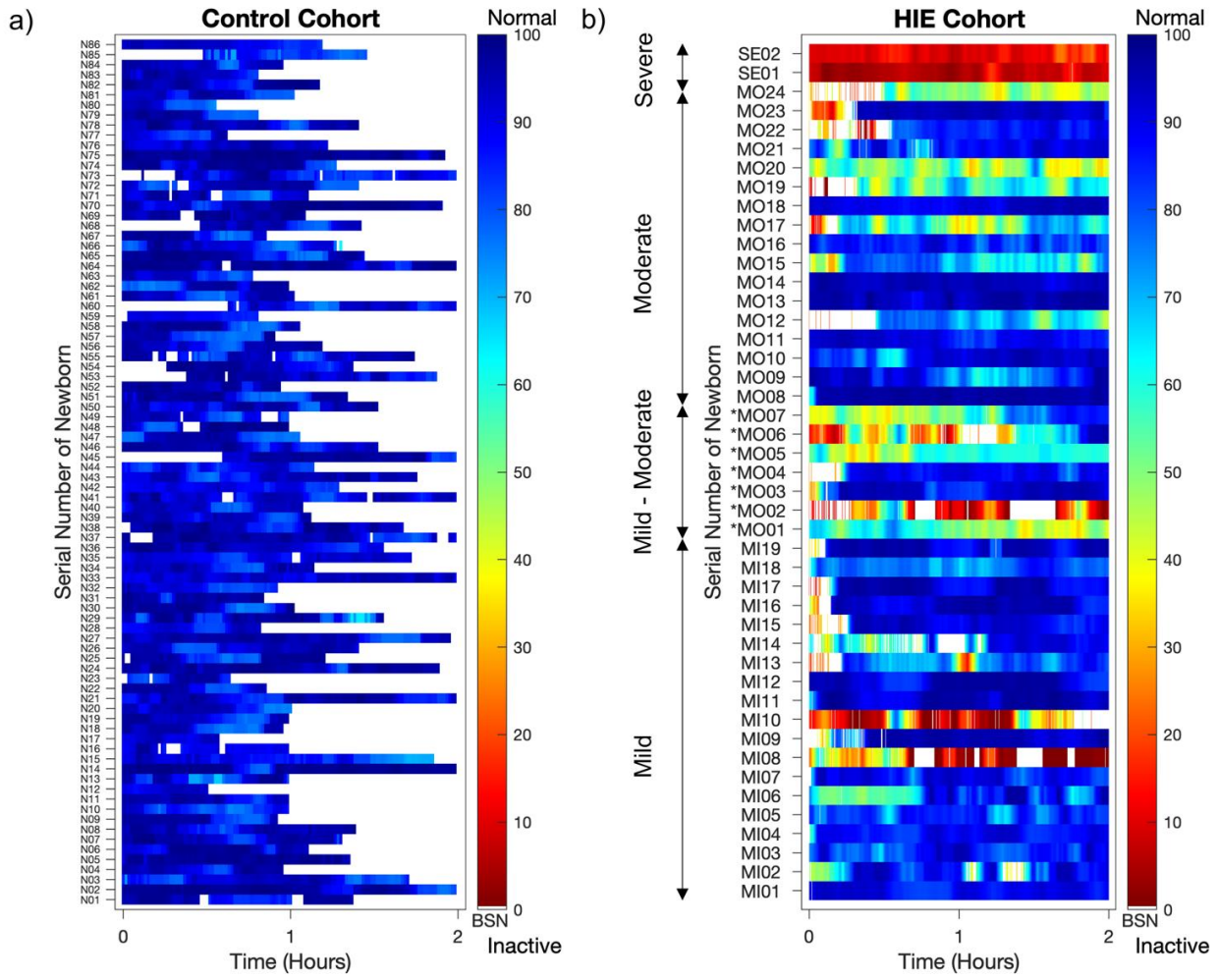


**Figure 2-1**. BSN values for two groups: normal newborns (a) and newborns with HIE (b). Each row in the figure represents the BSN values recorded over the first two hours for each newborn. The color bar is in arbitrary units, ranging from 0 (Inactive brain activity is represented by red) to 100 (normal brain activity is represented by blue). White spaces in the figure indicate missing data caused by artifacts or unavailability of data. Subject IDs with * in (b) indicate newborns (MO01 to MO07) who were initially classified as mild and later progressed to moderate are indicated as mild-moderate.

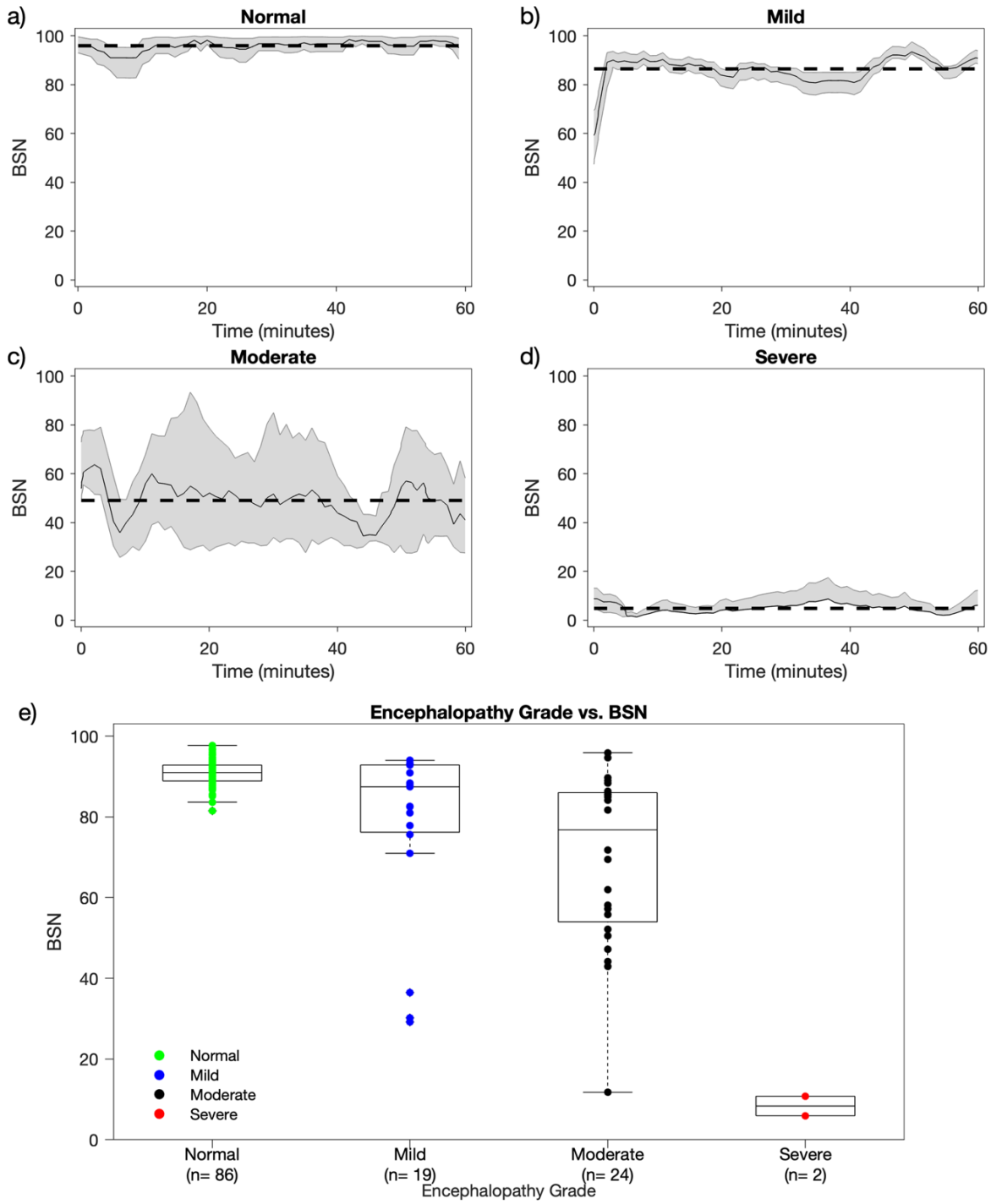


**Figure 2-2**. BSN value trend for a newborn: normal (a), mild (b), moderate (c), and severe (d), during the initial hour of recording. The shading in the figure represents the confidence of the classifier on the corresponding BSN values. The dashed line indicates the mean value of the trend. (e) The distribution of BSN values for all newborns is categorized based on the

encephalopathy grade. The moderate category comprises newborns with a moderate grade of encephalopathy, as well as those who were initially classified as mild but later progressed to severe encephalopathy.

In the univariate linear regression model that assessed the effect of BSN on TSS, BSN was negatively correlated with TSS, and the model explained 17% of the variation of TSS (i.e., $R^2$ of 0.17). It was found that for every 1-unit increase in BSN, TSS was decreased by 0.071 points (95% CI, -0.118 to -0.024; $p = 0.005$). The Shapiro-Wilk test ($p = 0.122$) and the Breusch-Pagan test ($p = 0.213$) suggested the normality of the residual and homoscedasticity, respectively. Figure 2-3 (a) displays the scatter plot of BSN and TSS, with a fitted line. Univariate logistic regression analysis showed that a higher score of BSN was associated with decreased odds for the occurrence of newborn HIE (OR, 0.794; 95% CI, 0.708 to 0.891; $p < 0.001$). Figure 2-3 (b) displays the ROC with the area under the curve (AUC). The BSN was classified HIE grade vs. normal, with an AUC of 0.808 (95% CI, 0.713 to 0.903), sensitivity of 0.667 and specificity of 0.942.

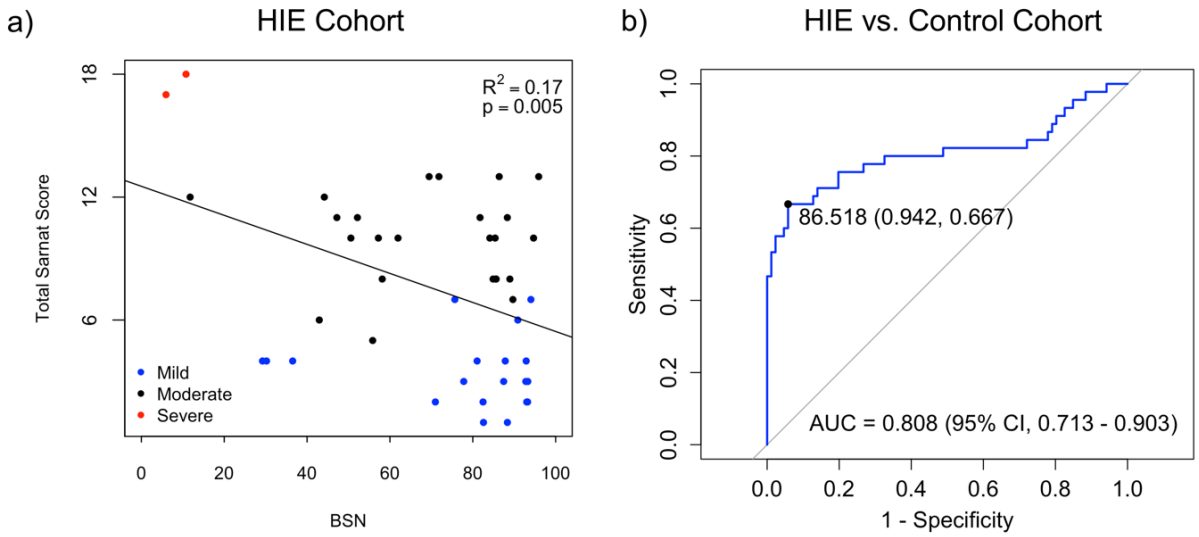


**Figure 2-3.** (a) Scatter plot illustrating the association between BSN and TSS. The black solid line represents the fitted line of simple linear regression. TSS exhibits a significant negative

correlation with BSN (regression coefficient = -0.071, R2=0.17, and P = 0.005). (b) The receiver operating characteristic (ROC) curve is generated for the classification of encephalopathy grade (normal versus HIE, including mild, mild-moderate, moderate, and severe categories) and BSN. The area under the curve (AUC) represents the area under the ROC curve compared to the line of non-significance, depicted in gray. A BSN value of 86.518 is the optimal threshold for discriminating between normal newborns and those with encephalopathy.

The results of ROC curves for global, cognitive, language, and motor outcomes at the age of two years are presented in Figure 2-4. In Figure 2-4 (a), it is evident that a BSN value of 86.518 effectively differentiated normal from abnormal global outcomes, achieving sensitivity of 0.75 and specificity of 0.912. The corresponding AUC value was 0.869 (95% CI, 0.779-0.958). Comparable findings were observed for cognitive, language, and motor outcomes, with the AUC value for global outcome slightly higher than the others. Additionally, the BSN threshold for cognition was marginally higher than the thresholds for the other outcomes. In addition, univariate logistic models reveal strong relationships between BSN and global, cognitive, language, and motor outcomes. Higher BSN scores are significantly associated with lower odds of abnormal global (OR, 0.854; 95% CI, 0.786 to 0.927; $p < 0.001$), cognitive (OR, 0.944; 95% CI, 0.918 to 0.971; $p < 0.001$), language (OR, 0.862; 95% CI, 0.798 to 0.930; $p < 0.001$), and motor outcomes (OR, 0.937; 95% CI, 0.908 to 0.967; $p < 0.001$).

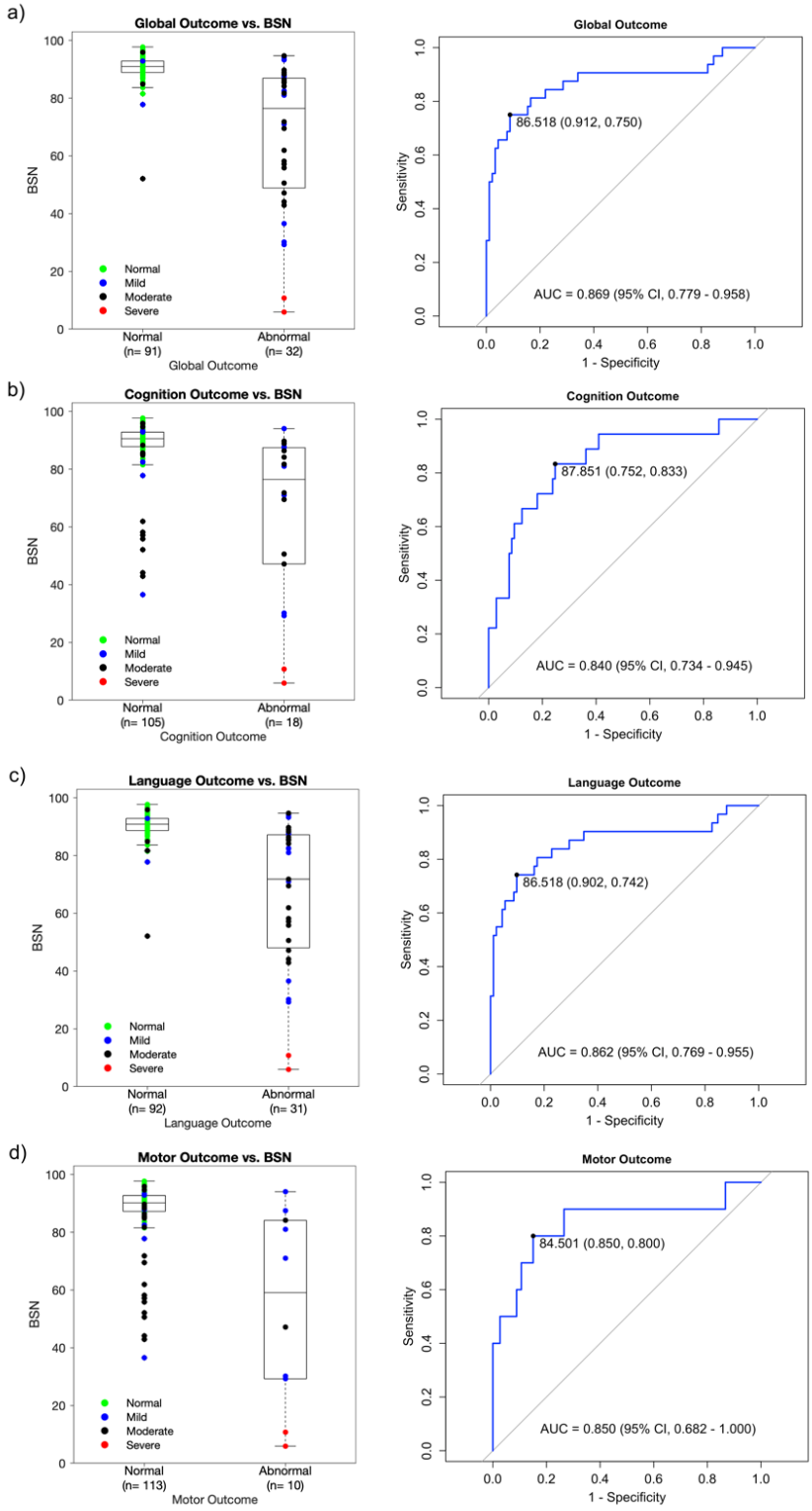


**Figure 2-4**. The distribution of BSN values for normal and abnormal neurodevelopmental outcomes at two years of age and the corresponding receiver operating characteristic (ROC)

curves for global (a), cognitive (b), language (c), and motor (d) outcomes. The area under the ROC curve (AUC) is indicated, depicting the comparison with the line of non-significance in gray.

## 2.4 Discussion

This study highlights BSN as a promising bedside biomarker to quantify brain health, severity of encephalopathy and predict neurodevelopmental outcome using the first hours of EEG recording. This is especially crucial when the neurological exam may not accurately determine the severity of encephalopathy within the first six hours after birth, particularly for identifying mild cases that would benefit from neuroprotection therapies. Furthermore, it has a potential to quantify evolving encephalopathy in the first days of life.

Heterogeneity across various encephalopathy grading systems like Sarnat, modified Sarnat exam, NICHD, and SIBEN, highlight the potential benefits of a standardized automated EEG quantitative system[22]. For instance, newborns, with mild encephalopathy a TSS ranging from 1 to 10 is possible, while moderate ranges from 6 to 14, and severe from 9 to 18. Chalak et al. reported that a TSS value of $\geq 5$ within first six hours of life predicted neurodevelopmental impairment and encephalopathy burden. The correlation between BSN and TSS in this study suggests that BSN could serve as a biomarker for assessing severity when trained and certified professionals are unavailable to conduct a neurological exam within the first day of life. The BSN value of 86.518 best discriminates HIE from normal. We and others have similarly reported spectral power, neurovascular coupling, and phase amplitude coupling also correlate with TSS [12, 23, 24].

Overall, BSN predicts encephalopathy severity and neurodevelopmental outcomes. The BSN value of 86.518 predicted Bayley-III outcome in language, cognition, and motor as well at the age of two years.

Moghadam et al. reported distinct BSN level differentiations based on EEG background activity determined from aEEG: BSN of 0 – 33 (median 14.8, 95% CI 12.8 -18.4) corresponds to inactive aEEG, a BSN of 27 – 61 (41.8, 38.4-43.4) corresponded to burst suppression, 61-91 (75.8, 70.4-73.6) corresponded to continuous normal voltage. The BSN values exceeding 90 were observed in EEG displaying more normal characteristics [15]. We observed that the BSN value of 86.518 best distinguishes normal from HIE cohort and predicts neurodevelopmental impairment. Clinicians could utilize this threshold value as a reference at the bedside. Previous studies utilizing spectral power have reported similar threshold values, which can be valuable biomarkers for clinicians in predicting encephalopathy severity or abnormal outcome on MRI [12, 25]. However, it's important to note that those studies lacked the inclusion of normal newborns, and their data analysis was conducted offline.

This study has several strengths. First, it evaluates a cloud-based tool that rapidly provides the trend of BSN values at the bedside, enabling immediate clinical decision-making. Second, the tool can identify EEG data with seizures and different types of artifacts that might be hard to identify with a human eye and reject segments with artifacts with visual inspection. Despite the small HIE cohort, the study successfully validated the use of BSN by comparing it with a normal cohort and predicting neurodevelopmental outcomes. Third, one of the significant advantages of this tool is its easy implementation at the bedside, requiring minimal data processing steps, such as high pass filtering. This simplicity makes it a potential tool to accurately assess the true severity of mild cases and determine the suitability of neuroprotective therapies within the first six hours

of life. Particularly in low-resource settings lacking physician availability for EEG review, BSN could play a crucial role in identifying newborns who would benefit from timely interventions.

Study limitations include the observational nature and small numbers with HIE derived from a single center. However, there is potential to expand the cohort in the future by including data from other sites participating in the COOLPRIME trial (https://clinicaltrials.gov/ct2/show/NCT04621279). In this current study, the analysis only considered inter and intra hemispheric central parietal bipolar electrodes. Nevertheless, we and others have shown electrodes in central parietal region to represent global HIE insults[12, 21, 23-26]. Moreover, Moghadam et al.[15] developed the algorithm using frontal parietal electrodes and validated it with frontal central electrodes, yielding no significant differences in outcomes.

It's worth noting that 69% of our HIE cohort is Hispanic, which highlights the importance of including these underserved and underrepresented patients in research studies. The BSN value is calculated using aEEG (amplitude-integrated electroencephalogram), and the interpretation might be affected by the specific algorithm used. However, Das et al. did not find any influence of aEEG algorithm in calculation neurovascular coupling[27]. Finally, neurodevelopmental trajectory needs to monitor for developing early intervention therapies because true severity of mild HIE may not know until school age [20, 28-34]. Future studies will include predicting neurodevelopmental outcome using multi-modal biomarkers include maternal and neonatal characteristics to identify combination of biomarkers that can best distinguishes the outcome.

## 2.5 Conclusion

BSN is a promising bedside tool for monitoring evolving encephalopathy in newborns and to predict neurodevelopmental outcomes. As a promising marker for continuous real-time monitoring of neonatal HIE, BSN is comparable with other published physiological biomarkers on long-term neurodevelopmental outcomes predictions. Moreover, larger studies with predictive modeling will be essential, which is particularly relevant when considering some of the measures may be independent to each other on predicting long-term neurodevelopmental outcomes. Subsequently, adding BSN into the muti-modal bedside monitor of neonatal HIE may assist clinicians in making prompt treatment decisions to reduce long-term neurodevelopmental impairment. It can help identify those who may benefit from additional interventions and protect those who may not require therapeutic hypothermia, thereby preventing potential adverse effects on their neurodevelopmental outcome.

# Chapter 3

# Quantification of Brain Networks in Neonatal Hypoxic-Ischemic Encephalopathy (HIE)

## 3.1 Introduction

Hypoxic-Ischemic Encephalopathy (HIE) is a condition characterized by oxygen and blood deprivation in the brain during or shortly after birth, which can lead to severe disabilities or even mortality among affected neonates. The severity of HIE varies from mild to severe, necessitating prompt decision-making for effective treatment. While electroencephalography (EEG) is commonly used for clinical monitoring of HIE-inflicted infants, there is a lack of studies investigating the neurophysiological networks in newborns with HIE using EEG recordings.

EEG-based functional connectivity analysis has shown promise in assessing neonatal brain development. Importantly, graph theory metrics have been employed to assess changes in brain networks and information flow due to diverse stimuli, diseases, cognitive decline, and altered consciousness states [35-37]. Analyzing EEG-based brain functional connectivity holds potential for developing early diagnosis and intervention strategies by identifying potential biomarkers, which could mitigate the risk of long-term neurological impairments in infants with HIE.

Consequently, a compelling need arises for quantifiable measures of brain functional connectivity in neonates with HIE, aiming to shed light on the underlying neural mechanisms of HIE. Our hypothesis posits that noticeable disparities exist in graph-theory-based (GTA) neurophysiological brain networks between newborns with mild and moderate HIE and their healthy counterparts, characterized by specific features. Specifically, our goal is to quantify the key parameters of the brain network in newborns with HIE using an eight-channel EEG

measurement. Furthermore, we anticipate that the key GTA matrices linked to HIE will generally exhibit smaller values compared to those observed in healthy newborns.

## 3.2 Method

### 3.2.1 Study participants

This study was based on a single-center prospective cohort having ≥ 36-week gestation inborn infants with HIE diagnosed within 6 hours (h) of birth in a level III neonatal intensive care unit from 2017 to 2019. The exclusion criteria include genetic syndromes, head circumference < 30 cm, and birthweight < 1800 g, as they interfere with the primary outcome.

In this study, the neonates with HIE include 16 with mild HIE, 15 moderate HIE. All newborns with HIE had metabolic acidosis, along with sentinel perinatal event and signs of encephalopathy within the first six hours of life. The classification of HIE was performed with Total Sarnat Score (TSS) in a scale from 0 to 18 which corresponding to normal and severe, by adding the scores of six categories includes level of consciousness, spontaneous activity, posture, tone, primitive reflexes, and autonomic system [5]. TSS was performed within 6 hours of age by experienced clinicians, to differentiate neonatal HIE severity into mild, moderate, or severe. Neonates with moderate to severe encephalopathy received 72 hours 33.5°C hypothermia therapy, achieved by placing them on a servo-controlled cooling blanket (Blanketrol II, Cincinnati Sub-Zero Products LLC, OH, USA) and maintaining their esophageal temperature.

### 3.2.2 EEG data acquisition

In this study, the EEG data of newborns with mild and moderate HIE was acquired at eight electrodes (Figure 3-1, Fz, Cz, C3, C4, P3, P4, O1, and O2) with 256 Hz sampling rate, based on the modified version of standard 10-20 montage (Nihon Kohden, Irvine, CA, USA). Those eight electrodes can cover the watershed regions that are typically affected in neonatal HIE, including intervascular boundary-zone white matter and cortical gray matter [19, 38-40]. All HIE datasets were recorded by a Moberg Component Neuromonitoring System monitor (Moberg Research, Inc., Ambler, PA, USA).

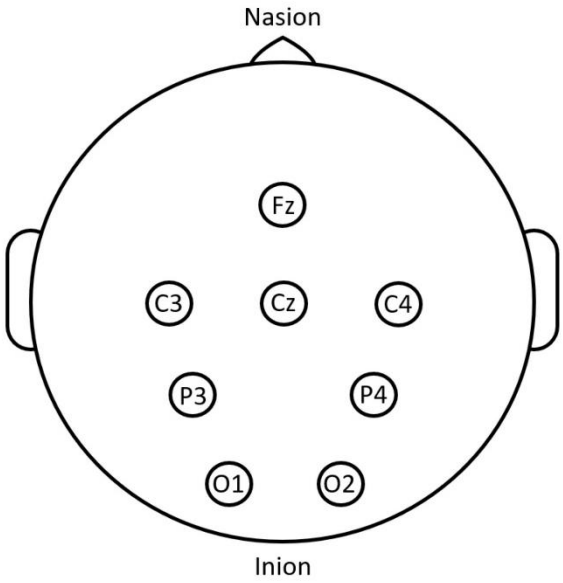


**Figure 3-1**. The location of eight-channel EEG electrodes for neonatal HIE, which overlying the watershed regions.

### 3.2.3 Overview of data processing pipeline

Each raw EEG dataset represents a time series of 8 channels collected from 31 subjects. As shown in Figure 3-2, the data processing pipeline includes four sections: (1) Preprocessing; (2) Power spectral density (PSD) analysis to obtain frequency-specific power topographies; (3) Construction

of connectivity matrices based on imaginary part of coherence analysis; (4) GTA-based global graphical brain connectivity analysis; (5) GTA-based nodal graphical brain connectivity analysis.

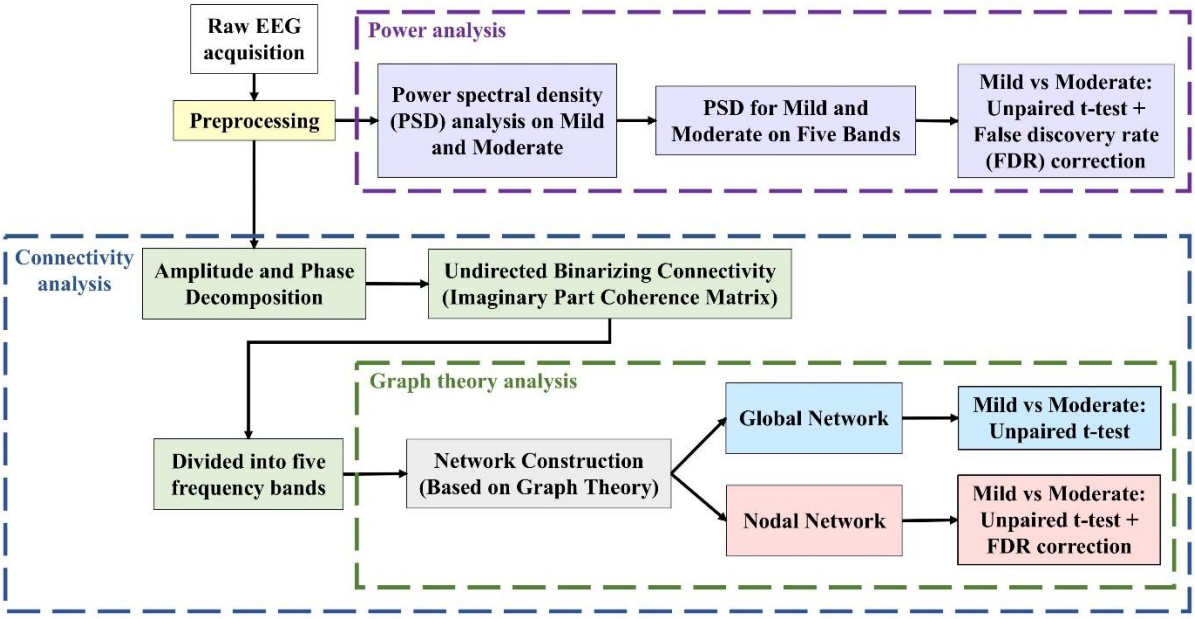


**Figure 3-2.** Flowchart of EEG data processing, including steps for: (1) Preprocessing (yellow box), (2) PSD-based analysis to get power topographies (purple boxes), (3) Construction of connectivity matrices (green boxes), (4) GTA-based global graphical brain connectivity (blue boxes), and (5) GTA-based nodal graphical brain connectivity (red boxes). The purple dashed box presents the steps for obtaining frequency-specific power topography. The blue dashed box indicates the analysis steps involved in connectivity analysis based on imaginary part of coherence analysis. The green dashed box signifies the process of analyzing the global and nodal brain network using graph theory.

### 3.2.4 Data preprocessing

To prepare the EEG data for electrophysiological network analysis, a series of preprocessing steps were needed to get the first 30 minutes of artifact-free EEG, as shown with the yellow box in Figure 3-2. All the EEG signal preprocessing steps were accomplished with MATLAB ® (MathWorks 2022a, MathWorks Inc., Natick, MA, USA). After EEG signals were band-pass

filtered to 0.5-100Hz, the 60 Hz line noise was eliminated with a notch filter. Then, EEG voltage signals were re-referenced based on the common mean of all eight channels, followed by removing artifacts spikes, short-time burst, flat line segments, and low-frequency drifts.

### 3.2.5 Channel-wise PSD-based analysis

After preprocessing, the 30 minutes clean data was divided into five different EEG frequency bands: delta (1-4Hz), theta (4-8Hz), alpha (8-12 Hz), beta (12-30 Hz), and gamma (30-55 Hz). Once the EEG signal has been decomposed into its frequency components, the power spectral density (PSD) can be calculated (Figure 3-2, purple boxes), which provides information about the distribution of power across different frequency bands in the signal. Since certain frequencies in the EEG signal are associated with different brain states, we can identify these frequency bands and use them to study changes in brain activity in response to different stimuli or conditions, by analyzing the PSD of the EEG signal.

To get PSD of preprocessed EEG data on five bands, "Pwelch" function was used with 4 seconds window length, 75% overlap, and four times the sampling frequency as the number of discrete Fourier transform points. For each frequency band, bandwidth-averaged PSD values are represented by $PSD_{band}$.

To illustrate the difference between Mild and Moderate HIE, ΔPower was calculated by subtracting the group mean power of Moderate HIE from respective group mean power of Mild HIE at each electrode for each of the five frequency bands:

$$\Delta Power = PSD_{band}^{Mild} - PSD_{band}^{Moderate} \quad \textbf{(1)}$$

### 3.2.6 Construction of connectivity matrices

By providing measures of network topology, graph theory helps to analyze the global brain network with measures such as degree, clustering coefficient, and path length. These measures can reveal important features of the network, including but not limited to the presence of highly connected hubs, the degree of local clustering, and the efficiency of information transfer between different brain regions.

Since correlations between the phases or amplitudes of EEG channels are interpreted as functional connectivity between all pairs of EEG electrodes, amplitude and phase decompositions were performed for all the 8 channels. Hence, the amplitude and phase of an EEG time-point could be represented as a complex number. Furthermore, Slepian sequences was utilized to taper the EEG signal in the time domain before performing the Fourier transform, using the 'ft_freqanalysis' function within FieldTrip toolbox [41, 42].

To measure connectivity, coherence is commonly utilized in frequency-domain, as an equivalent to the time-domain cross-correlation function. The coherence coefficient is computed for frequency of ω and yields a normalized coefficient between 0 and 1:

$$Coh_{xy}(\omega) = \frac{|S_{xy}(\omega)|}{\sqrt{S_{xx}(\omega)S_{yy}(\omega)}} \quad \textbf{(2)}$$

Sxx, Syy, and Sxy were calculated using complex values obtained with multitaper method, where Sxx and Syy respectively represent the power estimates of signals x and y, and Sxy denotes the averaged cross-spectral density term of these two signals.

However, volume conduction occurs when two or more EEG signals recorded from different scalp locations share a common source or generator, resulting in the appearance of spurious coherence. To minimize this issue, the imaginary part of coherence can be used by removing the magnitude of the operation from equation (2) and considering the imaginary part of Sxy, while

setting the cross-spectral density of the signals with 0 or 2π phase difference to zero. Hence, the 'ft_connectivityanalysis' function from FieldTrip toolbox was utilized for the computation of the imaginary part of coherence for all pairs of channels. For all pairs of electrodes in this study, the pairwise connectivity values were represented by 8 × 8 adjacency matrix.

For target temporal segments, the EEG data was divided into 10 sec epochs, and the adjacency matrices generated for all epochs on each frequency band were averaged. Then, these averaged matrices were binarized by varying the sparsity level and used for graph theory based global and nodal connectivity analyses. Afterward, the matrix was divided into five different EEG frequency bands, which were used for graph theory-based global and nodal connectivity analyses. The five frequency bands include delta (1-4 Hz), theta (4-8 Hz), alpha (8-12 Hz), beta (12-30 Hz), and gamma band (30-55 Hz).

### 3.2.7 GTA-based global graphical brain connectivity

As a user-friendly graph theory toolbox, GRETNA was used to quantify the global and nodal graphical metrics of brain network on five frequency bands [43]. This approach was repeated 19 times to assess the chosen metrics under a sparsity range of 5%–95%, with 5% as step length. For global network (Figure 3-2, blue boxes), five global graphical measures were included for analysis: Synchronization, Network Efficiency (Global efficiency), Small-World, Hierarchy, and Assortativity. The definitions of global graphical measures are listed in supplementary material A.

### 3.2.8 Comparison of GTA-based global brain networks between newborns with HIE and healthy newborns

To further investigate whether the GTA-based global brain networks of newborns with mild and moderate HIE are overall smaller than those of healthy newborns and adults, the global brain network of newborns with mild and moderate HIE was compared with resting-state GTA-based global brain networks of healthy newborns, young adults, and elderly adults.

The 60 healthy newborns (median age $\pm$ MAD: $12.5 \pm 6$ days; 35 males) included in the comparison were sourced from the study conducted by De Asis-Cruz et al [44]. In their research, the topological properties were assessed, including clustering coefficient, path length, small-world index, global efficiency, and local efficiency, based the Blood Oxygen Level-Dependent (BOLD) signals detected by Functional Magnetic Resonance Imaging (fMRI) using a band-pass filter of 0.01-0.1 Hz.

### 3.2.9 GTA-based nodal graphical brain connectivity

To analysis nodal connectivity (Figure 3-2, red boxes), the same approach was performed to get 8 × 8 imaginary part of coherence matrix as mentioned in 3.2.6. Then, six nodal graphical measures were obtained for comparison between Mild and Moderate HIE, using GRETNA toolbox: Nodal Clust Coeff (NCp), Nodal Shortest Path (NLp), Nodal Efficiency (Ne), Nodal Local Efficiency (NLe), Degree Centrality (Dc), Betweenness Centrality (Bc). The definitions of nodal graphical measures are listed in supplementary material B.

### 3.2.10 Statistical analysis

To statistically analysis the difference of PSD between Mild and Moderate HIE at each electrode for each of the five frequency bands, unpaired t-test followed by false discovery rate (FDR)

correction for multiple comparisons (eight channels) were performed between these two groups of HIE.

For GTA-based global graphical brain connectivity, to compare global network of Mild and Moderate HIE statistically, unpaired two-sample t-test was used for each global graphical measure at each sparsity level. For GTA-based nodal graphical brain connectivity, to quantify and compare nodal network of Mild and Moderate HIE statistically, unpaired t-test followed by FDR correction were used for each nodal graphical measure at each sparsity level.

## 3.3 Results

### 3.3.1 Channel-wise PSD-based analysis

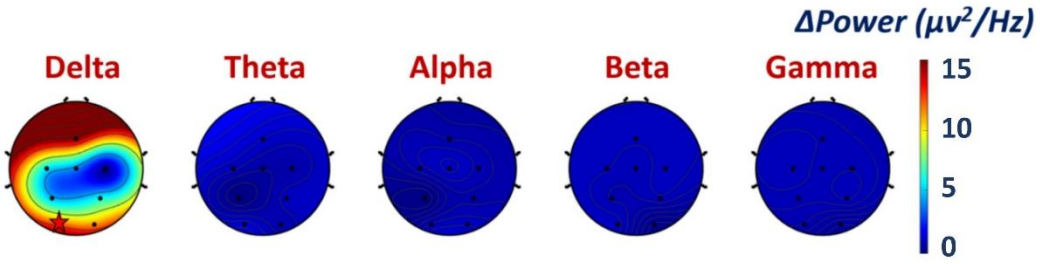


**Figure 3-3**. Comparison of Mild and Moderate HIE on ΔPower on five frequency bands. The channel showing significant difference between these two groups was marked with red asterisk.

In the channel-wise PSD comparison, newborns with Mild and Moderate HIE showed statistically significant differences at channels with FDR corrected $p < 0.05$, marked with red asterisk in Figure 3-3. Newborns with Mild HIE showed significantly higher PSD than those with Moderate HIE in the delta band at channel O1 (FDR corrected $p=0.0349$), with no significant differences observed in other frequency bands.

### 3.3.2 GTA-based global graphical brain connectivity

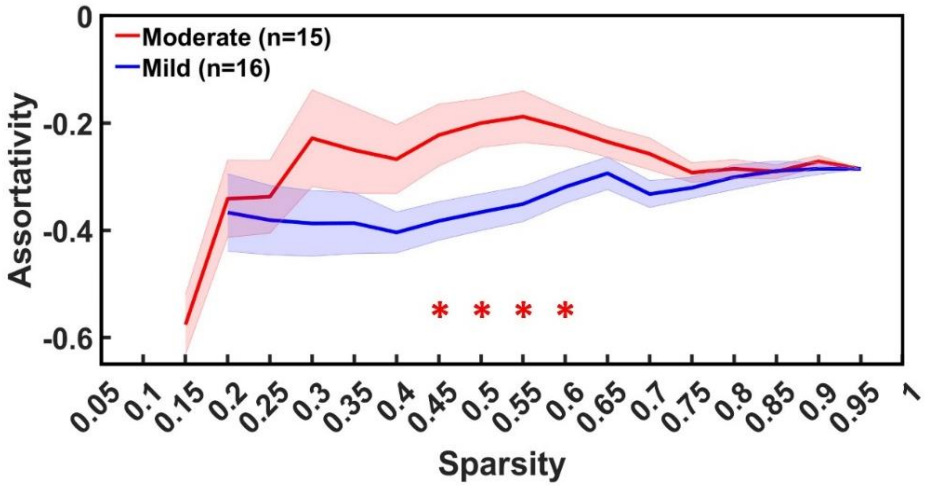


**Figure 3-4**. Comparison between Mild and Moderate HIE on assortativity of brain network was conducted across sparsity values ranging from 0.2 to 0.95. For Mild HIE group, the mean was plotted using a red solid line, while the standard error was represented by the red shadow. For Moderate HIE group, the mean values were depicted with a blue solid line, and the standard error was shown with blue shadow.

In the theta band, Moderate HIE had higher assortativity of brain network than Mild HIE within the sparsity range of 0.45 to 0.6, plotted with group mean and standard error in Figure 3-4. Assortativity measures the tendency of nodes in a network to be connected to nodes with similar degrees, such as those with similar connectivity patterns or functional properties [45]. Ranging from -1 to 1, negative values indicate that nodes with different properties are more likely to be connected to each other, while positive values indicate that nodes with similar properties are more likely to be connected. In other words, a higher assortativity in a brain network indicates that nodes or regions with similar properties or connectivity patterns are more strongly connected to each other within the network [46].

### 3.3.3 Comparison of GTA-based global brain networks of newborns with HIE and healthy newborns

Based on the absolute values of the quantified parameters in the delta band, the global network of newborns with HIE was quantified and compared to that of healthy newborns. Notable differences are reflected in three key parameters: Clustering coefficient (Cp), Global efficiency (Eg), and Local efficiency (Eloc), as shown in Figure 3-5. In Figure 3-5 (a), Cp of healthy newborns is shown to be consistently larger than Cp of newborns with HIE, within the threshold range from 0.025 to 0.45. As depicted in Figure 3-5 (b), within the sparsity range from 0.05 to 0.5, Eg of healthy newborns is consistently larger than Eg of newborns with HIE. The results in Figure 3-5 (c) demonstrate that Eloc of healthy newborns remains consistently larger than Eloc of newborns with HIE, within the sparsity range from 0.05 to 0.6.

Graph theory-based metrics provide insights into different aspects of brain network connectivity. Cp measures the tendency of neighboring nodes to cluster together, reflecting localized connectivity patterns [47, 48]. Eg evaluates the efficiency of information flow between all nodes, indicating the network's integration ability [49]. Eloc quantifies how effectively neighboring nodes communicate, revealing local information exchange efficiency within specific brain regions [50].

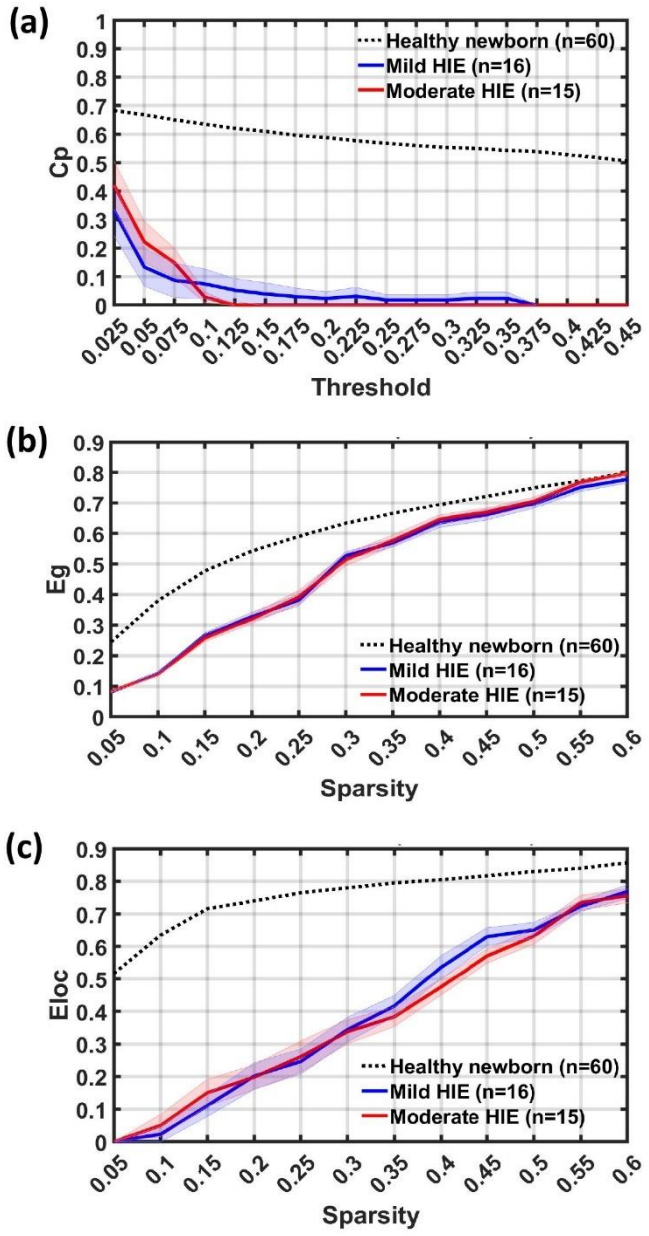


**Figure 3-5**. Characteristics of GTA-based global brain networks in newborns with HIE and healthy newborns. Newborns with mild and moderate HIE are represented in blue and red, respectively. The solid line and shaded area correspond to the mean values and standard error, respectively. The black dashed line represents the mean values of healthy full-term newborns. Quantification of key parameters in delta band were assessed, including (a) Clustering coefficient (Cp), (b) Global efficiency (Eg), and (c) Local efficiency (Eloc). For all figures except (a), network sparsity is plotted as the x-axis variable, as sparsity-based Cp is not available for healthy newborns.

### 3.3.4 GTA-based nodal graphical brain connectivity

As shown in Table 3-1, the mild HIE group showed significantly higher nodal cluster coefficient and nodal local efficiency than moderate HIE group, in delta band on channel P3 and in theta band on channel C3. Also, newborns with mild HIE had significantly lower betweenness centrality in theta band on channel C3 and degree centrality in alpha band on the same channel, than newborns with moderate HIE. Nodal cluster coefficient refers to the density of connections between a node and its neighbors, while nodal local efficiency refers to the efficiency of communication between a node and its neighbors [51, 52]. Betweenness centrality measures of the number of shortest paths that pass through a node or region of the brain [53-55].

| Features | δ Delta | θ Theta |
|---|---|---|
| Nodal Cluster Coefficient | Mild > Moderate on P3 | Mild > Moderate on C3 |
| Nodal Local Efficiency | Mild > Moderate on P3 | Mild > Moderate on C3 |
| Betweenness Centrality | | Mild < Moderate on C3 |

**Table 3-1.** Comparison of Mild and Moderate on GTA-based nodal graphical brain connectivity. All five bands were investigated, and this table only lists the bands and parameters that showed significance between the two groups. Statistical analysis was performed using unpaired t-tests followed by FDR correction for each nodal graphical measure at each sparsity level.

## 3.4 Discussion

The current analysis of HIE infant brain networks mainly involves fMRI [56, 57], diffusion magnetic resonance imaging (dMRI) [58], and F-deoxyglucose brain positron emission tomography scanning (FDG-PET) [59]. However, to date, there have been no studies reporting the use of EEG recordings and graph theory analysis to study the brain networks of HIE infants. The novelty of this research lies in investigating the electrophysiological brain networks of newborns

with mild and moderate HIE using EEG recordings. This approach may potentially serve as bedside monitoring of changes in infant brain functional networks caused by HIE. EEG recordings provide high temporal resolution of brain electrical activity, allowing us to capture the rapid dynamic changes in brain networks, which is crucial for understanding the impact of HIE on infant brain development.

Utilizing graph theory offers a framework to study the brain as a complex network of interconnected nodes. This approach enables the assessment of brain connectivity by analyzing the organization of different components and the strength of their connections. Based on graph theory, we can quantify the topological properties of the brain networks, such as clustering coefficient and shortest path length, to reveal the overall structure and functional characteristics of the brain networks in infants affected by HIE. Furthermore, contrasting brain networks in HIE infants with those of healthy peers enables a precise differentiation between HIE-induced and typical neonatal brain networks. This investigation deepens our comprehension of HIE's impact on brain function, yielding insights for early diagnosis and intervention. We anticipate this research will propel the integration of EEG technology into HIE studies and contribute to further exploration in related domains.

### 3.4.1 Channel-wise PSD-based analysis

Delta waves are slow brain waves that are typically seen in deep sleep or in states of decreased consciousness [60, 61]. In infants with HIE, an increase in delta power may indicate that the brain is struggling to maintain normal activity levels and is entering a state of reduced alertness or awareness [35-37]. During the 30 minutes period, we observed Mild HIE had significantly higher PSD than Moderate HIE on delta band, at marked channel O1.

An insightful interpretation for the observed phenomenon could be rooted in the brain's adaptive responses to the varying severities of Mild and Moderate HIE in infants. It is plausible that in the presence of Mild HIE, the infant brain endeavors to mitigate the impact of the condition by downregulating its energy demands and overall neural activity. This strategic reduction in brain activity might be aimed at prioritizing essential functions, such as respiration and circulation [62]. However, in cases of more severe HIE, such as Moderate HIE, the capacity of the infant brain to effectively employ the compensatory mechanism of energy reduction could be even more compromised, owing to the heightened severity of the condition. Consequently, the impairment in compensatory capabilities could culminate in a reduction in delta power, thereby reflecting the brain's diminished ability to support fundamental bodily functions.

### 3.4.2 GTA-based global graphical brain connectivity

Usually, assortativity is thought to contribute to the efficient processing of information in the brain, which allows specialized regions to work together in a coordinated manner. However, studies had shown that patients may have a higher assortativity of brain network than healthy individuals. This is thought to be due to the fact that certain diseases or conditions can affect specific brain regions or networks, leading to a disruption of the normal connectivity patterns within the brain. As a result, nodes that share similar connectivity patterns may become more strongly connected to each other, leading to a higher assortativity of the network. In recent studies for patients with Alzheimer's disease, increased assortativity within the brain's default mode network was reported, which was involved in self-referential thinking and mind-wandering [46, 63]. This increased assortativity may reflected a breakdown in the normal segregation and integration of brain regions, which was thought to underlie cognitive impairments in Alzheimer's disease. Several other studies

reported similar findings with different experimental protocols when assessing the impacts of Alzheimer's disease on communication between brain regions [64, 65]. These studies suggested that individuals with Alzheimer's disease may exhibit increased assortativity within the default mode network, which is a set of brain regions that are most active when the mind is at rest and not engaged in specific cognitive tasks. This increased assortativity may reflect a more selective and segregated pattern of connectivity within the network, potentially indicating disrupted communication between brain regions due to severity of encephalopathy.

For infants with Moderate HIE, their brain regions affected by HIE may have similar patterns of damage or altered connectivity, leading to increased segregation and reduced integration. In contrast, infants with Mild HIE may have more diverse patterns of brain connectivity, leading to lower assortativity in their brain networks. This discovery aligns with the outcomes derived from a systematic review of brain network organization in focal epilepsy [47]. For neonatal HIE, the incidence of epilepsy is influenced by the severity of HIE condition. Infants with more severe cases of HIE are more likely to develop epilepsy compared to those with milder forms of HIE. Therefore, it is imperative to undertake subsequent investigations to ascertain the extent of the correlation between this network pattern and epilepsy.

However, there was no significant difference between newborns with mild HIE and moderate HIE in other key parameters of global connectivity. The results may suggest that newborns with mild HIE can develop similar impaired brain functional network patterns as newborns with moderate HIE. In previous research, investigators focused more on the impact of moderate and severe HIE on infant brain development. By comparing the effects of mild and moderate HIE on brain functional network, we found that even in cases of mild HIE, there may still be a comparable degree of adverse impact on infant brain function, emphasizing the

importance of early detection and intervention to minimize the detrimental effects of HIE on infant brain development.

### 3.4.3 Comparison of GTA-based global brain networks of newborns with HIE and healthy newborns

Accessing several key GTA-based parameters, a further comparison of Cp, Eg, and Eloc was conducted among three groups, including newborns with mild and moderate HIE and healthy newborns. Cp measures the tendency of neighbors of a node to cluster together, indicating how closely interconnected brain regions are in a network. A higher clustering coefficient indicates that nodes in the network tend to form tightly-knit clusters or communities, suggesting a higher level of local connectivity and organization. Therefore, the larger Cp values in healthy newborns compared to newborns with HIE indicate that the brain networks of newborns with HIE have a less organized and less efficient local communication pattern in the delta band. This difference reflects significantly worse developmental or neurological conditions in newborns with HIE.

Eg measures how well information is transferred in a network. Thus, larger Eg indicates that the brain network has better overall information transmission capacity. The finding of Eg suggests that in the delta band, the brain networks of healthy newborns exhibit a higher level of global integration and information transfer efficiency compared to newborns with HIE. In other words, newborns with HIE exhibit lower efficiency and impaired communication pattern among distant brain regions in the delta band.

Quantifying how well neighbors of a node communicate with each other after the node is removed, Eloc reflects the information transmission efficiency of each node among its neighboring nodes. Higher Eloc typically implies that nodes have more efficient information transmission

among their neighbors. The result of Eloc implies that the healthy newborns show more efficient information transmission among their neighboring brain regions compared to newborns with HIE. This difference in local efficiency could potentially indicate that the brain networks of newborns with HIE may have much less effective communication and coordination among nearby brain regions, which could be related to the impairment caused by HIE on brain development and function.

### 3.4.4 GTA-based nodal graphical brain connectivity

Nodal clustering coefficient measures the extent to which the immediate neighbors of a specific node (brain region) in a brain network are also interconnected. Nodal local efficiency measures the efficiency of communication and information exchange between a specific brain region (node) and its neighboring nodes within a brain network. The significantly higher nodal cluster coefficient and nodal local efficiency in the delta band on the P3 channel and in the theta band on the C3 channel may indicate that newborns with mild HIE had more effective neural processing than those with moderate HIE.

Specifically, a low nodal clustering coefficient indicates that the neighbors of the node are less likely connected to each other, suggesting that the moderate HIE group has a lower degree of local information processing and functional specialization than the mild HIE group in the specific brain region covered by channels C3 and P3. A high nodal local efficiency indicates that a node is effectively connected to its neighbors, promoting efficient local information processing and functional integration. In comparison to the Moderate HIE group, the Mild HIE group can maintain more efficient information processing and integration within the local network neighborhood detected by channels C3 and P3.

Meanwhile, nodal betweenness centrality quantifies the number of shortest paths that pass through the specific node. A higher nodal betweenness centrality suggests that the region covered by channel C3 plays a crucial role in facilitating communication and information flow between different parts of the network in cases of moderate HIE.

From an anatomical perspective, channels C3 and P3 are positioned precisely within watershed regions, which are areas sensitive to the impact of HIE. Therefore, the differences in nodal connectivity observed in this study between the mild and moderate groups may suggest that the impairment of watershed regions worsens with a higher severity of encephalopathy.

### 3.4.5 Limitation of the study and future work

This study exhibits certain limitations primarily attributed to the utilization of distinct modalities when comparing newborns with HIE and healthy newborns. Specifically, these two experimental groups were based on different modalities, namely EEG and fMRI. These diverse experimental techniques offer unique advantages and constraints in the recording and assessment of brain function. EEG provides high temporal resolution but limited spatial resolution; fMRI, on the other hand, excels in spatial resolution but offers relatively lower temporal resolution.

Consequently, while these experimental modalities furnish valuable information concerning the neurophysiological mechanisms in HIE research, it is imperative to take into account the differences among them during data interpretation and result comparison. In future investigations, further exploration with the same experimental modalities and strategies to synergize their strengths will be instrumental in comprehensively understanding the neural network disparities among newborns with HIE and healthy newborns.

In our future in-depth research, the neurophysiological brain networks of newborns with HIE and healthy newborns will be compared based on EEG recording, to avoid confounding effects from different modalities. Then, the comparison will be conducted within the same frequency range, ensuring comparability when analyzing the brain networks of newborns with HIE and healthy neonates. Through this research design, we aim to accurately assess the differences in brain function between newborns with HIE and healthy newborns, gaining a deeper understanding of the progression of encephalopathy severity on infant brain development. We anticipate that these research findings may contribute to the development of more effective early diagnostic and intervention measures, ultimately improving the prognosis of infants with HIE and providing substantial support for the development of treatment strategies. With a more comprehensive understanding of the characteristics of brain networks in newborns with HIE, we may offer more precise information for clinical applications, defining potential biomarkers for real-time monitoring of brain function, promoting early intervention and treatment to improve long-term neurodevelopmental outcome.

## 3.5 Conclusion

In this prospective study, newborns with HIE underwent eight-channel EEG measurements to assess brain networks, with key parameters quantified through graph theory. Newborns with moderate HIE showed more selective global connectivity compared to those with mild HIE, possibly indicating disrupted inter-brain communication due to encephalopathy severity. Comparing HIE infants to healthy newborns revealed less organized and efficient brain networks, especially in delta band. Furthermore, the moderate HIE group exhibited weaker neural processing power than the mild group on channel C3 and P3, covering watershed zones. Notably, key

parameters of global connectivity showed no significant difference between mild and moderate HIE groups, implying similar brain functional impairments and the need for prompt intervention.

# Chapter 4

# Prefrontal Transcranial Photobiomodulation with 800-nm Laser Modulates Human Neurophysiological Networks

## 4.1. Introduction

Transcranial photobiomodulation (tPBM), also known as transcranial infrared laser stimulation (TILS), has shown potential in improving cognitive function, particularly in the areas of attention, memory, and executive function, as a non-invasive and safe intervention using near-infrared or infrared light. Recent studies have demonstrated that tPBM facilitates memory enhancement in both healthy humans and patients with certain neurological diseases [66-70]. To date, studies have proved that tPBM can increase cerebral blood flow and oxygenation in targeted brain regions, which enhance neuronal activity and improve cognitive performance [71-74]. However, the underlying electrophysiological mechanism of tPBM is still unclear and further research is needed to determine optimal parameters for tPBM applications, such as wavelength and treatment location. Previous studies investigating the effects of tPBM on brain activity have predominantly focused on hemodynamic and metabolic, or electrophysiological viewpoints. To date, few research has assessed the systematic modulation of the brain in response to left and right prefrontal tPBM using 800-nm laser.

Therefore, this research aims to investigate and quantify the modulation effects of left and right prefrontal 800-nm tPBM on neurophysiological networks using 19-channel wireless dry EEG. A more comprehensive understanding of the mechanisms underlying tPBM can be achieved by examining the topological networks and their modulation in response to tPBM. Specifically, employing Graph theory analysis (GTA), we evaluated the alterations in brain network and information flow induced by 800-nm prefrontal tPBM. Representing the brain as a network of

interconnected nodes (which refer to brain regions) and edges (which indicate the connections between regions), GTA-based brain network analysis enables the intricacies of connections and communication patterns within the brain [75].

## 4.2. Method

### 4.2.1 Study participants

Subjects were considered eligible if they met the inclusion criteria, which included being over 18 years of age, being healthy and pain-free individuals, irrespective of gender or ethnic background, and having the ability to provide informed consent. Exclusion criteria were as follows: (1) individuals with serious medical conditions, including neurological or psychiatric diseases; (2) those with a history of brain injuries or violent behavior; (3) individuals who had been institutionalized or imprisoned; (4) those taking long-term or short-term medication; (5) pregnant individuals; (6) smokers or those with diabetes; and (7) those unable to provide informed consent.

In total, thirty-one healthy subjects were recruited from the University of Texas at Arlington (UTA), who were the same as those in our recently reported studies on cerebral hemodynamic and metabolic activities [76, 77]. Each participant underwent five visits with a minimum interval of seven days between them. Due to the high sensitivity of wireless dry EEG to motion artifacts, five participants with excessive motion during one or more of the experiments were excluded from the analysis. Ultimately, 26 healthy young adults (14 males and 12 females) with $22.4 \pm 2.3$ years of age (i.e., average $\pm$ standard deviation) completed the two-visit experiments. All subjects were instructed to abstain from ingesting any beverages containing caffeine for a minimum of three hours preceding each visit. This study was conducted in

accordance with relevant federal guidelines and was approved by the Institutional Review Board (IRB) of UTA. All participants provided informed consent prior to participation.

### 4.2.2 EEG data acquisition

In this study, tPBM/sham was delivered on the left/right prefrontal location with a 4.16 cm diameter circular 800-nm laser beam, using a continuous-wave laser (Model CG-5000 Laser, Cell Gen. Therapeutics LLC, Dallas, TX, USA), which was cleared by the Food and Drug Administration (FDA). The setup for broadband near-infrared spectroscopy (bbNIRS) was positioned on the subjects' forehead for measurement during the pre-stimulation phase. It was temporarily removed during the stimulation to create space for the tPBM/sham procedure on the left/right frontal region. The setup was then placed back in the same location for post-stimulation measurement.

The data analyzed in this study were obtained from resting-state, bilateral measurements with 19-channel wireless dry EEG (CGX Quick-20 10–20 EEG system), which is one of the dual-mode (i.e., EEG and bbNIRS) modalities shown in Figure 1 (a) and (b). This section focuses on EEG signal for investigating the modulation effects of left/right prefrontal tPBM on neurophysiological networks with non-invasive 800-nm laser.

For each visit, the entire experiment was 22 minutes, including a 7 min pre (resting state), an 8 min tPBM/sham, and a 7 min post tPBM/sham period (resting state). Upon completion of the informed consent process, each participant was directed to assume a seated position comfortably on a chair, followed by a dual-mode probe placement on the participant’s head firmly. Subsequently, as shown in Figure 1 (c), the 19-channel EEG and bbNIRS apparatus started to record data at a sampling frequency of 500 Hz. This occurred during a 7 min period of resting state

both before and after tPBM/sham stimulation, while the participant maintained a state of eyes-closed wakefulness. The genuine stimulation intervention was delivered via 800-nm laser illumination targeted at the left/right frontal region with total power set to be 3.5 W, whereas the sham was performed with the laser power set to be 0.1 W and the laser aperture covered with a black cap. During tPBM/sham stimulation, participants were asked to wear protective goggles. The research was conducted in a single-blind crossover design, wherein every participant underwent sham tPBM and sham experiments in a random sequence (Figure 4-1).

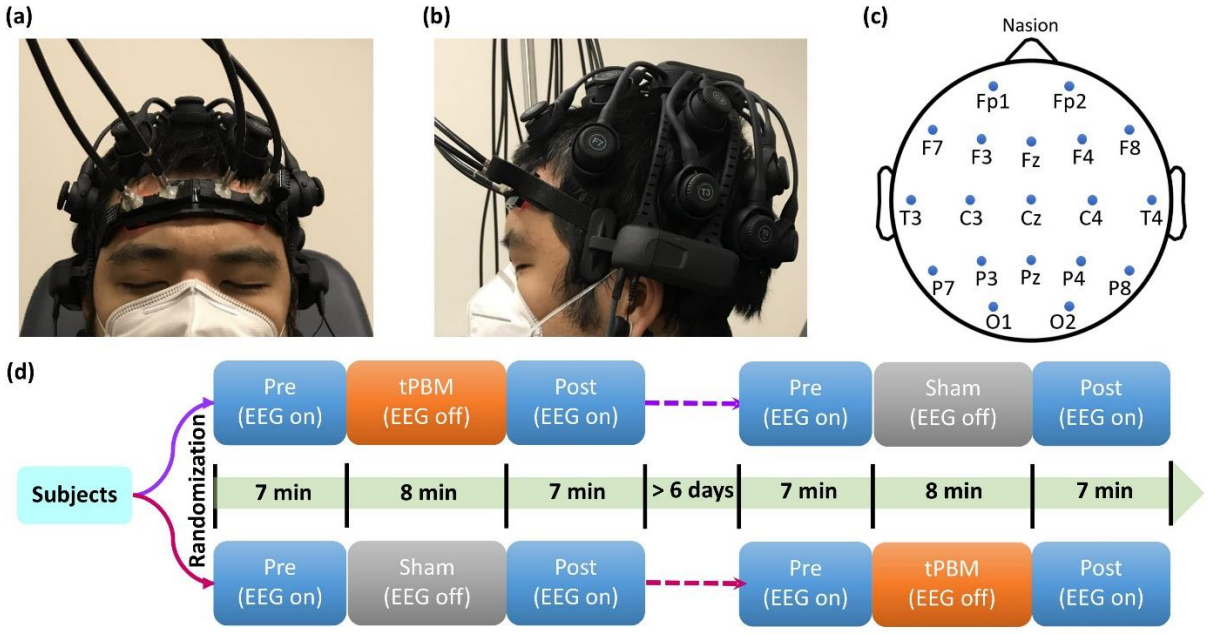


**Figure 4-1**. Experiment setup and protocol. (a) Front view of the dual-mode (EEG and bbNIRS) head probe setup (b) The side view of the dual-mode. While the 2-channel bbNIRS on the forehead is observable, the bbNIRS data are not the topic/subject of this section. The EEG datasets used for this study were taken during 7 min eyes-closed conditions with the setup shown. (c) The distribution of 19-channel wireless EEG (d) Experiment protocol for tPBM/sham

### 4.2.3 Overview of data processing pipeline

Each raw EEG dataset represents a 7-minute time series of 19 channels collected during active/sham tPBM experiments from 26 subjects. As shown in Figure 4-2, the data processing pipeline consists of four sections: (1) Preprocessing; (2) Construction of connectivity matrices based on imaginary part of coherence analysis; (3) GTA-based global graphical brain connectivity analysis; (4) Region-wise network analysis based on coherence strength of connectivity matrix.

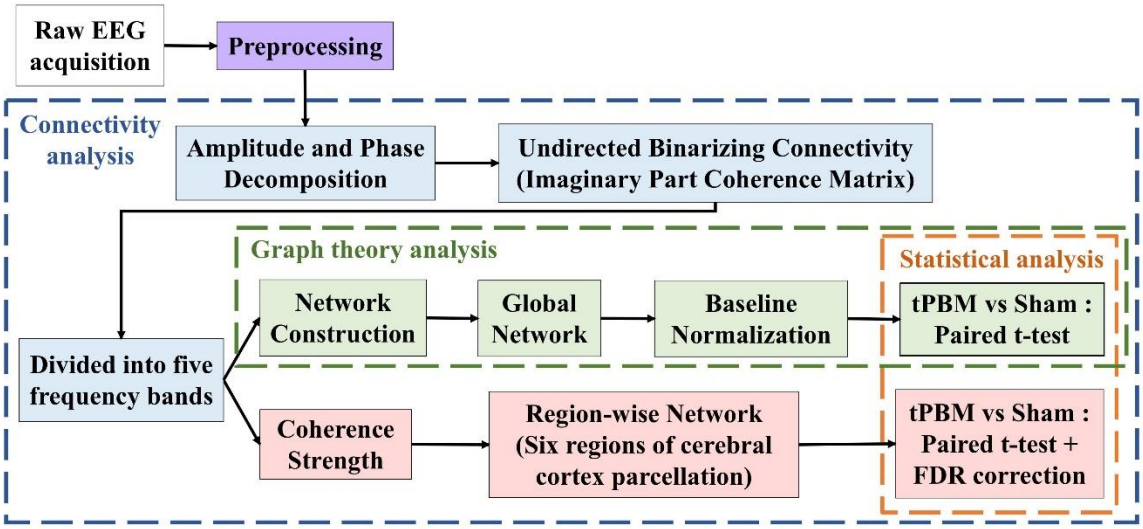


**Figure 4-2**. Flowchart of EEG data processing, including steps for (1) Preprocessing (purple box). (2) Construction of connectivity matrices (blue boxes). (3) GTA-based global graphical brain connectivity (green boxes). (4) Region-wise network analysis, based on coherence strength (red boxes). The purple dashed box indicates the analysis steps involved in connectivity analysis based on the imaginary part of coherence analysis. The green dashed box signifies the process of analyzing the global brain network using graph theory.

### 4.2.4 Data preprocessing

As depicted by the purple box in Figure 4-2, all EEG signal preprocessing steps were executed using MATLAB® (MathWorks 2022a, MathWorks Inc., Natick, MA, USA). The raw EEG data sampled at 500 Hz underwent bandpass filtering within the range of 1-55 Hz using a Butterworth

filter. Additionally, artificial spikes and flat segments were replaced with combined (50%-50%) signals from preceding and subsequent recordings. Subsequently, bad channels were interpolated using EEGLAB, an open-source MATLAB toolbox. For each EEG series, re-referencing was conducted by averaging the voltage across all 19 channels. Following this, independent component analysis (ICA) was applied to decompose the 19-channel EEG signals into underlying independent neural sources, aiming to eliminate motion artifacts such as eye movements and muscle activity.

### 4.2.5 Construction of connectivity matrices

By providing measures of network topology, graph theory helps to analyze the global brain network with measures such as degree, clustering coefficient, and path length. These measures can reveal important features of the network, including but not limited to the presence of highly connected hubs, the degree of local clustering, and the efficiency of information transfer between different brain regions.

Since correlations between the phases or amplitudes of EEG channels are interpreted as functional connectivity between all pairs of EEG electrodes, amplitude and phase decompositions were performed for all eight channels. Consequently, the amplitude and phase of an EEG time-point could be represented as a complex number. Furthermore, Slepian sequences were utilized to taper the EEG signal in the time domain before performing the Fourier transform, using the 'ft_freqanalysis' function within the FieldTrip toolbox [41, 42].

To measure connectivity, coherence is commonly utilized in the frequency domain as an equivalent to the time-domain cross-correlation function. The coherence coefficient is computed for a frequency of $\omega$ and yields a normalized coefficient between 0 and 1:

$$Coh_{xy}(\omega) = \frac{|S_{xy}(\omega)|}{\sqrt{S_{xx}(\omega)S_{yy}(\omega)}} \quad \textbf{(2)}$$

Sxx, Syy, and Sxy were calculated using complex values obtained with the multitaper method, where Sxx and Syy respectively represent the power estimates of signals x and y, and Sxy denotes the averaged cross-spectral density term of these two signals.

However, volume conduction occurs when two or more EEG signals recorded from different scalp locations share a common source or generator, resulting in the appearance of spurious coherence. To minimize this issue, the imaginary part of coherence can be used by removing the magnitude operation from equation (2) and considering the imaginary part of Sxy, while setting the cross-spectral density of the signals with 0 or 2π phase difference to zero. Hence, the 'ft_connectivityanalysis' function from the FieldTrip toolbox was utilized for computing the imaginary part of coherence for all pairs of channels. In this study, the pairwise connectivity values for all pairs of electrodes were represented by a 19 × 19 adjacency matrix.

For the target temporal segments, the EEG data was divided into 10-second epochs, and the generated adjacency matrices for all epochs in each frequency band were averaged. These averaged matrices were then binarized by varying the sparsity level. Afterward, the matrix was divided into five different EEG frequency bands, which were used for graph theory-based global and region-wise connectivity analyses. The five frequency bands include delta (1-4 Hz), theta (4-8 Hz), alpha (8-12 Hz), beta (12-30 Hz), and gamma band (30-55 Hz).

### 4.2.6 GTA-based global brain network

The user-friendly graph theory toolbox, GRETNA, was utilized to quantify the global and nodal graphical metrics of brain networks across five frequency bands [43]. This procedure was repeated

19 times to assess the selected metrics within a sparsity range of 5%–95%, with a step length of 5%.

Regarding the global network, five graphical measures were included for analysis: Synchronization (S), Network Efficiency (Global efficiency, N), Small-Worldness (Sw), Hierarchy (H), and Assortativity (A). The definitions of these global graphical measures are provided in supplementary material A.

To compare relative tPBM and relative sham for the same subject, key parameters of global connectivity were normalized for tPBM and sham group with the following equations: (1) $tPBM_{Relative} = (tPBM_{Post} - tPBM_{Pre}) / tPBM_{Pre}$). (2) $sham_{Relative} = (sham_{Post} - sham_{Pre}) / sham_{Pre}$. Then, the statistical comparison of global networks between tPBM and sham was realized using paired two-sample t-test for each global graphical measure at every sparsity level.

### 4.2.7 Adjacency-matrix-based region-wise network analysis

After performing graph theory on 19-channel EEG, we were interested in classifying these channels into six identified cortical regions on the human scalp, i.e., prefrontal, centraltemporal, parietal-occipital regions in left and right cerebral hemisphere. Consequently, the 19 nodes were grouped into six clusters, each comprising 2–3 electrodes (as depicted in Figure 4-4). After obtaining the 19 × 19 imaginary part of coherence matrix with FieldTrip, paired two-sample t-test followed by FDR correction were performed to compare ΔtPBM ($\Delta tPBM = tPBM_{Post} - tPBM_{Pre}$) and Δsham ($\Delta sham = sham_{Post} - sham_{Pre}$) on group-level.

## 4.3 Results

### 4.3.1 Modulation effects of 800-nm left prefrontal tPBM

**GTA-based global connection in the human cortex modulated by left prefrontal tPBM**

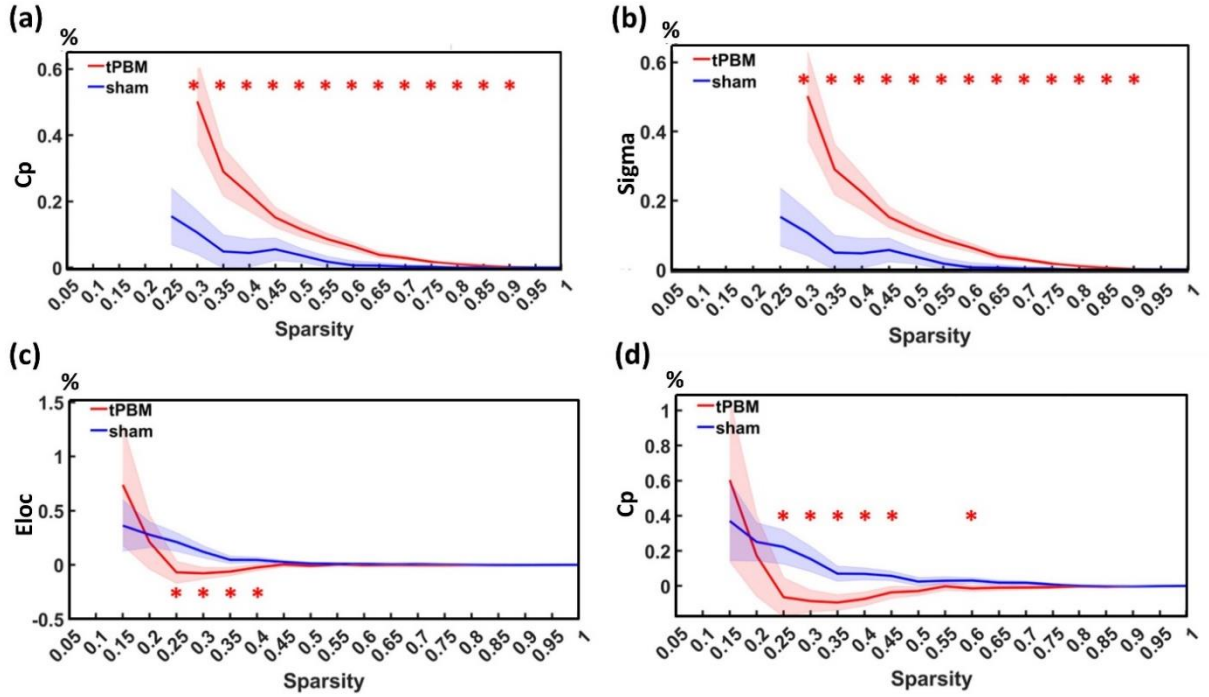


**Figure 4-3**. Comparison of 800-nm left prefrontal tPBM and sham on connectivity parameters. The significant differences ($p < 0.05$) between tPBM and sham are marked with red stars after two-sample paired t-test. (a) Clustering coefficient (Cp) on alpha band. (b) Sigma of Small-World on alpha band. (c) Local efficiency (Eloc) on delta band (d) Cp on delta band.

As the result of the comparison between relative tPBM and relative sham (Figure 4-3), tPBM created significantly higher metrics than sham in alpha band on Clustering Coefficient (Cp) and Sigma of Small-Word, both from sparsity 0.3 to 0.9 (Figure 4-3 ab). In delta band, tPBM generated significantly lower metrics than sham regarding effective Local Efficiency (Eloc) of Network Efficiency (from sparsity 0.25 to 0.4, Figure 4-3 c) and Cp of Small-Word (from sparsity 0.25 to 0.45, Figure 4-3 d). Cp measures the tendency of neighbors of a node to cluster together. Sigma

quantifies specialized/modularized and integrated/distributed information processing. Eloc evaluates how well neighbors of a node communicate with each other after the node is removed.

**Adjacency-matrix-based region-wise network analysis**

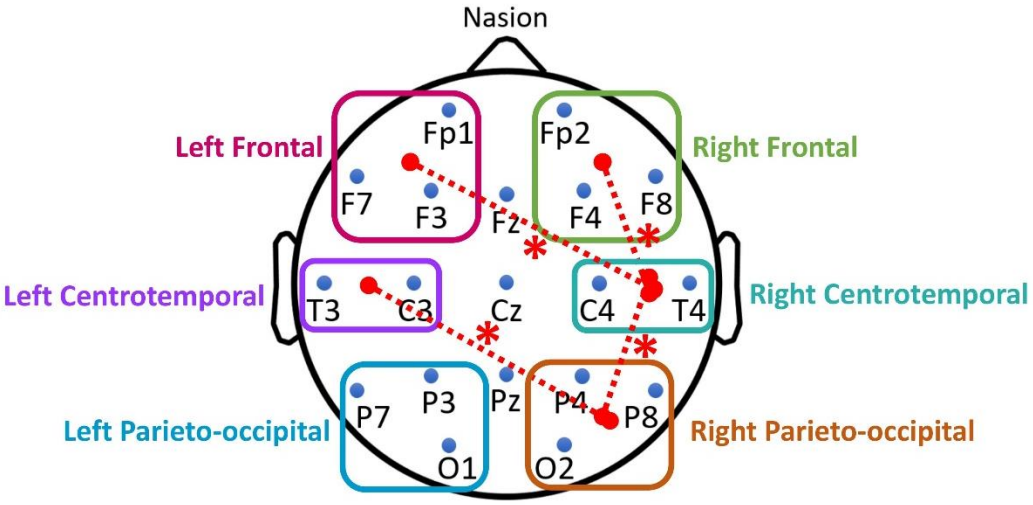


**Figure 4-4**. Comparison of the region-wise network between 800-nm left prefrontal tPBM and sham on alpha band. After paired t-test and FDR correction, the significantly increased ($p < 0.05$) connections modulated by tPBM are marked by the red stars.

After applying paired t-test and FDR correction, the coherence between the following regions demonstrated a statistically significant increase after tPBM treatment compared to sham within the alpha band: left frontal and right centrotemporal (p=0.0177), left centrotemporal and right parieto-occipital (p=0.0397), right frontal and right centrotemporal (p=0.0062), and right centrotemporal and right parieto-occipital (p=0.0062). In the beta band, the coherence between the left frontal and right centrotemporal regions exhibited a statistically significant increase (p=0.0111) after tPBM treatment compared to sham, using paired t-test followed by FDR correction (Figure 4-4).

### 4.3.2 Modulation effects of 800-nm right prefrontal tPBM

**GTA-based global connection in the human cortex modulated by right prefrontal tPBM**

Comparing relative tPBM and relative sham, as shown in Figure 4-5, tPBM resulted in significantly higher values than sham in the beta band for Normalized Clustering Coefficient (Gamma) and Sigma of Small-Word, both within the sparsity range of 0.35 to 0.45 (Figure 4-5 a and b). In the gamma band, tPBM gave rise to significantly lower values than sham regarding Global Efficiency (Eg) of Network Efficiency (within the sparsity range of 0.3 to 0.4, Figure 4-5 c), and significantly higher values than sham in terms of Shortest Path Length (Lp) of Small-Word (within the sparsity range of 0.2 to 0.4, Figure 4-5 d). Gamma measures the tendency of neighbors of a node to cluster together. Eg assess How well information is transferred in a network. Lp evaluates the average shortest distance between any two nodes.

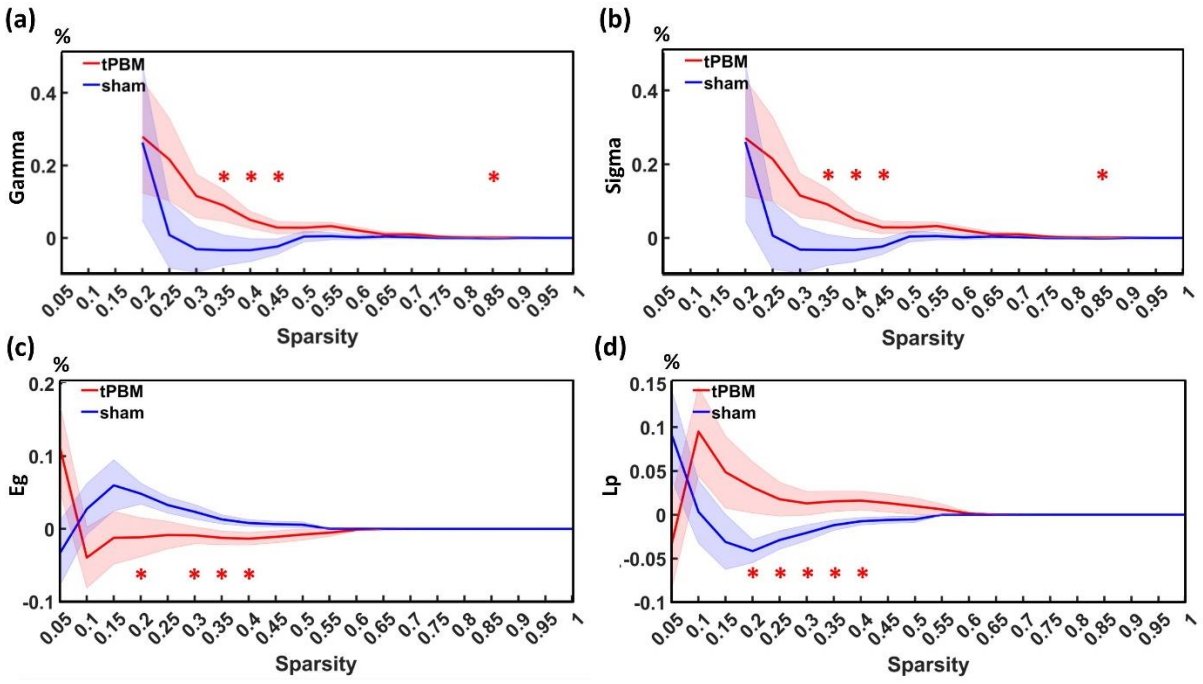

**Figure 4-5**. Comparison of 800-nm right prefrontal tPBM and sham on connectivity parameters. The significant differences ($p < 0.05$) between tPBM and sham are marked with red stars after Two-sample t-test. (a) Gamma (Normalized clustering coefficient) on beta band. (b) Sigma of Small-World on beta band. (c) Eg (Global efficiency) on gamma band (d) Lp (Shortest path length) on gamma band.

## 4.4. Discussion

There is an incomplete understanding of the topological mapping of the brain's electrophysiological network modulation in response to tPBM. Previous research by Wang et al. has shown that tPBM using 1064-nm laser can increase alpha and beta rhythms in frontal and parietal regions during eyes-open resting state as measured in healthy human using 64-channel EEG [67, 78]. However, the tPBM-induced functional network modulation has not been sufficiently studied and understood to identify changes in the interaction among different regions of the brain. Furthermore, the impact of left and right prefrontal tPBM on brain electrophysiology with 800-nm laser has not been investigated thus far.

### 4.4.1 Modulation effects of 800-nm left prefrontal tPBM

**GTA-based global connection in the human cortex modulated by left prefrontal tPBM**

Small-World refers to the network in which most nodes are not directly connected to one another but can be reached through a relatively small number of intermediate connections. Cp measures the average distance between any two nodes in the network and high Cp indicates that the network has a short path length, because the intermediate nodes in a Small-World network act as shortcuts which allow information to travel quickly and efficiently between nodes. On the other hand, the clustering coefficient measures how likely two nodes that are connected to a common neighbor

are to be connected to each other, which indicates if nodes in a Small-World network tend to form clusters or groups [79]. A high sigma value indicates that the network has a small-world structure with high clustering and short path lengths, while a low sigma value indicates that the network is more random in structure.

Eloc measures network efficiency that quantifies the ability of a network to transfer information efficiently between the immediate neighbors of a node, taking into account the network's overall topology [80]. The low Eloc value indicates that the network is less efficient in transmitting information between immediate neighbors of nodes. This could mean that there are certain regions or nodes in the network that are less well-connected than others, leading to reduced efficiency in local communication. A network with low Eloc may also have a higher number of long-range connections, which can reduce the efficiency of local information transfer [81]. This can occur if the long-range connections are less efficient than the shorter-range connections. Low Eloc values can also be observed in networks with high clustering coefficients, as the presence of highly connected clusters can reduce the efficiency of communication between immediate neighbors.

Studies have shown that the alpha band (8-12 Hz) is associated with relaxed wakefulness, attentional processes, and cognitive control, while the delta band (0.5-4 Hz) is associated with deep sleep, restorative processes, and emotional regulation [82, 83]. The results of this study indicated left prefrontal tPBM with 800-nm laser could enhance functional connectivity within the entire cortex in alpha band, which could lead to a more efficient and highly clustered network that may have positive effect on cognitive function. tPBM could also induce different effects on Small-World network measures depending on the frequency band of the brain waves being targeted. For example, a decrease in Cp of Small-World networks in the delta band indicates more dispersed

network with longer path lengths. This could potentially facilitate collaboration between regions with greater spatial separation.

**Region-wise network strength on five bands, with coherence matrix**

The observed changes in coherence within distinct frequency bands following tPBM treatment provide insights into the modulatory effects of this intervention on brain functional connectivity. In the alpha and beta band, the statistically significant increase in coherence between specific brain regions underscores the potential role of tPBM in promoting synchronized neural activity within these regions.

Current research widely posits that distinct anatomical structures of the brain play divergent roles when executing various functions and tasks [84-87]. Specifically, the left frontal region handles cognitive functions like decision-making, planning, and problem-solving. The right centrotemporal area processes auditory information and language comprehension. The left centrotemporal area is also linked to language processing and auditory perception. The right parieto-occipital region manages visual processing, spatial perception, and visual attention. The right frontal region regulates emotions, social interactions, and decision-making.

The observed significant increase in coherence between specific brain regions after tPBM treatment within the alpha band suggests that tPBM has the potential to enhance coordination and communication among these regions, thereby fostering collaboration in cognitive, sensory, and perceptual processes. Since left frontal region is associated with cognitive and right centrotemporal region is associated with the processing of visual and auditory stimuli, the increased coherence between these two regions in beta band may suggest the brain shows enhanced capability for integrating sensory information that related to cognitive processes. Furthermore, within the beta

band, the increase in coherence between the left frontal and right centrotemporal regions after tPBM treatment compared to the sham condition indicates that tPBM enhances information exchange and potentially promotes improved integration of cognitive and auditory processing pathways.

### 4.4.2 Modulation effects of 800-nm right prefrontal tPBM

**GTA-based global connection in the human cortex modulated by right prefrontal tPBM**

Metric Gamma derived from graph theory quantifies the level of local clustering or connectivity between neighboring nodes in the network, which can assess the efficiency of information processing within a brain network [35]. A high clustering coefficient indicates that the neighboring nodes of a given node are well interconnected, forming a tightly knit local neighborhood. On the other hand, a low clustering coefficient suggests that the neighboring nodes are less interconnected, forming a more sparsely connected neighborhood [88]. Providing insights into the local communication efficiency and the formation of functional modules or clusters within the brain, Gamma shows how information is processed and integrated within localized brain regions.

Eg can quantify the efficiency of information transfer and integration across the entire network, to assess how efficiently information can be transmitted between any two nodes in the brain network [81, 89]. A higher global efficiency value indicates a more efficient brain network, where information can be rapidly and effectively transmitted across different regions. In other words, Eg shows the overall integration and communication capacity of the brain network.

Lp measures the efficiency of communication between two nodes in the network, which calculates the smallest number of intermediate steps required to transmit information from one region of the brain to another [49, 90, 91]. A smaller Lp indicates a more efficient brain network,

as information can be transmitted quickly and directly between nodes. Hence, a larger Lp suggests a less efficient network with more indirect and longer routes for information transfer.

Researchers believe that the beta band is associated with active or engaged mental states, such as focused attention, problem-solving, and decision-making [92, 93]. Beta waves are commonly observed during awake and alert states when the brain is actively processing information and performing cognitive tasks [94, 95]. Associated with more complex cognitive processes and are believed to play a crucial role in information integration and binding, EEG signals in gamma band are often observed during tasks that involve sensory perception, memory formation, and higher-level cognitive functions [96, 97]. The results of this study indicated the right prefrontal 800-nm tPBM may elicit more organized and efficient local communication patterns while subjects were awake. Additionally, the increased sigma suggests the right prefrontal 800-nm tPBM may trigger a more balanced integration and segregation in brain networks during information processing. Interestingly, the overall information transfer efficiency of the brain network in the gamma band decreased, while the paths of information transmission became longer. This may suggest that the right prefrontal 800-nm tPBM induced a more relaxed state in the participants during the resting-state, leading to a temporary reduction in memory and cognitive activities.

### 4.4.3 Site-specific effects of left and right prefrontal tPBM

The 800-nm laser treatment applied to the left and right prefrontal regions in tPBM revealed distinct modulation effects, which were also observed in our previous study investigating cerebral hemodynamic and metabolic activities induced by 800-nm prefrontal tPBM [76, 77]. Specifically, when stimulating the left prefrontal area, tPBM primarily modulated key parameters

of the global network within the alpha and delta frequency bands. Quantitative analysis of these parameters indicated that the brain network becomes more efficient and highly clustered, potentially yielding a positive effect on cognitive function. Furthermore, in comparison to stimulating the right prefrontal region, the 800-nm stimulation applied to the left prefrontal region resulted in pronounced region-wise synchronized neural activity.

On the other hand, when stimulating the right prefrontal area, tPBM predominantly modulated key parameters of the global network within the beta and gamma frequency bands. Analysis of these parameters showed that the 800-nm laser applied to the right prefrontal region elicited more organized and efficient global communication patterns, while also triggering a more balanced integration and segregation during information processing.

### 4.4.4 Limitation of the study and future work

One limitation of this study is related to potential EEG setup movement. During the tPBM and sham experiments, EEG electrodes were removed from the Fp1/Fp2 channels. This process could lead to slight positional differences in the EEG channels during post-stimulation measurement, compared to their initial positions during pre-stimulation measurement. Such positional changes might impact data accuracy and create challenges when interpreting and comparing results.

Another limitation pertains to the eyes-closed resting state, where subjects might experience drowsiness. This drowsy state could potentially affect the quality of recorded data, potentially leading to reduced signal stability or the introduction of noise. These factors could influence the analysis results of brain networks.

For future studies, valuable insights could be gained by exploring the effects of various factors, including different wavelengths, light irradiance, stimulation doses, brain regions, and

subjects' ages. The effectiveness of specific brain regions may vary based on individual differences and light parameters. Additionally, different age groups might respond differently to the stimulation. Exploring these aspects can provide a more comprehensive understanding of photobiomodulation's effects on brain function. This, in turn, would offer valuable insights for clinical applications and guide further research endeavors.

## 4.5. Conclusion

This study underscores the site-specific effects of tPBM on brain function, wherein left and right prefrontal tPBM with the same wavelength can trigger distinct modulation effects. This suggests that the impact of brain stimulation may vary across different brain regions, possibly due to the differences of physiological structures among these regions, resulting in diverse responses to the stimulation. Furthermore, the analysis of key parameters of brain networks revealed that both left and right prefrontal tPBM significantly affected neurophysiological networks. These findings suggest that 800-nm tPBM on the prefrontal cortex can directly or indirectly regulate the connectivity patterns and information transmission in the brain. These findings are pivotal for tPBM application, ensuring optimal therapeutic outcomes for neurorehabilitation and brain disorder treatment. Further research is needed to validate and explore various brain regions and stimulation parameters, advancing tPBM in clinical practice.

# Chapter 5

# Future Work

## Prediction of long-term severities of newborns with HIE and advanced management in the first 72 hours of life

Neonatal Hypoxic Ischemic Encephalopathy (HIE) is a critical condition with significant implications for newborns worldwide. The utilization of the brain state of newborn (BSN) as a novel biomarker for prognostic assessment in HIE cases has shown promising results. However, for future work, there are several key areas that require further exploration to enhance the effectiveness and applicability of BSN and improve the management of HIE.

1. Expanding BSN training and data collection: To improve BSN's accuracy and reliability in stratifying HIE severity, extensive training using a larger dataset of EEG recordings from HIE newborns is essential. The inclusion of diverse and ample data will refine the BSN algorithm and enhance its ability to distinguish between mild, moderate, and severe HIE cases.
2. Machine learning-based prediction models: A large-scale studies are currently in progress, employing machine learning-based prediction models. These models utilize diverse markers and advanced algorithms, holding the promise of offering comprehensive and accurate prognostic insights for neonates with HIE. This integrated approach could enhance clinical decision-making by providing a holistic and accurate understanding of the condition.
3. Revisiting the definition of mild HIE: Defining mild HIE is a challenging aspect of its management. Addressing key questions surrounding the classification of mild HIE is imperative to improve diagnostic accuracy and therapeutic decisions. Several specific aspects are suggested for future work. (1) Considering the limited power of the current standard to differentiate mild HIE from normal newborns within the first six hours of life, exploring the

possibility of introducing subclasses to refine severity stratification is worth investigating. (2) Incorporating dynamic severity stratification based on the evolving nature of neonatal HIE may aid in adapting treatments as the condition progresses. (3) Accurately identifying infants who may benefit the most from therapeutic hypothermia (TH) is essential, as it can optimize treatment outcomes. (4) Establishing a specific therapeutic window for effective treatment in neonates with mild NE could account for the slower evolution of brain injury and improve the efficacy of interventions.

In summary, the application of BSN as a biomarker for prognostic assessment in neonatal HIE holds significant promise in improving clinical outcomes. To maximize its potential, future research should focus on expanding BSN training with more extensive EEG datasets, incorporating machine-learning-based prediction models, and redefining the classification of mild HIE. By addressing these key areas, we can enhance our understanding of HIE, optimize therapeutic strategies, and improve long-term neurological outcomes for affected infants. The continued collaborative efforts of researchers and clinicians are vital to advancing the management and care of neonatal HIE in the years to come.

**Potential research topics for future studies**

- To investigate the differences in brain network activity during the sleep cycle among different severities of HIE: This study aims to analyze the variations in neural connectivity and activity patterns across different sleep stages (such as active sleep and quiet sleep) in newborns with varying degrees of HIE severity. The objective is to uncover potential links between the severity of HIE and alterations in brain network dynamics during sleep.

- To explore the potential of using brain networks to predict the occurrence of epilepsy in newborns with HIE: This study aims to identify distinctive network patterns through machine learning algorithms that can serve as early indicators of epilepsy risk. The ultimate goal is to develop proactive and targeted interventions for newborns at risk of epilepsy due to HIE.
- To study tPBM modulation effects in neonates with HIE: A recent research (Groves et al., 2023) reported a photobiomodulation and caffeine treatment for acute kidney injury (AKI) in a hypoxic ischemic neonatal rat model using 670-nm red light. It has shown promise in reducing AKI induced by HIE in the modified Rice-Vannucci model. If further studies validate the potential of tPBM to alleviate AKI in neonatal HIE, it could pave the way for enhanced therapeutic strategies as an HIE management protocol.

# Chapter 6

# Conclusion

In conclusion, my dissertation focuses on the quantification of EEG-derived electrophysiological markers for two specific clinical and biomedical applications. The first application was to assess the potential of using the newborn brain state (BSN) to predict neurodevelopmental outcomes in infants with Hypoxic-Ischemic Encephalopathy (HIE). Furthermore, I explored how HIE can impact the topological connectivity of the neonatal brain based on 8-channel EEG reading. The second application focused on investigating the modulation effects of prefrontal transcranial photobiomodulation (tPBM) on neurophysiological networks in healthy young adults.

Specifically, the following objectives have been achieved:

1. The study confirmed that BSN is a promising bedside tool for monitoring evolving encephalopathy in newborns and predicting neurodevelopmental outcomes.
2. The study demonstrated that GTA-based brain networks can be quantified in neonates with HIE using an eight-channel EEG. The results revealed that the brain networks of neonates with HIE exhibited a lower level of efficiency compared to those observed in healthy full-term neonates and adults. Importantly, no statistically significant differences in these crucial parameters were observed between the mild and moderate HIE groups. This finding suggests a potential equivalence in the degree of brain functional impairment between neonates with mild and moderate HIE, underscoring the importance of prompt medical intervention.
3. My study illustrated that both left and right prefrontal 800-nm tPBM significantly affected neurophysiological networks. Moreover, the presence of site-specific effects of tPBM on brain function has been observed, where left and right prefrontal tPBM may elicit different modulation effects.

## Supplementary material

### A. The definitions of global graphical measures

| Features | Sub-features | Definition |
|---|---|---|
| Synchronization | s | Synchronization of network |
| | szscore | z-score of synchronization of network<br>szscore = (s – mean(srand)) / std(srand). |
| Network Efficiency | Eloc | Local efficiency of network |
| | Eg | Global efficient of network |
| Small-World | Cp | Clustering coefficient of network |
| | Gamma | Normalized clustering coefficient |
| | Lambda | Normalized characteristic path length |
| | Lp | Shortest path length of network |
| | Sigma | The ratio of Gamma and Lambda<br>Sigma = Gamma / Lambda. |
| Hierarchy | b | Hierarchy of network |
| | bzscore | z-score of hierarchy of network<br>bzscore = (b – mean(brand)) / std(brand). |
| Assortativity | r | Assortativity of network |
| | rzscore | z-score of assortativity of network<br>rzscore = (r – mean(rrand)) / std(rrand). |
| Note | srand | srand is a R×1 array, R is the number of randomized network.<br>It is the synchronization of randomized network. |
| | brand | brand is a R×1 array, R is the number of randomized network.<br>It is the hierarchy of randomized network. |
| | rrand | rrand is a R×1 array, R is the number of randomized network.<br>It is the assortativity of randomized network. |

**B. The definitions of nodal graphical measures**

| Features | Definition |
|---|---|
| Nodal Cluster Coefficient (NCp) | It measures the likelihood the neighborhoods of a given node are connected to each other. |
| Nodal Shortest Path (NLp) | It quantifies the mean distance or routing efficiency between a given node and all the other nodes in the network. |
| Nodal Efficiency (Ne) | It characterizes the efficiency of parallel information transfer of a given node in the network. |
| Nodal Local Efficiency (NLe) | It measures how efficient the communication is among the first neighbors of a given node when it is removed. |
| Degree Centrality (Dc) | It reflects the information communication ability of a given node in the functional network. |
| Betweenness Centrality (Bc) | It characterizes the effect of a given node on information flow between other nodes. |

# References


[1] J. Bryce, C. Boschi-Pinto, K. Shibuya, R. E. Black, and W. H. O. C. H. E. R. Group, "WHO estimates of the causes of death in children," *Lancet,* vol. 365, no. 9465, pp. 1147-52, Mar 26-Apr 1 2005, doi: 10.1016/S0140-6736(05)71877-8.

[2] R. Berger and Y. Garnier, "Pathophysiology of perinatal brain damage," *Brain Res Brain Res Rev,* vol. 30, no. 2, pp. 107-34, Aug 1999, doi: 10.1016/s0165-0173(99)00009-0.

[3] H. B. Sarnat and M. S. Sarnat, "Neonatal encephalopathy following fetal distress. A clinical and electroencephalographic study," *Arch Neurol,* vol. 33, no. 10, pp. 696-705, Oct 1976, doi: 10.1001/archneur.1976.00500100030012.

[4] C. Thompson *et al.*, "The value of a scoring system for hypoxic ischaemic encephalopathy in predicting neurodevelopmental outcome," *Acta paediatrica,* vol. 86, no. 7, pp. 757-761, 1997.

[5] L. F. Chalak, B. Adams-Huet, and G. Sant'Anna, "A Total Sarnat Score in Mild Hypoxic-ischemic Encephalopathy Can Detect Infants at Higher Risk of Disability," *J Pediatr,* vol. 214, pp. 217-221 e1, Nov 2019, doi: 10.1016/j.jpeds.2019.06.026.

[6] S. Shankaran *et al.*, "Whole-body hypothermia for neonates with hypoxic-ischemic encephalopathy," *N Engl J Med,* vol. 353, no. 15, pp. 1574-84, Oct 13 2005, doi: 10.1056/NEJMcps050929.

[7] S. Chawla, S. V. Bates, and S. Shankaran, "Is It Time for a Randomized Controlled Trial of Hypothermia for Mild Hypoxic-Ischemic Encephalopathy?," *J Pediatr,* vol. 220, pp. 241-244, May 2020, doi: 10.1016/j.jpeds.2019.11.030.

[8] A. C. Lee *et al.*, "Intrapartum-related neonatal encephalopathy incidence and impairment at regional and global levels for 2010 with trends from 1990," *Pediatric research,* vol. 74, no. 1, pp. 50-72, 2013.

[9] A. R. Laptook *et al.*, "Effect of therapeutic hypothermia initiated after 6 hours of age on death or disability among newborns with hypoxic-ischemic encephalopathy: a randomized clinical trial," *Jama,* vol. 318, no. 16, pp. 1550-1560, 2017.

[10] R. A. Shellhaas *et al.*, "The American Clinical Neurophysiology Society's Guideline on Continuous Electroencephalography Monitoring in Neonates," *J Clin Neurophysiol,* vol. 28, no. 6, pp. 611-7, Dec 2011, doi: 10.1097/WNP.0b013e31823e96d7.

[11] M. Chandrasekaran, B. Chaban, P. Montaldo, and S. Thayyil, "Predictive value of amplitude-integrated EEG (aEEG) after rescue hypothermic neuroprotection for hypoxic ischemic encephalopathy: a meta-analysis," *J Perinatol,* vol. 37, no. 6, pp. 684-689, Jun 2017, doi: 10.1038/jp.2017.14.

[12] S. Kota, K. Jasti, Y. Liu, H. Liu, R. Zhang, and L. Chalak, "EEG Spectral Power: A Proposed Physiological Biomarker to Classify the Hypoxic-Ischemic Encephalopathy Severity in Real Time," *Pediatr Neurol,* vol. 122, pp. 7-14, Sep 2021, doi: 10.1016/j.pediatrneurol.2021.06.001.

[13] M. A. Awal, M. M. Lai, G. Azemi, B. Boashash, and P. B. Colditz, "EEG background features that predict outcome in term neonates with hypoxic ischaemic encephalopathy: A structured review," *Clin Neurophysiol,* vol. 127, no. 1, pp. 285-296, Jan 2016, doi: 10.1016/j.clinph.2015.05.018.

[14] J. McLaren, G. L. Holmes, and M. T. Berg, "Functional Connectivity in Term Neonates With Hypoxic-Ischemic Encephalopathy Undergoing Therapeutic Hypothermia," *Pediatr Neurol,* vol. 94, pp. 74-79, May 2019, doi: 10.1016/j.pediatrneurol.2019.01.006.

[15] S. M. Moghadam *et al.*, "An automated bedside measure for monitoring neonatal cortical activity: a supervised deep learning-based electroencephalogram classifier with external cohort validation," *Lancet Digit Health,* vol. 4, no. 12, pp. e884-e892, Dec 2022, doi: 10.1016/S2589-7500(22)00196-0.

[16] N. Bayley, "Bayley scales of infant and toddler development," 2006.
[17] S. Shankaran *et al.*, "Effect of Depth and Duration of Cooling on Death or Disability at Age 18 Months Among Neonates With Hypoxic-Ischemic Encephalopathy: A Randomized Clinical Trial," *JAMA,* vol. 318, no. 1, pp. 57-67, Jul 4 2017, doi: 10.1001/jama.2017.7218.
[18] L. W. Impey, C. E. Greenwood, R. S. Black, P. S.-Y. Yeh, O. Sheil, and P. Doyle, "The relationship between intrapartum maternal fever and neonatal acidosis as risk factors for neonatal encephalopathy," *American journal of obstetrics and gynecology,* vol. 198, no. 1, pp. 49. e1-49. e6, 2008.
[19] P. S. Bobba, A. Malhotra, K. N. Sheth, S. N. Taylor, L. R. Ment, and S. Payabvash, "Brain injury patterns in hypoxic ischemic encephalopathy of term neonates," *J Neuroimaging,* vol. 33, no. 1, pp. 79-84, Jan 2023, doi: 10.1111/jon.13052.
[20] B. H. Walsh *et al.*, "The Frequency and Severity of Magnetic Resonance Imaging Abnormalities in Infants with Mild Neonatal Encephalopathy," *J Pediatr,* vol. 187, pp. 26-33 e1, Aug 2017, doi: 10.1016/j.jpeds.2017.03.065.
[21] S. V. Jain, J. M. Zempel, P. Srinivasakumar, M. Wallendorf, and A. Mathur, "Early EEG power predicts MRI injury in infants with hypoxic-ischemic encephalopathy," *J Perinatol,* vol. 37, no. 5, pp. 541-546, May 2017, doi: 10.1038/jp.2016.262.
[22] B. H. Walsh, C. Munster, H. El-Shibiny, E. Yang, T. E. Inder, and M. El-Dib, "Comparison of numerical and standard sarnat grading using the NICHD and SIBEN methods," *J Perinatol,* vol. 42, no. 3, pp. 328-334, Mar 2022, doi: 10.1038/s41372-021-01180-w.
[23] Y. Das *et al.*, "Wavelet-based neurovascular coupling can predict brain abnormalities in neonatal encephalopathy," *Neuroimage Clin,* vol. 32, p. 102856, 2021, doi: 10.1016/j.nicl.2021.102856.
[24] X. Wang *et al.*, "EEG phase-amplitude coupling to stratify encephalopathy severity in the developing brain," *Comput Methods Programs Biomed,* vol. 214, p. 106593, Feb 2022, doi: 10.1016/j.cmpb.2021.106593.
[25] S. Kota *et al.*, "Prognostic Value of Continuous Electroencephalogram Delta Power in Neonates With Hypoxic-Ischemic Encephalopathy," *J Child Neurol,* vol. 35, no. 8, pp. 517-525, Jul 2020, doi: 10.1177/0883073820915323.
[26] X. Wang *et al.*, "Feasibility of EEG Phase-Amplitude Coupling to Stratify Encephalopathy Severity in Neonatal HIE Using Short Time Window," *Brain Sci,* vol. 12, no. 7, Jun 29 2022, doi: 10.3390/brainsci12070854.
[27] Y. Das, H. Liu, F. Tian, S. Kota, R. Zhang, and L. F. Chalak, "Rigor of Neurovascular Coupling (NVC) Assessment in Newborns Using Different Amplitude EEG Algorithms," *Sci Rep,* vol. 10, no. 1, p. 9183, Jun 8 2020, doi: 10.1038/s41598-020-66227-y.
[28] G. Natarajan, A. Pappas, and S. Shankaran, "Outcomes in childhood following therapeutic hypothermia for neonatal hypoxic-ischemic encephalopathy (HIE)," in *Seminars in perinatology*, 2016, vol. 40, no. 8: Elsevier, pp. 549-555.
[29] S. Shankaran *et al.*, "Childhood outcomes after hypothermia for neonatal encephalopathy," *New England Journal of Medicine,* vol. 366, no. 22, pp. 2085-2092, 2012.
[30] R. Lee-Kelland, S. Jary, J. Tonks, F. M. Cowan, M. Thoresen, and E. Chakkarapani, "School-age outcomes of children without cerebral palsy cooled for neonatal hypoxic–ischaemic encephalopathy in 2008–2010," *Archives of Disease in Childhood-Fetal and Neonatal Edition,* vol. 105, no. 1, pp. 8-13, 2020.
[31] B. J. van Kooij, M. van Handel, R. A. Nievelstein, F. Groenendaal, M. J. Jongmans, and L. S. de Vries, "Serial MRI and neurodevelopmental outcome in 9- to 10-year-old children with neonatal encephalopathy," *J Pediatr,* vol. 157, no. 2, pp. 221-227 e2, Aug 2010, doi: 10.1016/j.jpeds.2010.02.016.

[32] D. M. Murray, C. M. O'Connor, C. A. Ryan, I. Korotchikova, and G. B. Boylan, "Early EEG Grade and Outcome at 5 Years After Mild Neonatal Hypoxic Ischemic Encephalopathy," *Pediatrics,* vol. 138, no. 4, Oct 2016, doi: 10.1542/peds.2016-0659.

[33] M. Finder, G. B. Boylan, D. Twomey, C. Ahearne, D. M. Murray, and B. Hallberg, "Two-Year Neurodevelopmental Outcomes After Mild Hypoxic Ischemic Encephalopathy in the Era of Therapeutic Hypothermia," *JAMA Pediatr,* vol. 174, no. 1, pp. 48-55, Jan 1 2020, doi: 10.1001/jamapediatrics.2019.4011.

[34] A. E. Torn, S. Hesselman, K. Johansen, J. Agren, A. K. Wikstrom, and M. Jonsson, "Outcomes in children after mild neonatal hypoxic ischaemic encephalopathy: A population-based cohort study," *BJOG,* May 18 2023, doi: 10.1111/1471-0528.17533.

[35] F. Vecchio *et al.*, "Human brain networks in cognitive decline: a graph theoretical analysis of cortical connectivity from EEG data," *J Alzheimers Dis,* vol. 41, no. 1, pp. 113-27, 2014, doi: 10.3233/JAD-132087.

[36] L. Ismail *et al.*, "Modeling Brain Functional Connectivity Patterns during an Isometric Arm Force Exertion Task at Different Levels of Perceived Exertion: A Graph Theoretical Approach," *Brain Sci,* vol. 12, no. 11, Nov 18 2022, doi: 10.3390/brainsci12111575.

[37] F. Vecchio *et al.*, "Cortical connectivity and memory performance in cognitive decline: A study via graph theory from EEG data," *Neuroscience,* vol. 316, pp. 143-50, Mar 1 2016, doi: 10.1016/j.neuroscience.2015.12.036.

[38] L. G. Gutierrez, A. Rovira, L. A. Portela, C. Leite Cda, and L. T. Lucato, "CT and MR in non-neonatal hypoxic-ischemic encephalopathy: radiological findings with pathophysiological correlations," *Neuroradiology,* vol. 52, no. 11, pp. 949-76, Nov 2010, doi: 10.1007/s00234-010-0728-z.

[39] K. P. Forbes, J. G. Pipe, and R. Bird, "Neonatal hypoxic-ischemic encephalopathy: detection with diffusion-weighted MR imaging," *AJNR Am J Neuroradiol,* vol. 21, no. 8, pp. 1490-6, Sep 2000. [Online]. Available: https://www.ncbi.nlm.nih.gov/pubmed/11003285.

[40] S. B. Trivedi *et al.*, "A validated clinical MRI injury scoring system in neonatal hypoxic-ischemic encephalopathy," *Pediatr Radiol,* vol. 47, no. 11, pp. 1491-1499, Oct 2017, doi: 10.1007/s00247-017-3893-y.

[41] T. Popov, R. Oostenveld, and J. M. Schoffelen, "FieldTrip Made Easy: An Analysis Protocol for Group Analysis of the Auditory Steady State Brain Response in Time, Frequency, and Space," *Front Neurosci,* vol. 12, p. 711, 2018, doi: 10.3389/fnins.2018.00711.

[42] J. Vorwerk, R. Oostenveld, M. C. Piastra, L. Magyari, and C. H. Wolters, "The FieldTrip-SimBio pipeline for EEG forward solutions," *Biomed Eng Online,* vol. 17, no. 1, p. 37, Mar 27 2018, doi: 10.1186/s12938-018-0463-y.

[43] J. Wang, X. Wang, M. Xia, X. Liao, A. Evans, and Y. He, "GRETNA: a graph theoretical network analysis toolbox for imaging connectomics," *Front Hum Neurosci,* vol. 9, p. 386, 2015, doi: 10.3389/fnhum.2015.00386.

[44] J. De Asis-Cruz, M. Bouyssi-Kobar, I. Evangelou, G. Vezina, and C. Limperopoulos, "Functional properties of resting state networks in healthy full-term newborns," *Sci Rep,* vol. 5, p. 17755, Dec 7 2015, doi: 10.1038/srep17755.

[45] E. C. van Straaten and C. J. Stam, "Structure out of chaos: functional brain network analysis with EEG, MEG, and functional MRI," *Eur Neuropsychopharmacol,* vol. 23, no. 1, pp. 7-18, Jan 2013, doi: 10.1016/j.euroneuro.2012.10.010.

[46] C. J. Stam *et al.*, "Graph theoretical analysis of magnetoencephalographic functional connectivity in Alzheimer's disease," *Brain,* vol. 132, no. Pt 1, pp. 213-24, Jan 2009, doi: 10.1093/brain/awn262.

[47] E. van Diessen, W. J. Zweiphenning, F. E. Jansen, C. J. Stam, K. P. Braun, and W. M. Otte, "Brain Network Organization in Focal Epilepsy: A Systematic Review and Meta-Analysis," *PLoS One,* vol. 9, no. 12, p. e114606, 2014, doi: 10.1371/journal.pone.0114606.

[48] N. Masuda, M. Sakaki, T. Ezaki, and T. Watanabe, "Clustering Coefficients for Correlation Networks," *Front Neuroinform,* vol. 12, p. 7, 2018, doi: 10.3389/fninf.2018.00007.

[49] E. Bullmore and O. Sporns, "The economy of brain network organization," *Nat Rev Neurosci,* vol. 13, no. 5, pp. 336-49, Apr 13 2012, doi: 10.1038/nrn3214.

[50] J. Royer *et al.*, "Epilepsy and brain network hubs," *Epilepsia,* vol. 63, no. 3, pp. 537-550, Mar 2022, doi: 10.1111/epi.17171.

[51] R. Prajapati and I. A. Emerson, "Global and regional connectivity analysis of resting-state function MRI brain images using graph theory in Parkinson's disease," *Int J Neurosci,* vol. 131, no. 2, pp. 105-115, Feb 2021, doi: 10.1080/00207454.2020.1733559.

[52] Y. Wang, E. Ghumare, R. Vandenberghe, and P. Dupont, "Comparison of Different Generalizations of Clustering Coefficient and Local Efficiency for Weighted Undirected Graphs," *Neural Comput,* vol. 29, no. 2, pp. 313-331, Feb 2017, doi: 10.1162/NECO_a_00914.

[53] E. van Diessen, W. M. Otte, K. P. Braun, C. J. Stam, and F. E. Jansen, "Improved diagnosis in children with partial epilepsy using a multivariable prediction model based on EEG network characteristics," *PLoS One,* vol. 8, no. 4, p. e59764, 2013, doi: 10.1371/journal.pone.0059764.

[54] V. Verbavatz and M. Barthelemy, "Betweenness centrality in dense spatial networks," *Phys Rev E,* vol. 105, no. 5-1, p. 054303, May 2022, doi: 10.1103/PhysRevE.105.054303.

[55] B. T. Grobelny, D. London, T. C. Hill, E. North, P. Dugan, and W. K. Doyle, "Betweenness centrality of intracranial electroencephalography networks and surgical epilepsy outcome," *Clin Neurophysiol,* vol. 129, no. 9, pp. 1804-1812, Sep 2018, doi: 10.1016/j.clinph.2018.02.135.

[56] Y. Wang *et al.*, "Changes of Functional Brain Network in Neonates with Different Degrees of Hypoxic-Ischemic Encephalopathy," *Brain Connect,* Jul 26 2023, doi: 10.1089/brain.2022.0073.

[57] H. X. Li *et al.*, "Resting-state network complexity and magnitude changes in neonates with severe hypoxic ischemic encephalopathy," *Neural Regen Res,* vol. 14, no. 4, pp. 642-648, Apr 2019, doi: 10.4103/1673-5374.247468.

[58] A. Ramirez *et al.*, "Neonatal brain injury influences structural connectivity and childhood functional outcomes," *PLoS One,* vol. 17, no. 1, p. e0262310, 2022, doi: 10.1371/journal.pone.0262310.

[59] Z. He *et al.*, "Brain Metabolic Connectivity Patterns in Patients with Prolonged Disorder of Consciousness after Hypoxic-Ischemic Injury: A Preliminary Study," *Brain Sci,* vol. 12, no. 7, Jul 7 2022, doi: 10.3390/brainsci12070892.

[60] T. T. Dang-Vu *et al.*, "Cerebral correlates of delta waves during non-REM sleep revisited," *Neuroimage,* vol. 28, no. 1, pp. 14-21, Oct 15 2005, doi: 10.1016/j.neuroimage.2005.05.028.

[61] S. G. Horovitz *et al.*, "Decoupling of the brain's default mode network during deep sleep," *Proc Natl Acad Sci U S A,* vol. 106, no. 27, pp. 11376-81, Jul 7 2009, doi: 10.1073/pnas.0901435106.

[62] E. Tagliazucchi, M. Behrens, and H. Laufs, "Sleep neuroimaging and models of consciousness," *Front Psychol,* vol. 4, p. 256, 2013, doi: 10.3389/fpsyg.2013.00256.

[63] Y. Luo *et al.*, "Alterations of Brain Networks in Alzheimer's Disease and Mild Cognitive Impairment: A Resting State fMRI Study Based on a Population-specific Brain Template," *Neuroscience,* vol. 452, pp. 192-207, Jan 1 2021, doi: 10.1016/j.neuroscience.2020.10.023.

[64] S. Lim, F. Radicchi, M. P. van den Heuvel, and O. Sporns, "Discordant attributes of structural and functional brain connectivity in a two-layer multiplex network," *Sci Rep,* vol. 9, no. 1, p. 2885, Feb 27 2019, doi: 10.1038/s41598-019-39243-w.

[65] S. Galantucci *et al.*, "Structural Brain Connectome and Cognitive Impairment in Parkinson Disease," *Radiology,* vol. 283, no. 2, pp. 515-525, May 2017, doi: 10.1148/radiol.2016160274.

[66] S. Shahdadian, X. Wang, H. Wanniarachchi, A. Chaudhari, N. C. D. Truong, and H. Liu, "Neuromodulation of brain power topography and network topology by prefrontal transcranial photobiomodulation," *J Neural Eng,* vol. 19, no. 6, Nov 17 2022, doi: 10.1088/1741-2552/ac9ede.

[67] X. Wang, H. Wanniarachchi, A. Wu, F. Gonzalez-Lima, and H. Liu, "Transcranial photobiomodulation and thermal stimulation induce distinct topographies of EEG alpha and beta power changes in healthy humans," *Sci Rep,* vol. 11, no. 1, p. 18917, Sep 23 2021, doi: 10.1038/s41598-021-97987-w.

[68] X. Wang, L. C. Ma, S. Shahdadian, A. Wu, N. C. D. Truong, and H. Liu, "Metabolic Connectivity and Hemodynamic-Metabolic Coherence of Human Prefrontal Cortex at Rest and Post Photobiomodulation Assessed by Dual-Channel Broadband NIRS," *Metabolites,* vol. 12, no. 1, Jan 5 2022, doi: 10.3390/metabo12010042.

[69] F. Salehpour and S. H. Rasta, "The potential of transcranial photobiomodulation therapy for treatment of major depressive disorder," *Rev Neurosci,* vol. 28, no. 4, pp. 441-453, May 24 2017, doi: 10.1515/revneuro-2016-0087.

[70] A. Jahan, M. A. Nazari, J. Mahmoudi, F. Salehpour, and M. M. Salimi, "Transcranial near-infrared photobiomodulation could modulate brain electrophysiological features and attentional performance in healthy young adults," *Lasers Med Sci,* vol. 34, no. 6, pp. 1193-1200, Aug 2019, doi: 10.1007/s10103-018-02710-3.

[71] C. L. Saucedo *et al.*, "Transcranial laser stimulation: Mitochondrial and cerebrovascular effects in younger and older healthy adults," *Brain Stimul,* vol. 14, no. 2, pp. 440-449, Mar-Apr 2021, doi: 10.1016/j.brs.2021.02.011.

[72] M. R. Hamblin, "Photobiomodulation for traumatic brain injury and stroke," *J Neurosci Res,* vol. 96, no. 4, pp. 731-743, Apr 2018, doi: 10.1002/jnr.24190.

[73] F. Tian, S. N. Hase, F. Gonzalez-Lima, and H. Liu, "Transcranial laser stimulation improves human cerebral oxygenation," *Lasers Surg Med,* vol. 48, no. 4, pp. 343-9, Apr 2016, doi: 10.1002/lsm.22471.

[74] E. Vargas *et al.*, "Beneficial neurocognitive effects of transcranial laser in older adults," *Lasers Med Sci,* vol. 32, no. 5, pp. 1153-1162, Jul 2017, doi: 10.1007/s10103-017-2221-y.

[75] Y. He and A. Evans, "Graph theoretical modeling of brain connectivity," *Curr Opin Neurol,* vol. 23, no. 4, pp. 341-50, Aug 2010, doi: 10.1097/WCO.0b013e32833aa567.

[76] S. Shahdadian, X. Wang, S. Kang, C. Carter, and H. Liu, "Site-specific effects of 800- and 850-nm forehead transcranial photobiomodulation on prefrontal bilateral connectivity and unilateral coupling in young adults," *Neurophotonics,* vol. 10, no. 2, p. 025012, Apr 2023, doi: 10.1117/1.NPh.10.2.025012.

[77] S. Shahdadian, X. Wang, S. Kang, C. Carter, A. Chaudhari, and H. Liu, "Prefrontal cortical connectivity and coupling of infraslow oscillation in the resting human brain: a 2-channel broadband NIRS study," *Cereb Cortex Commun,* vol. 3, no. 3, p. tgac033, 2022, doi: 10.1093/texcom/tgac033.

[78] X. Wang *et al.*, "Transcranial photobiomodulation with 1064-nm laser modulates brain electroencephalogram rhythms," *Neurophotonics,* vol. 6, no. 2, p. 025013, Apr 2019, doi: 10.1117/1.NPh.6.2.025013.

[79] L. Song *et al.*, "Human Fetal Brain Connectome: Structural Network Development from Middle Fetal Stage to Birth," *Front Neurosci,* vol. 11, p. 561, 2017, doi: 10.3389/fnins.2017.00561.

[80] V. Latora and M. Marchiori, "Efficient behavior of small-world networks," *Phys Rev Lett,* vol. 87, no. 19, p. 198701, Nov 5 2001, doi: 10.1103/PhysRevLett.87.198701.

[81] M. P. van den Heuvel, C. J. Stam, R. S. Kahn, and H. E. Hulshoff Pol, "Efficiency of functional brain networks and intellectual performance," *J Neurosci,* vol. 29, no. 23, pp. 7619-24, Jun 10 2009, doi: 10.1523/JNEUROSCI.1443-09.2009.

[82] R. A. Shellhaas, J. W. Burns, F. Hassan, M. D. Carlson, J. D. E. Barks, and R. D. Chervin, "Neonatal Sleep-Wake Analyses Predict 18-month Neurodevelopmental Outcomes," *Sleep,* vol. 40, no. 11, Nov 1 2017, doi: 10.1093/sleep/zsx144.

[83] L. Bennet, K. L. Fyfe, S. R. Yiallourou, H. Merk, F. Y. Wong, and R. S. Horne, "Discrimination of sleep states using continuous cerebral bedside monitoring (amplitude-integrated electroencephalography) compared to polysomnography in infants," *Acta Paediatr,* vol. 105, no. 12, pp. e582-e587, Dec 2016, doi: 10.1111/apa.13602.

[84] L. Pessoa, "Understanding brain networks and brain organization," *Phys Life Rev,* vol. 11, no. 3, pp. 400-35, Sep 2014, doi: 10.1016/j.plrev.2014.03.005.

[85] S. Genon, A. Reid, R. Langner, K. Amunts, and S. B. Eickhoff, "How to Characterize the Function of a Brain Region," *Trends Cogn Sci,* vol. 22, no. 4, pp. 350-364, Apr 2018, doi: 10.1016/j.tics.2018.01.010.

[86] M. L. Anderson, J. Kinnison, and L. Pessoa, "Describing functional diversity of brain regions and brain networks," *Neuroimage,* vol. 73, pp. 50-8, Jun 2013, doi: 10.1016/j.neuroimage.2013.01.071.

[87] C. Horien, A. S. Greene, R. T. Constable, and D. Scheinost, "Regions and Connections: Complementary Approaches to Characterize Brain Organization and Function," *Neuroscientist,* vol. 26, no. 2, pp. 117-133, Apr 2020, doi: 10.1177/1073858419860115.

[88] K. Supekar, V. Menon, D. Rubin, M. Musen, and M. D. Greicius, "Network analysis of intrinsic functional brain connectivity in Alzheimer's disease," *PLoS Comput Biol,* vol. 4, no. 6, p. e1000100, Jun 27 2008, doi: 10.1371/journal.pcbi.1000100.

[89] F. de Pasquale, S. Della Penna, O. Sporns, G. L. Romani, and M. Corbetta, "A Dynamic Core Network and Global Efficiency in the Resting Human Brain," *Cereb Cortex,* vol. 26, no. 10, pp. 4015-33, Oct 2016, doi: 10.1093/cercor/bhv185.

[90] C. Seguin, O. Sporns, and A. Zalesky, "Brain network communication: concepts, models and applications," *Nat Rev Neurosci,* Jul 12 2023, doi: 10.1038/s41583-023-00718-5.

[91] G. Chen, G. Chen, C. Xie, and S. J. Li, "Negative functional connectivity and its dependence on the shortest path length of positive network in the resting-state human brain," *Brain Connect,* vol. 1, no. 3, pp. 195-206, 2011, doi: 10.1089/brain.2011.0025.

[92] T. Akerstedt and M. Gillberg, "Subjective and objective sleepiness in the active individual," *Int J Neurosci,* vol. 52, no. 1-2, pp. 29-37, May 1990, doi: 10.3109/00207459008994241.

[93] M. A. Boksem, T. F. Meijman, and M. M. Lorist, "Effects of mental fatigue on attention: an ERP study," *Brain Res Cogn Brain Res,* vol. 25, no. 1, pp. 107-16, Sep 2005, doi: 10.1016/j.cogbrainres.2005.04.011.

[94] G. Borghini, L. Astolfi, G. Vecchiato, D. Mattia, and F. Babiloni, "Measuring neurophysiological signals in aircraft pilots and car drivers for the assessment of mental workload, fatigue and drowsiness," *Neurosci Biobehav Rev,* vol. 44, pp. 58-75, Jul 2014, doi: 10.1016/j.neubiorev.2012.10.003.

[95] C. Neuper and G. Pfurtscheller, "Event-related dynamics of cortical rhythms: frequency-specific features and functional correlates," *Int J Psychophysiol,* vol. 43, no. 1, pp. 41-58, Dec 2001, doi: 10.1016/s0167-8760(01)00178-7.

[96] O. Jensen, J. Kaiser, and J. P. Lachaux, "Human gamma-frequency oscillations associated with attention and memory," *Trends Neurosci,* vol. 30, no. 7, pp. 317-24, Jul 2007, doi: 10.1016/j.tins.2007.05.001.

[97] M. Lundqvist, J. Rose, P. Herman, S. L. Brincat, T. J. Buschman, and E. K. Miller, "Gamma and Beta Bursts Underlie Working Memory," *Neuron,* vol. 90, no. 1, pp. 152-164, Apr 6 2016, doi: 10.1016/j.neuron.2016.02.028.

# Appendix: MATLAB codes for this dissertation

The MATLAB codes utilized for each aim are documented as follows.

### M.1 MATLAB codes for Aim 1 (Chapter 2)

```
%% To access BabaCloud:
% BABA cloud: https://babacloud.fi/login/?next=/

%% Get 1 hours artifact-free data and build bipolar EEG montages
clc; close all; clearvars;
cd E:\UTSW\HIE_neonates\SUB45\Matlab
fout = sprintf('SUB45_EEG_1h.mat');
dirlist = dir('EEG,Composite,SampleSeries,Composite*.mat');
fn = length(dirlist);
load(dirlist(1).name,'start_date_time','comp_elements','units');
cn = length(comp_elements);
clear dirlist
element = comp_elements(:);
for idx = 1:9
   fin = sprintf('EEG,Composite,SampleSeries,Composite,Amp1020,data_part%dof35.mat',idx);
%change 35 to the number matches the recording
   load(fin,'time_vector','measurement_data');
   if idx == 1
      time = time_vector;
      data = measurement_data(:,:);
   else
      time = [time time_vector];
      data = [data measurement_data(:,:)];
   end
   clear fin time_vector measurement_data
end
clear idx
data_1h = data(:,1:round(1*256*3600)+1);
Chs_EEG = data_1h;
eeg_C3 = Chs_EEG(1,1:end);
eeg_C4 = Chs_EEG(2,1:end);
eeg_P3 = Chs_EEG(7,1:end);
eeg_P4 = Chs_EEG(8,1:end);
C3_C4 = eeg_C3 - eeg_C4;
P3_P4 = eeg_P3 - eeg_P4;
C3_P3 = eeg_C3 - eeg_P3;
C4_P4 = eeg_C4 - eeg_P4;
EEG = [C3_C4; P3_P4; C3_P3; C4_P4];
element = {'C3_C4'; 'P3_P4'; 'C3_P3'; 'C4_P4'};
cd D:\UTSW\TESTING5\MATfiles_forEDF
```

```
save(fout,'start_date_time','element','units','time','EEG');
clear element time EEG fout data cn fn
close all

%  Convert EEG data from MAT to EDF
clc; close all; clearvars;
files = dir('E:\UTSW\TESTING5\forBaBaCloud\MATfiles_forEDF');
for iFiles = 3 : length(files)
   load(strcat(files(iFiles).folder, '\', files(iFiles).name))
   filename = [files(iFiles).name(1:end-4) '.edf']; % the same Filename only in EDF
   ns = length(element);              % # channels
   fs = round(1/(time(2)-time(1)));    % sampling frequency
   BB = size(EEG);                    % recording length
   len = floor(BB(2)/fs);             % recording length in sec
   scx = ones(ns,1);                  % scaling
   bp_f_high = 0.3;                   % cut off frequency
   order = 4;                        % 4th order filter, low pass
   [b,a] = butter(order,([bp_f_high]/(fs/2)),'high');
   dat = {};
   for iCh = 1:size(EEG,1)
      % filtering
      dat{iCh} = filtfilt(b,a,EEG(iCh,:)); % Copy EEG to dat
   end

   % Extract date and time of recording
   start_date_time = ('20 03 2019, 12:50:09');
   date_time = datetime(start_date_time,'Format','dd MM yyyy, HH:mm:ss');
   yy = num2str(year(date_time));
   formatSpec = '%02.f';

   % Write EDF header
   hdr{1} = ['0' ; char(32*ones(7,1)); ...
      char(32*ones(160,1)); ...
      num2str(day(date_time),formatSpec)';'.';...
      num2str(month(date_time),formatSpec)';'.';...
      yy(3:4)';...
      num2str(hour(date_time),formatSpec)';'.';...
      num2str(minute(date_time),formatSpec)';'.';...
      num2str(second(date_time),formatSpec)';char(32*ones(8,1)); char(32*ones(44,1)) ; ...
      num2str(len)' ; char(32*ones(8-length(num2str(len)),1)) ; '1' ;...
      char(32*ones(7,1)) ; num2str(ns)' ; char(32*ones(4-length(num2str(ns)),1))];
   dstr1 = element;
   % Label is ns*16 chars (Make sure each label has 16 characters if you
   % want to change the label name)
   hdr{2} = [];
   for kk = 1:ns; hdr{2} = [hdr{2} ; dstr1{kk}' ; char(32*ones(16-length(dstr1{kk}),1))]; end
```

```
% Transducer type (ns*80 chars)
hdr{3} = [];
for kk = 1:ns; hdr{3} = [hdr{3} ; char(32*ones(64,1)) ; ['AgAgCL electrode']']; end
% Physical dimension (ns*8 chars)
hdr{4} = [];
for kk = 1:ns; hdr{4} = [hdr{4} ; char(32*ones(6,1)) ; units'] ; end
% Physical minimum (ns*8 chars)
val2 = (2^15-1).*scx; val1 = -(2^15).*scx;
hdr{5} = [];
for kk = 1:ns
   dum = val1(kk);
   switch floor(log10(abs(dum)))
      case 4
         hdr{5} = [hdr{5} ; num2str(dum, '%5.1f')'];
      case 3
         hdr{5} = [hdr{5} ; num2str(dum, '%4.2f')'];
      case 2
         hdr{5} = [hdr{5} ; num2str(dum, '%3.3f')'];
      case 1
         hdr{5} = [hdr{5} ; num2str(dum, '%2.4f')'];
   end
end
% Physical maximum (ns*8 chars)
hdr{6} = [];
for kk = 1:ns
   dum = val2(kk);
   switch floor(log10(abs(dum)))
      case 4
         hdr{6} = [hdr{6} ; num2str(dum, '%5.1f')' ; char(32)];
      case 3
         hdr{6} = [hdr{6} ; num2str(dum, '%4.2f')' ; char(32)];
      case 2
         hdr{6} = [hdr{6} ; num2str(dum, '%3.3f')' ; char(32)];
      case 1
         hdr{6} = [hdr{6} ; num2str(dum, '%2.4f')' ; char(32)];
   end
end
% Digital minimum (ns*8 chars)
hdr{7} = [];
for kk = 1:ns; hdr{7} = [hdr{7} ; num2str(-32768)' ; char(32*ones(2,1))]; end
% Digital maximum (ns*8 chars)
hdr{8} = [];
for kk = 1:ns; hdr{8} = [hdr{8} ; num2str(32767)' ; char(32*ones(3,1))]; end
% Prefiltering
hdr{9} = [];
for kk = 1:ns; hdr{9} = [hdr{9} ; char(32*ones(80,1))]; end
```

```
   % Number of samples per record
   hdr{10} = [];
   for kk = 1:ns; hdr{10} = [hdr{10} ; num2str(fs)' ; char(32*ones(8-length(num2str(fs)),1))];
end
   % Reserved section
   hdr{11} = [];
   for kk = 1:ns; hdr{11} = [hdr{11} ; char(32*ones(32,1))]; end
   % Header length
   h = 0;
   for kk = 1:11
      h = h + length(hdr{kk});
   end
   h1 = [num2str(h)' ; char(32*ones(8-length(num2str(h)),1))];
   hdr{1}(185:192) = h1;

   cd E:\UTSW\TESTING5\forBaBaCloud\EDF_files
   write_edf(filename, dat, hdr);
end

% Analysis CSV file from BabaCloud
clc; close all; clearvars;
path = 'E:\UTSW\TESTING5\forBaBaCloud\BabaCloudOutput\datafiles\';    % change to your
path
for i =1:45
realpath = strcat(path,'UTSW_UTSW_test2_2022-04-
07_SUB',num2str(i),'_EEG_6h_babyEEG_result','\');  % change to your folder
cd(realpath);
subject = i;
datain = readtable('UTSW_test2_Classifiers_result.csv');

% Define quantifiable parameters
NBS_raw = datain(12,1);
NBS_cell = NBS_raw{1,1};
splitcells_NBS = regexp(NBS_cell, '\s+', 'split');
NBS_cell = vertcat(splitcells_NBS{:});
NBS = str2double(NBS_cell);
clear NBS_raw NBS_cell splitcells_NBS NBS_cell
NBS_mean = mean(NBS);
NBS_std = std(NBS);
save('outputs.mat','subject','NBS','SST','NBS_mean','NBS_std');
clear subject NBS NBS_mean NBS_std
          end

%%% Function write_edf
function dum1 = write_edf(filename, dat, hdr);
% [data, hdr, label] = write_edf(filename);
```

```
%
% This functions writes an EDF file as per the format outlined in
%  http://www.edfplus.info/specs/edf.html. Note this version uses a
%  pre-existing header so the function is limited.
%
% INPUT: filename - EDF file name
%              dat - a cell array containing the data in the file (int16 format)
%               hdr - a cell array the header file information in ASCII format
%
% Nathan Stevenson

fid = fopen(filename, 'w');

% WRITE HEADER (see next commented section as to what each bits relates to with respect to the EDF specification)
c1 = fwrite(fid, hdr{1}, 'char');
c2 = fwrite(fid, hdr{2}, 'char');
c3 = fwrite(fid, hdr{3}, 'char');
c4 = fwrite(fid, hdr{4}, 'char');
c5 = fwrite(fid, hdr{5}, 'char');
c6 = fwrite(fid, hdr{6}, 'char');
c7 = fwrite(fid, hdr{7}, 'char');
c8 = fwrite(fid, hdr{8}, 'char');
c9 = fwrite(fid, hdr{9}, 'char');
c10 = fwrite(fid, hdr{10}, 'char');
c11 = fwrite(fid, hdr{11}, 'char');

% CORRESPONDING COMPONNET OF HEADER IN EDF FORMAT
% hdr{1} = fread(fid, 256, 'char');        % CONTAINS PATIENT INFORMATION, RECORDING INFORMATION
% ns = char(hdr{1}(253:256))';             % NUMBER OF SIGNALS
% hdr{2} = fread(fid, ns*16, 'char');    % LABEL channel label, temp or HR
% hdr{3} = fread(fid, ns*80,'char');     % TRANSDUCER TYPE
% hdr{4} = fread(fid, ns*8,'char');      % PHYSICAL DIMENSION, voltage - temperature
% hdr{5} = fread(fid, ns*8,'char');      % PHYSICAL MIN
% hdr{6} = fread(fid, ns*8,'char');      % PHYSICAL MAX
% hdr{7} = fread(fid, ns*8,'char');      % DIGITAL MIN
% hdr{8} = fread(fid, ns*8,'char');      % DIGITAL MAX
% hdr{9} = fread(fid, ns*80,'char');     % PRE FILTERING
% hdr{10} = fread(fid, ns*8, 'char');    % SAMPLING NO rec
% hdr{11} = fread(fid, ns*32,'char');     % RESERVED

len_s = str2num(char(hdr{1}(235:244))');        % START DATE AND TIME and a RESERVED
ns = char(hdr{1}(253:256))';
ns = str2num(ns);
nsamp = str2num(char(hdr{10})');
```

```
for ii = 1:len_s;
   for jj = 1:length(nsamp);
      r1 = nsamp(jj)*(ii-1)+1; r2 = ii*nsamp(jj);
      d1 =  dat{jj}(r1:r2);
      fwrite(fid, d1, 'short');
   end
end
dum1 = fclose(fid);
```

**M.2 MATLAB codes for Aim 2 (Chapter 3)**

```
%%% Preprocessing
clear all; clc;
fs=256;
Target_timelength = 0.5;
excluded_timelength = 0;
people_Mild = [2,4:8,10,12,14:17,21:23,25];
for i = 1:16
   for j = 1:9
      subject_mild{i,j}=strcat('F:\HIE_Brain_network\EEG for Shu\HIE EEG
(+)\HIE_neonates\Ctrl',num2str(people_Mild(i)),'\Matlab\EEG,Composite,SampleSeries,Compo
site,Amp1020,data_part',num2str(j),'.mat');
   end
end
mild_data = [];
for i = 1:16
   for j = 1:9
      temp = load(subject_mild{i,j});
      mild_data = [mild_data, temp.measurement_data];
   end
   all_mild_data(:,:,i) = mild_data;
   mild_data = [];
end

people_Moderate = [4:11,13:14,16,18:21];
for i=1:15
   for j = 1:9
      subject_moderate{i,j}=strcat('F:\HIE_Brain_network\EEG for Shu\HIE EEG
(+)\HIE_neonates\HIE',num2str(people_Moderate(i)),'\Matlab\EEG,Composite,SampleSeries,Co
mposite,Amp1020,data_part',num2str(j),'.mat');
   end
end
moderate_data = [];
for i = 1:15
   for j = 1:9
```

```
        temp = load(subject_moderate{i,j});
        moderate_data = [moderate_data, temp.measurement_data];
    end
    all_moderate_data(:,:,i) = moderate_data;
    moderate_data = [];
end

for i = 1:16
    dataIn=double(all_mild_data(:,:,i));
    EEG.data = dataIn(8,:);
    EEG.nbchan = 8;
    %% high pass filter
    fl=0.5;
    [b,a]=butter(2,fl/(fs/2) ,'high');
    prependLen=10*fs;
    nChannels=size(dataIn,1);
    dataIn=cat(2,zeros(nChannels,prependLen)+dataIn(:,1),dataIn); % Adding extra zeros to the
begining to create zero padding for the filter
    dataOut1=filter(b,a,dataIn,[],2);
    dataOut1=dataOut1(:,prependLen+1:end);

    %% low pass filter
    fl=100;
    [b,a]=butter(2,fl/(fs/2) ,'low');
    prependLen=10*fs;
    nChannels=size(dataOut1,1);
    dataIn1=cat(2,zeros(nChannels,prependLen)+dataOut1(:,1),dataOut1); % Adding extra zeros
to the begining to create zero padding for the filter
    dataOut=filter(b,a,dataIn1,[],2);
    dataOut=dataOut(:,prependLen+1:end);

    %% Remove 60 Hz
    [b,a]=butter(4,[58/(fs/2) 62/(fs/2)] ,'stop');
    dataOut=cat(2,zeros(nChannels,prependLen),dataOut);
    dataOut=filter(b,a,dataOut,[],2);
    dataOut=dataOut(:,prependLen+1:end);
    [b,a]=butter(4,[43/(fs/2) 45/(fs/2)] ,'stop');
    dataOut=cat(2,zeros(nChannels,prependLen),dataOut);
    dataOut=filter(b,a,dataOut,[],2);
    dataOut=dataOut(:,prependLen+1:end);
    [b,a]=butter(4,[75/(fs/2) 77/(fs/2)] ,'stop');
    dataOut=cat(2,zeros(nChannels,prependLen),dataOut);
    dataOut=filter(b,a,dataOut,[],2);
    dataOut=dataOut(:,prependLen+1:end);

    % rereference to the common mean
```

```
    dataOut=dataOut-repmat(mean(dataOut,1),nChannels,1);
    dataOut = dataOut(:,(fs*60*60*excluded_timelength+1):(fs*60*60*6));
    un_processed_mild(:,:,i) = dataOut;
    t = linspace(1/fs,(60*60*(6-excluded_timelength)-1),length(un_processed_mild));

    for ii = 1:8
        epoch_temp = buffer(dataOut(ii,:),fs);
        std_epoch = std(epoch_temp,[],1);
        std_epoch(std_epoch > 50 | std_epoch < 0.01) = NaN;
        std_epoch_all = repmat(std_epoch,[fs,1]);
        epoch_temp1 = epoch_temp;
        epoch_temp1(isnan(std_epoch_all)) = [];
        epoch_temp1(abs(epoch_temp1) > 4*std(epoch_temp1)) = [];
        if ii == 1
            data_final(ii,:) = epoch_temp1;
        else
            if length(epoch_temp1) < length(data_final)
                data_final = data_final(:,1:length(epoch_temp1));
                data_final(ii,:) = epoch_temp1;
            else data_final(ii,:) = epoch_temp1(1:length(data_final));
            end
        end

        pre_processed_mild_temp{i} = data_final;
        clear epoch_temp1
    end
    clear data_final
end

for sub = 1:length(people_Mild)
     pre_processed_mild_temp_temp = cell2mat(pre_processed_mild_temp(1,sub));
     pre_processed_mild(:,:,sub) =
pre_processed_mild_temp_temp(:,1:(fs*60*60*Target_timelength+1));
end

% moderate pre-process
for i = 1:15
    dataIn=double(all_moderate_data(:,:,i));
    EEG.data = dataIn(8,:);
    EEG.nbchan = 8;
    %% high pass filter
    fl=0.5;
    [b,a]=butter(2,fl/(fs/2) ,'high');
        prependLen=10*fs;
    nChannels=size(dataIn,1);
```

```
   dataIn=cat(2,zeros(nChannels,prependLen)+dataIn(:,1),dataIn); % Adding extra zeros to the
begining to create zero padding for the filter
   dataOut1=filter(b,a,dataIn,[],2);
   dataOut1=dataOut1(:,prependLen+1:end);

   %% low pass filter
   fl=100;
   [b,a]=butter(2,fl/(fs/2) ,'low');
   prependLen=10*fs;
   nChannels=size(dataOut1,1);
   dataIn1=cat(2,zeros(nChannels,prependLen)+dataOut1(:,1),dataOut1); % Adding extra zeros
to the begining to create zero padding for the filter
   dataOut=filter(b,a,dataIn1,[],2);
   dataOut=dataOut(:,prependLen+1:end);

   %% remove 60 Hz
   [b,a]=butter(4,[58/(fs/2) 62/(fs/2)] ,'stop');
   dataOut=cat(2,zeros(nChannels,prependLen),dataOut);
   dataOut=filter(b,a,dataOut,[],2);
   dataOut=dataOut(:,prependLen+1:end);
   [b,a]=butter(4,[43/(fs/2) 45/(fs/2)] ,'stop');
   dataOut=cat(2,zeros(nChannels,prependLen),dataOut);
   dataOut=filter(b,a,dataOut,[],2);
   dataOut=dataOut(:,prependLen+1:end);
   [b,a]=butter(4,[75/(fs/2) 77/(fs/2)] ,'stop');
   dataOut=cat(2,zeros(nChannels,prependLen),dataOut);
   dataOut=filter(b,a,dataOut,[],2);
   dataOut=dataOut(:,prependLen+1:end);

   %% rereference to the common mean
   dataOut=dataOut-repmat(mean(dataOut,1),nChannels,1);
   dataOut = dataOut(:,(fs*60*60*excluded_timelength+1):(fs*60*60*6));
   un_processed_moderate(:,:,i) = dataOut;
   t = linspace(1/fs,(60*60*(6-excluded_timelength)-1),length(un_processed_moderate));
   for ii = 1:8
      epoch_temp = buffer(dataOut(ii,:),fs);
      std_epoch = std(epoch_temp,[],1);
      std_epoch(std_epoch > 50 | std_epoch < 0.01) = NaN;
      std_epoch_all = repmat(std_epoch,[fs,1]);
      epoch_temp1 = epoch_temp;
      epoch_temp1(isnan(std_epoch_all)) = [];
      epoch_temp1(abs(epoch_temp1) > 4*std(epoch_temp1)) = [];
      if ii == 1
         data_final(ii,:) = epoch_temp1;
      else
         if length(epoch_temp1) < length(data_final)
```

```
            data_final = data_final(:,1:length(epoch_temp1));
            data_final(ii,:) = epoch_temp1;
        else data_final(ii,:) = epoch_temp1(1:length(data_final));
        end
    end

    pre_processed_moderate_temp{i} = data_final;
    clear epoch_temp1
  end
  clear data_final
end

% Convert cell to double with target length
for sub = 1:length(people_Moderate)
pre_processed_moderate_temp_temp = cell2mat(pre_processed_moderate_temp(1,sub));
pre_processed_moderate(:,:,sub) =
pre_processed_moderate_temp_temp(:,1:(fs*60*60*Target_timelength+1));
end
cd(strcat('F:\HIE_Brain_network\EEG for Shu\SK_HIE_results'))
save('F:\HIE_Brain_network\EEG for
Shu\SK_HIE_results\HIE_pre_processed','fs','SK_chan_names','people_Mild','people_Moderate',
'Target_timelength','excluded_timelength','pre_processed_mild','pre_processed_moderate')

%% Get coh via fieldtrip
clear;
clc;
ft_defaults;
conn_method  = 'coh';
freq_low = [1,4,8,12,30];
freq_high = [4,8,12,30,55];
time_low = [0];
time_high = [30];
cd(strcat('E:\HIE_Brain_network\EEG for Shu\SK_HIE_results'))
load HIE_pre_processed
cd(strcat('F:\HIE_Brain_network\EEG for Shu\SK_Code_HIE'))
load SK_EEG.mat
EEG_type = pre_processed_moderate;   % change between pre_processed_mild and
pre_processed_moderate
EEG_type_str = 'pre_processed_moderate';
for mm = 1:size(EEG_type,3)
  SK_EEG.trial{1,1} = [];
  SK_EEG.trial{1,1} = EEG_type(:,:,mm);
  cfg        = [];
  cfg.channel = SK_EEG.label;
  data       = ft_selectdata(cfg,SK_EEG);
```

```
% convert elec positions in mm
elec       = ft_convert_units(SK_EEG.elec,'mm');
data.elec   = SK_EEG.elec;
for ii = 1:5
   for jj = 1:1
      %% resegment the data into chunks
      cfg        = [];
      cfg.toilim  = [time_low(jj)*60 time_high(jj)*60];
      dataseg1    = ft_redefinetrial(cfg,data);
      cfg        = [];
      cfg.length  = 10;
      dataseg     = ft_redefinetrial(cfg,dataseg1);

% compute sensor level Fourier spectra, to be used for cross-spectral density computation.
      cfg           = [];
      cfg.method     = 'mtmfft';
      cfg.output     = 'fourier';
      cfg.keeptrials = 'yes';
      cfg.tapsmofrq  = 1;
      cfg.foilim     = [freq_low(ii) freq_high(ii)];
      cfg.pad        = 'nextpow2';
      freq           = ft_freqanalysis(cfg, dataseg);
      %%% following two lines for Cluster based permutation test
      cfg.output     = 'pow';
      freq2          = ft_freqanalysis(cfg, dataseg);
      %% compute connectivity
      cfg        = [];
      % freq.freq = mean(freq.freq);
      cfg.method  = conn_method;
      cfg.complex = 'absimag';
      source_conn = ft_connectivityanalysis(cfg, freq);
      source_conn_all(:,:,jj,ii) = mean(source_conn.cohspctrm,3);
   end
end

cd(strcat('F:\HIE_Brain_network\EEG for Shu\SK_HIE_results\Result_after_Fieldtrip'))
save([EEG_type_str,'_','SUB',num2str(mm),'_',conn_method,'_','4hr','.mat'],'source_conn_all');
end

%% get data into different five bands
clear;
clc;
fd_name = 'F:\HIE_Brain_network\EEG for Shu\SK_HIE_results\Result_after_Fieldtrip';
conn_method  = 'coh';
EEG_type_str = 'pre_processed_mild';   % change between pre_processed_mild and
pre_processed_moderate
```

```
group_name = 'mild';    % change: mild or moderate

for mm = [1:16]    % number of subjects: Mild 16, Moderate 15
   sub_name = ['SUB',num2str(mm)];
   load([fd_name,'/',EEG_type_str,'_',sub_name,'_coh_30.mat']);
   b_delta = squeeze(source_conn_all(:,:,:,1));
   b_theta = squeeze(source_conn_all(:,:,:,2));
   b_alpha = squeeze(source_conn_all(:,:,:,3));
   b_beta = squeeze(source_conn_all(:,:,:,4));
   b_gamma = squeeze(source_conn_all(:,:,:,5));
   cd(strcat(fd_name,'/Diff_bands/','Band1'))
   save([group_name,'_',sub_name,'_',conn_method,'_','30','.mat'],'b_delta');
   cd(strcat(fd_name,'/Diff_bands/','Band2'))
   save([group_name,'_',sub_name,'_',conn_method,'_','30','.mat'],'b_theta');
   cd(strcat(fd_name,'/Diff_bands/','Band3'))
   save([group_name,'_',sub_name,'_',conn_method,'_','30','.mat'],'b_alpha');
   cd(strcat(fd_name,'/Diff_bands/','Band4'))
   save([group_name,'_',sub_name,'_',conn_method,'_','30','.mat'],'b_beta');
   cd(strcat(fd_name,'/Diff_bands/','Band5'))
   save([group_name,'_',sub_name,'_',conn_method,'_','30','.mat'],'b_gamma');
end

%% Run Gretna (within Gretna)


%%% PSD analysis via pwelch

% load data
clc; close all; clearvars;
eeglab
cd(strcat('F:\HIE_Brain_network\EEG for Shu\SK_HIE_results\30min'))
load('HIE_pre_processed');
G1_name = 'Mild';
G2_name = 'Moderate';
G1 = pre_processed_mild;
G2 = pre_processed_moderate;
clear pre_processed_mild pre_processed_moderate

%%% PSD (via pwelch)
for sub = 1:length(people_Mild)
   for Ch = 1:8
      [pxx_G1(Ch,:,sub) f1] = pwelch(G1(Ch,:,sub), 4*fs, 3*fs, 4*fs, fs,'psd');
   end
end
for sub = 1:length(people_Moderate)
   for Ch = 1:8
      [pxx_G2(Ch,:,sub) f1] = pwelch(G2(Ch,:,sub), 4*fs, 3*fs, 4*fs, fs,'psd');
```

```
    end
end

% plot all channels on one pages
FigN1 = figure('color','w')
for i = 1:8
    subplot(2,4,i)
    pxx_G1_mean = median(pxx_G1(i,:,:),3);
    pxx_G1_sem = std(pxx_G1(i,:,:),0,3)/sqrt(size(pxx_G1(i,:,:),3));
    pxx_G2_mean = median(pxx_G2(i,:,:),3);
    pxx_G2_sem = std(pxx_G2(i,:,:),0,3)/sqrt(size(pxx_G2(i,:,:),3));
    hold on;
    shadedErrorBar(f1,pxx_G1_mean, pxx_G1_sem,'b',1)
    hold on;
    shadedErrorBar(f1,pxx_G2_mean, pxx_G2_sem,'r',1)
      xlim([1 55])
    ylim([0 8])
    hold on
    xlabel('Frequency (Hz)')
    ylabel('Power (μV^2/Hz)')
    xticks([1 4 8 12 30 55])
    yticks([0 4 8])
    title(SK_chan_names{i})
    set(gca,'fontsize',15,'fontweight','bold','linewidth',1.5)
end
cd('F:\HIE_Brain_network\EEG for Shu\SK_HIE_results\30min\Power')
saveas(FigN1,'AllCh_PSD_withErrorBar_nfft434fs_to55Hz_withMedian.png','png');
save('F:\HIE_Brain_network\EEG for
Shu\SK_HIE_results\Power\Mild_vs_Moderate_nfft434fs','fs','f1','SK_chan_names','G1_name','
G2_name','pxx_G1','pxx_G2')


% plot Mild and Moderate
FigN2 = figure('color','w')
colors = distinguishable_colors(8);
for i = 1:8
    subplot(2,1,1)
    pxx_G1_mean = mean(pxx_G1(i,:,:),3);
    pxx_G1_sem = std(pxx_G1(i,:,:),0,3)/sqrt(size(pxx_G1(i,:,:),3));
    hold on;
    shadedErrorBar(f1,pxx_G1_mean, pxx_G1_sem, {'color', colors(i,:)},1);
    xlim([1 55])
    ylim([0 8])
    hold on
    xlabel('Frequency (Hz)')
    ylabel('Power (μV^2/Hz)')
    xticks([1 4 8 12 30 55])
```

```
    yticks([0 4 8])
    title(G1_name)
    set(gca,'fontsize',15,'fontweight','bold','linewidth',1.5)
    hold on
    subplot(2,1,2)
    pxx_G2_mean = mean(pxx_G2(i,:,:),3);
    pxx_G2_sem = std(pxx_G2(i,:,:),0,3)/sqrt(size(pxx_G2(i,:,:),3));
    hold on;
    shadedErrorBar(f1,pxx_G2_mean, pxx_G2_sem, {'color', colors(i,:)},1)
    xlim([1 55])
    ylim([0 8])
    hold on
    xlabel('Frequency (Hz)')
    ylabel('Power (μV^2/Hz)')
    xticks([1 4 8 12 30 55])
    yticks([0 4 8])
    title(G2_name)
    set(gca,'fontsize',15,'fontweight','bold','linewidth',1.5)
end
cd('F:\HIE_Brain_network\EEG for Shu\SK_HIE_results\30min\Power')
saveas(FigN2,'Mild_Moderate_PSD_withErrorBar_nfft434fs_to55Hz_withMean.png','png');

%% topoplot
eeglab
locfile = 'SK_BioSemi8.loc';
dif_PSD = mean(pxx_G1,3) - mean(pxx_G2,3);  % Mild - Moderate
dif_PSD_Band1 = dif_PSD(:,5:17);       % 1-4Hz
dif_PSD_Band2 = dif_PSD(:,18:33);      % 4-8Hz
dif_PSD_Band3 = dif_PSD(:,34:49);      % 8-12Hz
dif_PSD_Band4 = dif_PSD(:,50:121);     % 12-30Hz
dif_PSD_Band5 = dif_PSD(:,122:221);    % 30-55Hz
tp_Band1 = mean(dif_PSD_Band1,2);
tp_Band2 = mean(dif_PSD_Band2,2);
tp_Band3 = mean(dif_PSD_Band3,2);
tp_Band4 = mean(dif_PSD_Band4,2);
tp_Band5 = mean(dif_PSD_Band5,2);
tp_Band = [tp_Band1,tp_Band2,tp_Band3,tp_Band4,tp_Band5];

FigT1 = figure('color','w')
for Band = 1:5
    subplot(1,6,Band)
    topoplot(tp_Band(:,Band),locfile, 'electrodes','on');
    title(['Band',num2str(Band)]);
    Clim_min = min( min (tp_Band));
    Clim_max = max( max (tp_Band));
    set(gca,'Clim',[Clim_min Clim_max])
```

```
    tf = gca;
    tf.FontSize = 28;
end

sgt = sgtitle('HIE Power (Mild - Moderate)');
sgt.FontSize = 30;
subplot(1,6,6)
colormap;colorbar('FontSize',28);
caxis([Clim_min Clim_max])
cd('F:\HIE_Brain_network\EEG for Shu\SK_HIE_results\Power')
saveas(gcf,strcat('topoplot_Power_Mild-Moderate_nfft434fs_withCh.png'),'png');

% t-test & FDR
clc; close all; clearvars;
cd('F:\HIE_Brain_network\EEG for Shu\SK_HIE_results\30min\Power')
load('Mild_vs_Moderate_nfft434fs');
pxx_G1_Band1 = squeeze(mean(pxx_G1(:,5:17,:),2));       % 1-4Hz
pxx_G1_Band2 = squeeze(mean(pxx_G1(:,18:33,:),2));      % 4-8Hz
pxx_G1_Band3 = squeeze(mean(pxx_G1(:,34:49,:),2));      % 8-12Hz
pxx_G1_Band4 = squeeze(mean(pxx_G1(:,50:121,:),2));     % 12-30Hz
pxx_G1_Band5 = squeeze(mean(pxx_G1(:,122:221,:),2));    % 30-55Hz
pxx_G1_Bands(:,:,1) = pxx_G1_Band1;
pxx_G1_Bands(:,:,2) = pxx_G1_Band2;
pxx_G1_Bands(:,:,3) = pxx_G1_Band3;
pxx_G1_Bands(:,:,4) = pxx_G1_Band4;
pxx_G1_Bands(:,:,5) = pxx_G1_Band5;
pxx_G2_Band1 = squeeze(mean(pxx_G2(:,5:17,:),2));       % 1-4Hz
pxx_G2_Band2 = squeeze(mean(pxx_G2(:,18:33,:),2));      % 4-8Hz
pxx_G2_Band3 = squeeze(mean(pxx_G2(:,34:49,:),2));      % 8-12Hz
pxx_G2_Band4 = squeeze(mean(pxx_G2(:,50:121,:),2));     % 12-30Hz
pxx_G2_Band5 = squeeze(mean(pxx_G2(:,122:221,:),2));    % 30-55Hz
pxx_G2_Bands(:,:,1) = pxx_G2_Band1;
pxx_G2_Bands(:,:,2) = pxx_G2_Band2;
pxx_G2_Bands(:,:,3) = pxx_G2_Band3;
pxx_G2_Bands(:,:,4) = pxx_G2_Band4;
pxx_G2_Bands(:,:,5) = pxx_G2_Band5;

for band = 1:5
    pm_pxx_G1 = permute(pxx_G1_Bands,[2 1 3]);        % change order of dimension
    pm_pxx_G2 = permute(pxx_G2_Bands,[2 1 3]);
end
size(pm_pxx_G1)
size(pm_pxx_G1)
for band = 1:5
    for col = 1:8
```

```
        [ht,pt,cit,statst] = ttest2(pm_pxx_G1(:,col,band),pm_pxx_G2(:,col,band),'alpha', 0.05,
'Vartype','unequal', 'tail', 'both');  % use ttest2 for Independent two-sample t-test
        ht_all(col,band) = ht;
        pt_all(col,band) = pt;
    end
end

size(ht_all)
size(pt_all)
if any(pt_all(:) == 0)
    disp('pt_all has 0 value')
else
    disp('pt_all does not has any 0 value')
end

for band = 1:5
    [h_r, Crit_p_r, ci_r, p_r]  = fdr_bh(pt_all(:,band), 0.05);
    h_r_all(:,band) = h_r;
    p_r_all(:,band) = p_r;
end
size(h_r_all)
size(p_r_all)

% number of significant p value
if any(ht_all(:) == 1)
    disp('ht_all >= 1')
    num_sig_ttest = sum(ht_all(:) == 1);
    disp(num_sig_ttest)
else
    disp('all ttest p-value not significant')
end
if any(h_r_all(:) == 1)
    disp('h_r_all >= 1')
    num_sig_fdr = sum(h_r_all(:) == 1);
    disp(num_sig_fdr)
else
    disp('all FDR p-value not significant')
end

% number of sig ttest p-value in each band
for band = 1:5
    num_sig_ttest_indBand = sum(ht_all(:,band) == 1);
    num_sig_ttest_Bands(:,band) = num_sig_ttest_indBand;
end
disp(num_sig_ttest_Bands);

% number of sig FDR p-value in each band
```

```
for band = 1:5
   num_sig_fdr_indBand = sum(sum(h_r_all(:,band) == 1));
   num_sig_fdr_Bands(:,band) = num_sig_fdr_indBand;
end
disp(num_sig_fdr_Bands);

% sig increase or decrease
change_amount_temp = mean(pm_pxx_G1,1) - mean(pm_pxx_G2,1);
change_amount = squeeze(change_amount_temp);

% sig ttest p-value & FDR p-value with change_amount
sig_ttest_with_change = change_amount .* ht_all;
sig_FDR_with_change = change_amount .* h_r_all;

cd('F:\HIE_Brain_network\EEG for Shu\SK_HIE_results\30min\Power')
save('Mild_vs_Moderate_Power_ttest_FDR.mat','ht_all','pt_all','h_r_all','p_r_all','change_amount
','sig_ttest_with_change','sig_FDR_with_change');


%%% Global network analysis
clear;
clc;
GN_path = 'F:\HIE_Brain_network\EEG for Shu\SK_HIE_results\30min_after_First1hr\Gretna';
Mild_or_Mode = 'Mild';
Band_name = 'Band1';

% Global Network
% Synchronization (GS1 = s_All_Thres; GS2 = szscore_All_Thres)
cd(strcat(GN_path,'/',Mild_or_Mode,'/',Band_name,'\Synchronization'))
GS1 = readmatrix('s_All_Thres.txt');
GS2 = readmatrix('szscore_All_Thres.txt');
if Mild_or_Mode == 'Mild'
   Mild_GS1 = GS1;
   Mild_GS2 = GS2;
else
   Mode_GS1 = GS1;
   Mode_GS2 = GS2;
end

% NetworkEfficiency (GN1 = Eloc_All_Thres; GN2 = Eg_All_Thres)
cd(strcat(GN_path,'/',Mild_or_Mode,'/',Band_name,'\NetworkEfficiency'))
GN1 = readmatrix('Eloc_All_Thres.txt');
GN2 = readmatrix('Eg_All_Thres.txt');
if Mild_or_Mode == 'Mild'
   Mild_GN1 = GN1;
   Mild_GN2 = GN2;
```

```
else
   Mode_GN1 = GN1;
   Mode_GN2 = GN2;
end

% SmallWorld (GSw1 = Cp_All_Thres; GSw2 = Gamma_All_Thres; GSw3 =
%              Lambda_All_Thres; GSw4 = Lp_All_Thres; GSw5 =
%              Sigma_All_Thres)
cd(strcat(GN_path,'/',Mild_or_Mode,'/',Band_name,'\SmallWorld'))
GSw1 = readmatrix('Cp_All_Thres.txt');
GSw2 = readmatrix('Gamma_All_Thres.txt');
GSw3 = readmatrix('Lambda_All_Thres.txt');
GSw4 = readmatrix('Lp_All_Thres.txt');
GSw5 = readmatrix('Sigma_All_Thres.txt');
if Mild_or_Mode == 'Mild'
   Mild_GSw1 = GSw1;
   Mild_GSw2 = GSw2;
   Mild_GSw3 = GSw3;
   Mild_GSw4 = GSw4;
   Mild_GSw5 = GSw5;
else
   Mode_GSw1 = GSw1;
   Mode_GSw2 = GSw2;
   Mode_GSw3 = GSw3;
   Mode_GSw4 = GSw4;
   Mode_GSw5 = GSw5;
end

% Hierarchy (GH1 = b_All_Thres; GH2 = bzscore_All_Thres)
cd(strcat(GN_path,'/',Mild_or_Mode,'/',Band_name,'\Hierarchy'))
GH1 = readmatrix('b_All_Thres.txt');
GH2 = readmatrix('bzscore_All_Thres.txt');
if Mild_or_Mode == 'Mild'
   Mild_GH1 = GH1;
   Mild_GH2 = GH2;
else
   Mode_GH1 = GH1;
   Mode_GH2 = GH2;
end

% Assortativity (GA1 = r_All_Thres; GA2 = rzscore_All_Thres)
cd(strcat(GN_path,'/',Mild_or_Mode,'/',Band_name,'\Assortativity'))
GA1 = readmatrix('r_All_Thres.txt');
GA2 = readmatrix('rzscore_All_Thres.txt');
if Mild_or_Mode == 'Mild'
   Mild_GA1 = GA1;
```

```
        Mild_GA2 = GA2;
    else
        Mode_GA1 = GA1;
        Mode_GA2 = GA2;
    end

    PltA = Mild_GN2;
    PltB = Mode_GN2;
    [ht,pt,cit,statst] = ttest2(PltB,PltA,'alpha', 0.05, 'Vartype','unequal', 'tail', 'both');
    Output_ttest = [ht; pt];
    if any(ht(:) == 1)
        disp('ht >= 1')
        num_sig = sum(ht(:) == 1);          % We want at least three continus sig, otherwise ignore
        disp(num_sig)
    else
        disp('all p value not significant')
    end

    % Add normal groups
    PltC = Normal_Eg(2,:);
    C_Sparsity = 0.05:0.05:0.6;

    % Plot
    close all
    feature_name = 'Eg';
    Sparsity = 0.05:0.05:1;
    PltA_mean = mean(PltA,1);
    PltA_sem = std(PltA)/sqrt(size(PltA,1));
    PltB_mean = mean(PltB,1);
    PltB_sem = std(PltB)/sqrt(size(PltB,1));
    FigM = figure(1);
    set(gcf,'Position', get(0, 'Screensize'),'color','w');
    hold on;
    plot(C_Sparsity,PltC,'k:', 'linewidth',4)
    plot(Sparsity,PltA_mean,'b',Sparsity,PltB_mean,'r','linewidth',4)
    Location = [0.21 0.8 0.1 0.1] ;
    set(0,'DefaultLegendAutoUpdate','off')
    legend('boxoff')
    hold on;
    shadedErrorBar(Sparsity,PltA_mean, PltA_sem,'b',1)
    hold on;
    shadedErrorBar(Sparsity,PltB_mean, PltB_sem,'r',1)
    legend('Healthy newborn (n=60)','Mild HIE (n=16)','Moderate HIE (n=15)',
'Location',Location,'Orientation','Vertical')
    grid on
    set(gca,'fontweight','bold','fontsize',26,'linewidth',4,'box','on');
```

```
xlabel('Sparsity'); ylabel(feature_name);
title('Global Network (Delta band)')
cd 'F:\EEG for Shu\SK_HIE_results\30min\Graph_theory\Global_Network'
saveas(gcf,strcat('Eg_Delta_band_OnlyAdd_Normal_Shorten.png'),'png');              %


%%% Nodal network analysis
clear;
clc;
Group1 = 'Mild';
Group2 = 'Mode';
network_method = 'BetweennessCentrality';
fd_name = 'F:\HIE_Brain_network\EEG for Shu\SK_HIE_results\Gretna';
for jj = 1:5
   Band_fd = ['Band',num2str(jj)];
   G1 = load([fd_name,'/',Group1,'/',Band_fd,'/',network_method,'/',network_method,'.mat']);
   G1_all(1:16,:,:,jj) = squeeze(G1.Bc);      % choose from: NCp NLp Ne NLe Dc Bc
end
for jj = 1:5
   Band_fd = ['Band',num2str(jj)];
   G2 = load([fd_name,'/',Group2,'/',Band_fd,'/',network_method,'/',network_method,'.mat']);
   G2_all(1:15,:,:,jj) = squeeze(G2.Bc);      % choose from: NCp NLp Ne NLe Dc Bc
end
G1_mean = mean(G1_all,1);
G1_Median = median(G1_all,1);
G2_mean = mean(G2_all,1);
G2_Median = median(G2_all,1);

% t-test
for band = 1:5
   for sparsity = 1:20
      for ch_num = 1:8
         [ht,pt,cit,statst] =
ttest2(G1_all(:,ch_num,sparsity,band)',G2_all(:,ch_num,sparsity,band)','alpha', 0.05,
'Vartype','unequal', 'tail', 'both');
         ht_all(ch_num,sparsity,band) = ht;
         pt_all(ch_num,sparsity,band) = pt;
      end
   end
end

% FDR
for band = 1:5
   for sparsity = 1:19   % not 1:20, to avoid NaN
      [h_r, Crit_p_r, ci_r, p_r]  = fdr_bh(pt_all(:,sparsity,band), 0.05);
      h_r_all(:,sparsity,band) = h_r;
      p_r_all(:,sparsity,band) = p_r;
```

```
    end
end

% Bonferroni correction
for band = 1:5
    for sparsity = 1:19   % not 1:20, to avoid NaN
        for ch_num = 1:8
            if pt_all(ch_num,sparsity,band) < (0.05/8)
                h_Bf_all(ch_num,sparsity,band) = ht_all(ch_num,sparsity,band);  % or use '= 1'
            else
                h_Bf_all(ch_num,sparsity,band) = 0;
            end
        end
    end
end

% number of significant p value
if any(ht_all(:) == 1)
    disp('ht_all >= 1')
    num_sig_ttest = sum(ht_all(:) == 1);            % We want at least three continus sig, otherwise
ignore
    disp(num_sig_ttest)
else
    disp('all ttest p-value not significant')
end

if any(h_r_all(:) == 1)
    disp('h_r_all >= 1')
    num_sig_fdr = sum(h_r_all(:) == 1);            % We want at least three continus sig, otherwise
ignore
    disp(num_sig_fdr)
else
    disp('all FDR p-value not significant')
end

if any(h_Bf_all(:) == 1)
    disp('h_Bf_all >= 1')
    num_sig_Bf = sum(h_Bf_all(:) == 1);             % We want at least three continus sig, otherwise
ignore
    disp(num_sig_Bf)
else
    disp('all p-value after Bonferroni correction are not significant')
end

% number of sig ttest p-value for each band
for band = 1:5
```

```
   num_sig_ttest_indBand = sum(sum(ht_all(:,:,band) == 1));
   num_sig_ttest_Bands(:,band) = num_sig_ttest_indBand;
end
disp(num_sig_ttest_Bands);

% number of sig FDR p-value for each band
for band = 1:5
   num_sig_fdr_indBand = sum(sum(h_r_all(:,:,band) == 1));
   num_sig_fdr_Bands(:,band) = num_sig_fdr_indBand;
end
disp(num_sig_fdr_Bands);

% number of sig p-value after Bonferroni correction for each band
for band = 1:5
   num_sig_Bf_indBand = sum(sum(h_Bf_all(:,:,band) == 1));
   num_sig_Bf_Bands(:,band) = num_sig_Bf_indBand;
end
disp(num_sig_Bf_Bands);

% number of sig ttest p-value for each sparsity under each band
for band = 1:5
   for sparsity = 1:19
      num_sig_ttest_ind = sum(ht_all(:,sparsity,band) == 1);
      num_sig_ttest_all(:,sparsity,band) = num_sig_ttest_ind;
   end
end
loc_sig_t = find(num_sig_ttest_all(:) >= 1);   % use >= 1 for 8 channels
[row_t, col_sparsity_t, height_band_t] = ind2sub(size(num_sig_ttest_all),loc_sig_t);
sum_sig_ttest = [row_t, col_sparsity_t, height_band_t];
disp(sum_sig_ttest)

% total number of sig FDR p-value for each sparsity under each band
for band = 1:5
   for sparsity = 1:19
      num_sig_fdr_ind = sum(h_r_all(:,sparsity,band) == 1);
      num_sig_fdr_all(:,sparsity,band) = num_sig_fdr_ind;
   end
end
loc_sig_f = find(num_sig_fdr_all(:) >= 1);
[row_f, col_sparsity_f, height_band_f] = ind2sub(size(num_sig_fdr_all),loc_sig_f);
sum_sig_fdr = [row_f, col_sparsity_f, height_band_f];
disp(sum_sig_fdr)

% check total number of sig p-value after Bonferroni correction for each sparsity under each
band
for band = 1:5
```

```
    for sparsity = 1:19
        num_sig_Bf_ind = sum(h_Bf_all(:,sparsity,band) == 1);
        num_sig_Bf_all(:,sparsity,band) = num_sig_Bf_ind;
    end
end
loc_sig_Bf = find(num_sig_Bf_all(:) >= 1);
[row_B, col_sparsity_B, height_band_B] = ind2sub(size(num_sig_Bf_all),loc_sig_Bf);
sum_sig_Bf = [row_B, col_sparsity_B, height_band_B];
disp(sum_sig_Bf)

% channels/regions location for target sparsity&band, which are sig after FDR
for L = 1:size(sum_sig_fdr,1)
    if sum_sig_fdr(L,2) >= 4 && sum_sig_fdr(L,2) <= 14
        target_sig_fdr(L,1) = sum_sig_fdr(L,2);
        target_sig_fdr(L,2) = sum_sig_fdr(L,3);
    end
end
target_sig_fdr_all = target_sig_fdr(all(target_sig_fdr,2),:);

for L = 1:size(target_sig_fdr_all,1)
    target_sig_fdr_loc_temp = h_r_all(:,target_sig_fdr_all(L,1),target_sig_fdr_all(L,2));
    target_sig_fdr_loc(L,1:8) = target_sig_fdr_loc_temp';
end

% channels/regions location for target sparsity&band, which are sig after Bonferroni correction
for L = 1:size(sum_sig_Bf,1)
    %     if sum_sig_Bf(L,2) >= 4 && sum_sig_Bf(L,2) <= 14  && sum_sig_Bf(L,3) ~= 5   %
focuse on sparsity 0.3-0.5 (6-10 row), without Gamma band
    if sum_sig_Bf(L,2) >= 4 && sum_sig_Bf(L,2) <= 14
        target_sig_Bf(L,1) = sum_sig_Bf(L,2);
        target_sig_Bf(L,2) = sum_sig_Bf(L,3);
    end
end
target_sig_Bf_all = target_sig_Bf(all(target_sig_Bf,2),:);

for L = 1:size(target_sig_Bf_all,1)
    target_sig_Bf_loc_temp = h_Bf_all(:,target_sig_Bf_all(L,1),target_sig_Bf_all(L,2));
    target_sig_Bf_loc(L,1:8) = target_sig_Bf_loc_temp';    % 8 channels use '1:8'
end

% check sig increase/decrease
change_amount_temp = mean(G1_all,1) - mean(G2_all,1);
change_amount = squeeze(change_amount_temp);

% check FDR
```

```
all_sig_change_fdr = h_r_all .* change_amount(:,1:19,:);    % change_amount: 1st col for num
of Ch/region, 2nd col for sparsity, 3rd col for bands

for L = 1:size(target_sig_fdr_all,1)
   target_sig_change_fdr_temp =
all_sig_change_fdr(:,target_sig_fdr_all(L,1),target_sig_fdr_all(L,2));
   target_sig_change_fdr(L,1:8) = target_sig_change_fdr_temp';
end

target_sig_fdr_new_temp =
[target_sig_change_fdr,target_sig_fdr_all,sum(target_sig_fdr_loc,2)];
target_sig_fdr_new = target_sig_fdr_new_temp;
target_sig_fdr_new(:,9) = target_sig_fdr_new_temp(:,9)*0.05;

%%% check for Bonferroni correction
all_sig_change_Bf = h_Bf_all .* change_amount(:,1:19,:);
for L = 1:size(target_sig_Bf_all,1)
   target_sig_change_Bf_temp =
all_sig_change_Bf(:,target_sig_Bf_all(L,1),target_sig_Bf_all(L,2));
   target_sig_change_Bf(L,1:8) = target_sig_change_Bf_temp';
end

target_sig_Bf_new_temp = [target_sig_change_Bf,target_sig_Bf_all,sum(target_sig_Bf_loc,2)];
target_sig_Bf_new = target_sig_Bf_new_temp;
target_sig_Bf_new(:,9) = target_sig_Bf_new_temp(:,9)*0.05;
cd 'F:\HIE_Brain_network\EEG for Shu\SK_HIE_results\Graph_theory\Nodal_Network'
save(['Mild_vs_Moderate_Bands','_',network_method,'.mat'],'num_sig_fdr_all','num_sig_Bf_all',
'sum_sig_fdr','sum_sig_Bf','target_sig_fdr_new','target_sig_Bf_new','network_method','pt_all','ht
_all','p_r_all','h_r_all','h_Bf_all','target_sig_fdr_loc','target_sig_Bf_loc');
```

**M.3 MATLAB codes for Aim 3 (Chapter 4)**

```
%% Prepocessing
close all;
clear all;
clc
addpath 'C:\Users\sxk1519\OneDrive - University of Texas at
Arlington\Notebooks\EEGLab\eeglab2021.1\functions';
addpath 'C:\Users\sxk1519\OneDrive - University of Texas at
Arlington\Notebooks\Quik20\EEG_FALL2021\Code\FromXinlong_pca_ica';
addpath 'C:\Users\sxk1519\OneDrive - University of Texas at
Arlington\Notebooks\Quik20\EEG_FALL2021\Code\SK_For_pre_and_power';
eeglab
path = 'C:\Users\sxk1519\OneDrive - University of Texas at
Arlington\Notebooks\Quik20\EEG_FALL2021\808R\';
```

```
for i = [1:8, 10:33]
   realpath = strcat(path,'SUB',num2str(i),'\');
   EEG = pop_biosig(strcat(realpath,'SUB',num2str(i),'_B_R808.bdf'));
   EEG = eeg_checkset( EEG );
   % above are using EEGLAB built-in functions to load .bdf data

   data= EEG.data(1:19,:);
   dataIn=double(data);
   fs=EEG.srate;

% high pass
   fl = 1;
   [b,a] = butter(2,fl/(fs/2) ,'high');
   prependLen = 0*fs;
   nChannels = size(dataIn,1);
   dataIn1 = [zeros(nChannels,prependLen),dataIn];
   dataOut1 = filtfilt(b,a,dataIn1');
   dataOut2 = dataOut1(prependLen+1:end,:);
   dataOut_hp = dataOut2';

% low pass
   fl = 55;
   [b,a] = butter(2,fl/(fs/2) ,'low');
      prependLen = 0*fs;
   nChannels = size(dataOut_hp,1);
   dataIn2 = [zeros(nChannels,prependLen),dataOut_hp];
   dataOut3 = filtfilt(b,a,dataIn2');
   dataOut4 = dataOut3(prependLen+1:end,:);
   dataOut = dataOut4';

% NaN the cns created artificial spikes
   eeg_temp = dataOut;
   for ch_n = 1:19;
      TH_4std_upper = median(eeg_temp(ch_n,:)) + 4*std(eeg_temp(ch_n,:));
      TH_4std_lower = median(eeg_temp(ch_n,:)) - 4*std(eeg_temp(ch_n,:));
      timer = length(eeg_temp(ch_n,:));

      for j = 1:length(eeg_temp(ch_n,:))
         if eeg_temp(ch_n,j) > TH_4std_upper
            eeg_temp(ch_n,j)=NaN;
         end
         if eeg_temp(ch_n,j) < TH_4std_lower
            eeg_temp(ch_n,j)=NaN;
         end
         j=j+1;
      end
```

```
    clear j
  end

  sum_nan = sum(isnan(eeg_temp),2);
  time_nan_sec = sum_nan./fs;

%Denan by interpolated Data
  eeg_temp2 = dataOut';
  temp2 = filloutliers(eeg_temp2,'nearest','median');
  temp2 = temp2';
  EEG.data = temp2(1:19,:);

% Replace bad seg
  locfile = 'SK_BioSemi19.loc';
  [Zica, W, T, mu] = fastICA(temp2(1:19,:),19,'kurtosis',1);
  icaw = pinv(W*T);
  FigN = figure
  for j = 1:19
    subplot(4,5,j)
    topoplot(icaw(:,j),locfile, 'electrodes','off');
    title(j);
    colormap(jet);
  end
    EEG.icaweights = W;

% ICs
  EEG.icasphere = T;
  EEG.icawinv = icaw;
  EEG.chanlocs = EEG.chanlocs(1:19,:);
  EEG = pop_editset(EEG, 'chanlocs', 'SK_BioSemi19.loc');
  EEG = pop_select( EEG,'time',[0 420],'channel',{'F7' 'Fp1' 'Fp2' 'F8' 'F3' 'Fz' 'F4' 'C3' 'Cz' 'P8'
'P7' 'Pz' 'P4' 'T3' 'P3' 'O1' 'O2' 'C4' 'T4'});

% save plot before replace bad ch
  cd(strcat(realpath))
  save(strcat(realpath,'R808_B_PreEEGLAB.set'),'EEG')
end

% Remove artifacts in EEGLAB
eeglab
locfile = 'SK_BioSemi19.loc';
clear data dataOut1 dataIn f1 a b fs
clear prependLen nChanneLS dataBeforeRPCA A_hat E_hat iter
clear U S V dataIn dataIn1 ans c fl
EEG.data = dataOut(1:19,:);
```

```
% run ICA usin the function fastICA
[Zica, W, T, mu] = fastICA(dataOut(1:19,:),19,'kurtosis',1);
icaw = pinv(W*T);

% plot the ICs
FigN = figure
for j = 1:19
   subplot(4,5,j)
   topoplot(icaw(:,j),locfile, 'electrodes','off');
   title(j);
  colormap(jet);
end

% EEGLAB need following modification to plot the result
EEG.icaweights = W;
EEG.icasphere = T;
EEG.icawinv = icaw;
EEG.chanlocs = EEG.chanlocs(1:19,:);
EEG = pop_editset(EEG, 'chanlocs', 'SK_BioSemi19.loc');
EEG = pop_select( EEG,'time',[0 420],'channel',{'F7' 'Fp1' 'Fp2' 'F8' 'F3' 'Fz' 'F4' 'C3' 'Cz' 'P8'
'P7' 'Pz' 'P4' 'T3' 'P3' 'O1' 'O2' 'C4' 'T4'});
fin = sprintf('SUB%d',i);
cd(strcat('E:\Quik20\EEG_FALL2021\808R\',fin))
save(strcat(realpath,'B_RS_afterICA.set'),'EEG')
saveas(FigN,strcat('SUB',num2str(i),'B_RS_Icsplot.png'),'png');

% transfer_eeglab_to_fieldtrip
path = 'C:\Users\sxk1519\Documents\Quik20\EEG_FALL2021\808R\';
fd_name = 'C:\Users\sxk1519\Documents\Quik20\EEG_FALL2021\808R\808R_Post\'
for ii = [1:3,6:8,10,11,13:28,31,33] \
   realpath = strcat(path,'SUB',num2str(i),'\');
   sub_fd = ['SUB',num2str(ii)];
   EEG = pop_loadset([path,'/',sub_fd,'/','R808_B_PostEEGLAB.set']);
   transferred_EEG = eeglab2fieldtrip(EEG,'raw','none');
    save([fd_name,'/',sub_fd,'_Ftrip.mat'],'transferred_EEG');
end


%% Network analysis
clear;
clc;
ft_defaults;
conn_method  = 'coh';
freq_low = [1,4,8,12,30];
freq_high = [4,8,12,30,55];
time_low = [0,2,4,6];
```

```
time_high = [2,4,6,7];
fd_name = 'C:\Users\sxk1519\Documents\Quik20\EEG_FALL2021\808L\808L_Pre';
for mm = [1:3,6:8,10,11,13:28,31,33] %% number of subjects
   sub_name = ['SUB',num2str(mm)];
   EEG = load([fd_name,'/',sub_name,'_Ftrip.mat'],'transferred_EEG');
   cfg        = [];
   cfg.channel = EEG.transferred_EEG.label;
   data       = ft_selectdata(cfg,EEG.transferred_EEG);
   elec       = ft_convert_units(EEG.transferred_EEG.elec,'mm');
   data.elec   = EEG.transferred_EEG.elec;
   for ii = 1:5
      for jj = 1:1
         cfg        = [];
         cfg.toilim  = [time_low(jj)*60 time_high(jj)*60];
         dataseg1       = ft_redefinetrial(cfg,data);
         cfg        = [];
         cfg.length  = 10;
         dataseg       = ft_redefinetrial(cfg,dataseg1);

% compute sensor level Fourier spectra, to be used for cross-spectral density computation
         cfg           = [];
         cfg.method     = 'mtmfft';
         cfg.output     = 'fourier';
         cfg.keeptrials = 'yes';
         cfg.tapsmofrq  = 1;
         cfg.foilim     = [freq_low(ii) freq_high(ii)];
         cfg.pad        = 'nextpow2';
         freq          = ft_freqanalysis(cfg, dataseg);

% compute connectivity
         cfg        = [];
         % freq.freq = mean(freq.freq);
         cfg.method  = conn_method;
         cfg.complex = 'absimag';
         source_conn = ft_connectivityanalysis(cfg, freq);
         source_conn_all(:,:,jj,ii) = mean(source_conn.cohspctrm,3);
      end
   end
save([fd_name,'/',sub_name,'_',conn_method,'_','2221','.mat'],'source_conn_all');
end

% get data into different five bands
clear;
clc;
fd_name = 'C:\Users\sxk1519\Documents\Quik20\EEG_FALL2021\808R\808R_Post';
conn_method  = 'coh';
```

```
for mm = [1:3,6:8,10,11,13:28,31,33]

   sub_name = ['SUB',num2str(mm)];
   load([fd_name,'/',sub_name,'_coh_2221.mat']);
   b_delta = squeeze(source_conn_all(:,:,1,1));
   b_theta = squeeze(source_conn_all(:,:,1,2));
   b_alpha = squeeze(source_conn_all(:,:,1,3));
   b_beta = squeeze(source_conn_all(:,:,1,4));
   b_gamma = squeeze(source_conn_all(:,:,1,5));

   cd(strcat(fd_name,'/','Diff_bands\1_4'))
   save([sub_name,'_',conn_method,'_','2221','.mat'],'b_delta');
   cd(strcat(fd_name,'/','Diff_bands\4_8'))
   save([sub_name,'_',conn_method,'_','2221','.mat'],'b_theta');
   cd(strcat(fd_name,'/','Diff_bands\8_12'))
   save([sub_name,'_',conn_method,'_','2221','.mat'],'b_alpha');
   cd(strcat(fd_name,'/','Diff_bands\12_30'))
   save([sub_name,'_',conn_method,'_','2221','.mat'],'b_beta');
   cd(strcat(fd_name,'/','Diff_bands\30_55'))
   save([sub_name,'_',conn_method,'_','2221','.mat'],'b_gamma');
end

% Run Gretna

% Gretna output analysis
clear;
clc;
GN_path = 'D:\Quik20\EEG_FALL2021\808L';
Pre_or_Post = 'Pre';
Band_name = 'Band1';

% GTA_Global Network
% Synchronization (GS1 = s_All_Thres; GS2 = szscore_All_Thres)
cd(strcat(GN_path,'/','808L_',Pre_or_Post,'/',Band_name,'\Synchronization'))
GS1 = readmatrix('s_All_Thres.txt');
GS2 = readmatrix('szscore_All_Thres.txt');
if Pre_or_Post == 'Pre'
   Pre_GS1 = GS1;
   Pre_GS2 = GS2;
else
   Post_GS1 = GS1;
   Post_GS2 = GS2;
end

% NetworkEfficiency (GN1 = Eloc_All_Thres; GN2 = Eg_All_Thres)
cd(strcat(GN_path,'/','808L_',Pre_or_Post,'/',Band_name,'\NetworkEfficiency'))
```

```
GN1 = readmatrix('Eloc_All_Thres.txt');
GN2 = readmatrix('Eg_All_Thres.txt');
if Pre_or_Post == 'Pre'
   Pre_GN1 = GN1;
   Pre_GN2 = GN2;
else
   Post_GN1 = GN1;
   Post_GN2 = GN2;
end

% SmallWorld (GSw1 = Cp_All_Thres; GSw2 = Gamma_All_Thres; GSw3 =
%             Lambda_All_Thres; GSw4 = Lp_All_Thres; GSw5 =
%             Sigma_All_Thres)
cd(strcat(GN_path,'/','808L_',Pre_or_Post,'/',Band_name,'\SmallWorld'))
GSw1 = readmatrix('Cp_All_Thres.txt');
GSw2 = readmatrix('Gamma_All_Thres.txt');
GSw3 = readmatrix('Lambda_All_Thres.txt');
GSw4 = readmatrix('Lp_All_Thres.txt');
GSw5 = readmatrix('Sigma_All_Thres.txt');
if Pre_or_Post == 'Pre'
   Pre_GSw1 = GSw1;
   Pre_GSw2 = GSw2;
   Pre_GSw3 = GSw3;
   Pre_GSw4 = GSw4;
   Pre_GSw5 = GSw5;
else
   Post_GSw1 = GSw1;
   Post_GSw2 = GSw2;
   Post_GSw3 = GSw3;
   Post_GSw4 = GSw4;
   Post_GSw5 = GSw5;
end

% Hierarchy (GH1 = b_All_Thres; GH2 = bzscore_All_Thres)
cd(strcat(GN_path,'/','808L_',Pre_or_Post,'/',Band_name,'\Hierarchy'))
GH1 = readmatrix('b_All_Thres.txt');
GH2 = readmatrix('bzscore_All_Thres.txt');
if Pre_or_Post == 'Pre'
   Pre_GH1 = GH1;
   Pre_GH2 = GH2;
else
   Post_GH1 = GH1;
   Post_GH2 = GH2;
end

% Assortativity (GA1 = r_All_Thres; GA2 = rzscore_All_Thres)
```

```
cd(strcat(GN_path,'/','808L_',Pre_or_Post,'/',Band_name,'\Assortativity'))
GA1 = readmatrix('r_All_Thres.txt');
GA2 = readmatrix('rzscore_All_Thres.txt');
if Pre_or_Post == 'Pre'
   Pre_GA1 = GA1;
   Pre_GA2 = GA2;
else
   Post_GA1 = GA1;
   Post_GA2 = GA2;
end

PltA = Pre_GH1;
PltB = Post_GH1;
[ht,pt,cit,statst] = ttest(PltB,PltA,'alpha', 0.05, 'tail', 'both');
Output_ttest = [ht; pt];
if any(ht(:) == 1)
   disp('ht >= 1')
   num_sig = sum(ht(:) == 1);
   disp(num_sig)
else
   disp('all p value not significant')
end

% Plot
feature_name = 'b of Hierarchy';
Sparsity = 0.05:0.05:1;
PltA_mean = mean(PltA,1);
PltA_sem = std(PltA)/sqrt(size(PltA,1));
PltB_mean = mean(PltB,1);
PltB_sem = std(PltB)/sqrt(size(PltB,1));
FigM = figure(1);
set(gcf,'Position', get(0, 'Screensize'),'color','w');
plot(Sparsity,PltB_mean,'r',Sparsity,PltA_mean,'b','linewidth',4)
Location = [0.16 0.8 0.1 0.1] ;
legend('Post','Pre','Location',Location,'Orientation','Vertical')
set(0,'DefaultLegendAutoUpdate','off')
legend('boxoff')

hold on;
shadedErrorBar(Sparsity,PltB_mean, PltB_sem,'r',1)
hold on;
shadedErrorBar(Sparsity,PltA_mean, PltA_sem,'b',1)

set(gca,'XLim',[min(Sparsity),max(Sparsity)],'XTick',Sparsity,'XTickLabel',num2str(Sparsity),'
XTickLabelRotation',45)
set(gca,'fontweight','bold','fontsize',33,'linewidth',4,'box','off');
```

```
xlabel('Sparsity'); ylabel(feature_name);
title('Global Network (Theta band)')
cd D:\Quik20\EEG_FALL2021\808R\Global_network\Plot_RSPre_RSPos
saveas(gcf,strcat('b_Hierarchy_Theta_band.png'),'png');


%% Six regions with Coherence matrix

clear;
clc;
cd C:\Users\sxk1519\Documents\Quik20\EEG_FALL2021\808R\RS_Pre\Diff_bands
load('coh_2221_Bands_Pre.mat');
G1_all = mm_Bands_Pre;
cd C:\Users\sxk1519\Documents\Quik20\EEG_FALL2021\808R\808R_Pre\Diff_bands
load('coh_2221_Bands_Pre.mat');
G2_all = mm_Bands_Pre;
size(G2_all)

% tPBM_Post-Pre vs sham_Post-pre
cd C:\Users\sxk1519\Documents\Quik20\EEG_FALL2021\808R\RS_Pos\Diff_bands
load('coh_2221_Bands_Pos.mat');
G3_all = mm_Bands_Pos;
cd C:\Users\sxk1519\Documents\Quik20\EEG_FALL2021\808R\808R_Pos\Diff_bands
load('coh_2221_Bands_Pos.mat');
G4_all = mm_Bands_Pos;
G1_all = G3_all;
G2_all = G4_all;
pm_G1 = permute(G1_all,[3 1 2 4]);
pm_G2 = permute(G2_all,[3 1 2 4]);

% build regions for t-Test
Reg1 = [1,2,5];
Reg2 = [14,8];
Reg3 = [11,15,16];
Reg4 = [3,7,4];
Reg5 = [18,19];
Reg6 = [13,10,17];
pm_G = pm_G2;      % choose from pm_G1 or pm_G2
for band = 1:5
   for sub = 1:26

% for 1st col in new 6*6 matrix
       set_ele = [];
       for s = Reg1
          for k = Reg2
             temp_ele = pm_G(sub,s,k,band);
             set_ele = union(set_ele,temp_ele);
```

```
            new_Reg_1_2 = mean(set_ele, 2);
        end
    end

    set_ele = [];
    for s = Reg1
        for k = Reg3
            temp_ele = pm_G(sub,s,k,band);
            set_ele = union(set_ele,temp_ele);
            new_Reg_1_3 = mean(set_ele, 2);
        end
    end

    set_ele = [];
    for s = Reg1
        for k = Reg4
            temp_ele = pm_G(sub,s,k,band);
            set_ele = union(set_ele,temp_ele);
            new_Reg_1_4 = mean(set_ele, 2);
        end
    end

    set_ele = [];
    for s = Reg1
        for k = Reg5
            temp_ele = pm_G(sub,s,k,band);
            set_ele = union(set_ele,temp_ele);
            new_Reg_1_5 = mean(set_ele, 2);
        end
    end

    set_ele = [];
    for s = Reg1
        for k = Reg6
            temp_ele = pm_G(sub,s,k,band);
            set_ele = union(set_ele,temp_ele);
            new_Reg_1_6 = mean(set_ele, 2);
        end
    end

% for 2nd col in new 6*6 matrix
    set_ele = [];
    for s = Reg2
        for k = Reg3
            temp_ele = pm_G(sub,s,k,band);
            set_ele = union(set_ele,temp_ele);
```

```
            new_Reg_2_3 = mean(set_ele, 2);
        end
    end

    set_ele = [];
    for s = Reg2
        for k = Reg4
            temp_ele = pm_G(sub,s,k,band);
            set_ele = union(set_ele,temp_ele);
            new_Reg_2_4 = mean(set_ele, 2);
        end
    end

    set_ele = [];
    for s = Reg2
        for k = Reg5
            temp_ele = pm_G(sub,s,k,band);
            set_ele = union(set_ele,temp_ele);
            new_Reg_2_5 = mean(set_ele, 2);
        end
    end

    set_ele = [];
    for s = Reg2
        for k = Reg6
            temp_ele = pm_G(sub,s,k,band);
            set_ele = union(set_ele,temp_ele);
            new_Reg_2_6 = mean(set_ele, 2);
        end
    end

% for 3rd col in new 6*6 matrix
    set_ele = [];
    for s = Reg3
        for k = Reg4
            temp_ele = pm_G(sub,s,k,band);
            set_ele = union(set_ele,temp_ele);
            new_Reg_3_4 = mean(set_ele, 2);
        end
    end

    set_ele = [];
    for s = Reg3
        for k = Reg5
            temp_ele = pm_G(sub,s,k,band);
            set_ele = union(set_ele,temp_ele);
```

```
            new_Reg_3_5 = mean(set_ele, 2);
        end
    end

    set_ele = [];
    for s = Reg3
        for k = Reg6
            temp_ele = pm_G(sub,s,k,band);
            set_ele = union(set_ele,temp_ele);
            new_Reg_3_6 = mean(set_ele, 2);
        end
    end

% for 4th col in new 6*6 matrix
    set_ele = [];
    for s = Reg4
        for k = Reg5
            temp_ele = pm_G(sub,s,k,band);
            set_ele = union(set_ele,temp_ele);
            new_Reg_4_5 = mean(set_ele, 2);
        end
    end

    set_ele = [];
    for s = Reg4
        for k = Reg6
            temp_ele = pm_G(sub,s,k,band);
            set_ele = union(set_ele,temp_ele);
            new_Reg_4_6 = mean(set_ele, 2);
        end
    end

% for 5th col in new 6*6 matrix
    set_ele = [];
    for s = Reg5
        for k = Reg6
            temp_ele = pm_G(sub,s,k,band);
            set_ele = union(set_ele,temp_ele);
            new_Reg_5_6 = mean(set_ele, 2);
        end
    end

    new_Reg_all = [new_Reg_1_2; new_Reg_1_3; new_Reg_1_4; new_Reg_1_5;
new_Reg_1_6;
        new_Reg_2_3; new_Reg_2_4; new_Reg_2_5; new_Reg_2_6;
        new_Reg_3_4; new_Reg_3_5; new_Reg_3_6;
```

```
            new_Reg_4_5; new_Reg_4_6;
            new_Reg_5_6];
        new_pm_G(sub,:,band) = new_Reg_all;
    end
end
if pm_G == pm_G1
    new_pm_G1 = new_pm_G;
else
    new_pm_G2 = new_pm_G;
end

% t-test
for band = 1:5
    for new_matrix_ele = 1:15
        [ht,pt,cit,statst] =
ttest(new_pm_G1(:,new_matrix_ele,band),new_pm_G2(:,new_matrix_ele,band),'alpha', 0.05,
'tail', 'both');
        ht_all(new_matrix_ele,band) = ht;
        pt_all(new_matrix_ele,band) = pt;
    end
end

if any(pt_all(:) == 0)
    disp('pt_all has 0 value')
else
    disp('pt_all does not has any 0 value')
end

% FDR
for band = 1:5
    [h_r, Crit_p_r, ci_r, p_r]  = fdr_bh(pt_all(:,band), 0.05);
    h_r_all(:,band) = h_r;
    p_r_all(:,band) = p_r;
end

% number of significant p value
if any(ht_all(:) == 1)
    disp('ht_all >= 1')
    num_sig_ttest = sum(ht_all(:) == 1);
    disp(num_sig_ttest)
else
    disp('all ttest p-value not significant')
end

if any(h_r_all(:) == 1)
    disp('h_r_all >= 1')
```

```
   num_sig_fdr = sum(h_r_all(:) == 1);
   disp(num_sig_fdr)
else
   disp('all FDR p-value not significant')
end

% number of sig ttest p-value for each band
for band = 1:5
   num_sig_ttest_indBand = sum(sum(ht_all(:,band) == 1));
   num_sig_ttest_Bands(:,band) = num_sig_ttest_indBand;
end
disp(num_sig_ttest_Bands);

% number of sig FDR p-value for each band
for band = 1:5
   num_sig_fdr_indBand = sum(sum(h_r_all(:,band) == 1));
   num_sig_fdr_Bands(:,band) = num_sig_fdr_indBand;
end
disp(num_sig_fdr_Bands);

% check sig increase or decrease
change_amount_temp = mean(new_pm_G2,1) - mean(new_pm_G1,1);
change_amount = squeeze(change_amount_temp);

cd
C:\Users\sxk1519\Documents\Quik20\EEG_FALL2021\808R\BrainNetViewer\SixReg_with_Co
herence_matrix
save('R808_Post_vs_RS_Post_Bands.mat','ht_all','pt_all','h_r_all','p_r_all','num_sig_ttest_Bands'
,'num_sig_fdr_Bands','change_amount');
```